ANALYSIS AND DESIGN OF FREQUENCY SELECTIVE SURFACE FOR TRANSMISSION IN S-BAND AND REFLECTION IN Ku/Ka-BAND FOR SATELLITE COMMUNICATION

by

Garima Bharti

a thesis submitted for fulfilment of the requirements

for the degree of

Doctor of Philosophy

in

Electronics and Communication Engineering

DEPARTMENT OF ELECTRONICS AND COMMUNICATION ENGINEERING
JAYPEE UNIVERSITY OF INFORMATION TECHNOLOGY
WAKNAGHAT, SOLAN - 173234
INDIA

Roll No. 126004 **June 2015**

Date:

Candidate's Declaration

I hereby certify that the work which is being presented in the thesis entitled "*Analysis and Design of Frequency Selective Surface for Transmission in S-Band and Reflection in Ku/Ka-Band for Satellite Communication*" in fulfilment of the requirement for the award of the degree of *Doctor of Philosophy* in Electronics and Communication Engineering and submitted in the Department of Electronics and Communication Engineering of Jaypee University of Information Technology, Waknaghat (H.P), India is an authentic record of my own work, carried out during the period from July 2012 to June 2015, under the supervision of **Prof. Ghanshyam Singh.**

The matter presented in this thesis has not been submitted by me for the award of any other degree in this Institute or any other Institute/University.

Garima Bharti
(Enrolment No. 126004)

This is to certify that the above statement made by the candidate is correct to the best of our knowledge.

Prof. Ghanshyam Singh
Professor,
Department of Electronics and Communication Engineering

Dedicated to my brother (Ankush)...

ACKNOWLEDGMENT

First of all, I express most sincere gratitude to my advisor, Prof. (Dr.) Ghanshyam Singh for his guidance, support and encouragement. His vast experience and deep understanding of the subject proved to be immense help to me, and also his profound view-points and extraordinary motivation enlightened me in many ways. I am highly indebted for his guidance, support and cooperation. I shall always remain grateful to him. I am grateful to Dr. Kumud Ranjan Jha, for his valuable guidance that helps me improving my work.

My sincere thank to Vice-Chancellor, Director and Academic Head, Dean (Academic and Research), Director, and Head ECE Department, Jaypee University of Information Technology, Solan for providing me all the needed support to complete this work. I sincerely thank to the members of DPMC committee, Dr. Pradeep Kumar, Dr. Shruti Jain and Dr. Nitin for their constructive feedback and valuable suggestions. I gratefully acknowledge Indian Space Research Organization vide Project No. ISRO/RES/4/579/10-11 for financial aid. I also sincerely thank to Shri Rajeev Jyoti (Head, Antenna System Group (ASG), Space Application Centre-Ahmedabad), Dr. K. Ganesha Raj (Deputy, Director RESPOND, ISRO Headquarter Bangalore), Smt. Ankita Patel (Sr. Scientific Assistant-A) and Shri Vikas Patel (Coordinator-RESPOND).

I give my greatest gratitude to my parents, who have been offering all round support during the period of my studies and research. It is the boundless blessings and endless sacrifice of my parents. They have shown immense patience and supported me in every possible way. I owe everything to them. I express my profound thanks to my husband, Divanshu Sharma for his unconditional love, support and patience throughout my research. I am heartily thankful to my parents-in-laws and sister-in-law, Megha for their faithful support during the final stages of this Ph.D. My words alone can never express my gratitude to them.

I would like to pay high regards to my Taya ji and Tayi ji for their motivation throughout my research work and lifting me uphill this phase of life. I would like to extend warm thanks to my brother Amit Kamal, Puneet Kamal and Saurabh Rattan for their love and care.

I also thank my friends (Saras, Shweta, Aastha, Keerti, Oshin and Neha) for bringing me laughter and encouraging me while I was depressed and stressed out throughout these years. I would like to thank all those people from the core of my heart who made this thesis possible.

In the last but not least, I thank the ultimate source of energy of every particle in the universe, the Almighty, for giving me enough energy and strength to complete the work.

(Garima Bharti)

PUBLICATIONS

JOURNALS

[1] Garima Bharti, K R Jha, G. Singh, and Rajeev Jyoti, "Azimuthally periodic wedge shaped metallic vane loaded circular ring frequency selective surface," *International Journal of Microwave and Wireless Technologies*, vol. 7, no. 1, pp. 95-106, 2015. http://dx.doi.org/10.1017/S1759078714000488

[2] Garima Bharti, K R Jha, G. Singh, and Rajeev Jyoti, "Angular stable, dual polarized and multiband modified circular ring frequency selective surface", *Frequenz: Journal of RF Engineering and Telecommunication*, vol. 69, no. 5-6, pp. 199-206, March 2015. DOI: 10.1515/freq-2014-0067

[3] Garima Bharti, K R Jha, G. Singh, and Rajeev Jyoti, "Design of angular and polarization stable modified circular ring frequency selective surface for satellite communication systems", *International Journal of Microwave and Wireless Technologies*, March 2015. http://dx.doi.org/10.1017/S1759078715000331

[4] Garima Bharti, K R Jha, G. Singh, and Rajeev Jyoti, "Design of dual polarized and angular stable new bandpass frequency selective surface in X-band", *Telecommunication System*, (Online) March 2015. http://dx.doi.org/10.1007/s11235-015-0012-y

[5] Garima Bharti, K R Jha and G. Singh, "A simple synthesis technique of single square loop frequency selective surface at terahertz frequency", *OPTIK: International Journal for Light Electron Optics*, vol. 125, no. 21, pp. 6428-6435, 2014. http://dx.doi.org/10.1016/j.ijleo.2014.08.009

[6] Garima Bharti, K R Jha, G. Singh and Rajeev Jyoti, "Design of azimuthally periodic wedge shaped circular ring bandpass frequency selective surface using transmission-line method", *Wireless Personal Communication,* (Accepted), June 2015.

[7] Garima Bharti, K R Jha, G. Singh and Rajeev Jyoti, "Planar tri-band frequency selective surface with transmission in S-band and reflection in Ka/Ku-band", *Radioelectronics and Communication System*, (Accepted), May 2015.

Under Review

[8] Garima Bharti, K R Jha, G. Singh and Rajeev Jyoti, "An overview of frequency selective surface for wireless communication perspective", *Telecommunication System* (Under Review) Jan. 2015.

[9] K R Jha, Garima Bharti, G. Singh and Rajeev Jyoti, "A novel synthesis technique with resonant constituting element for dual-polarized and angular stable bandstop frequency selective surface", *Electromagnetics*, (Under Review), Jan. 2015.

[10] K R Jha, Garima Bharti, G. Singh, and Rajeev Jyoti, "Dual-polarized and angular stable bandpass FSS structure with resonant constituting elements", International Journal of Circuit Theory and Applications, (Under Review) Jan. 2015.

CONFERENCES

[11] Garima Bharti, K R Jha, G. Singh, and Rajeev Jyoti, "Analysis of circular ring frequency selective surface at Ka/ Ku band," *Proc. of 3rd IEEE International Advance Computing Conference*, 22- 23 Feb, 2013, India, pp. 169-172. http://dx.doi.org/10.1109/IAdCC.2013.6514215

[12] Garima Bharti, K R Jha, G. Singh, and Rajeev Jyoti, "Circular ring frequency selective surface: a novel synthesis technique," *Proc. of 6th International Conference on Contemporary Computing (IC3-2013)*, Aug. 8-10, 2013, India, pp. 491-496. http://dx.doi.org/10.1109/IC3.2013.6612245

LIST OF FIGURES

LIST OF TABLES

ABSTRACT

Frequency selective surface (FSS) is an array of periodically arranged patches on the dielectric substrate/apertures in the metallic screen, which exhibits total reflection and transmission, respectively despite of the fact that the patch/aperture is just a small fraction of the total FSS area. It is the most relevant periodic structure, which finds various applications in microwave regime of the electromagnetic spectrum such as satellite communication, radio broadcasting, radomes, electromagnetic shielding, improving the purity of the received signal and enhancing the gain/directivity of the antenna. However, the electromagnetic behavior of the FSS structures is a function of frequency, angle-of-incidence (AOI) and polarization of the incident waves, which make it a potential candidate to use as spatial filters in variety of microwave applications such as radomes and satellite communication. The unit-cell geometry of FSS structure that is used in the microwave regime of the electromagnetic spectrum has to be very simple because the fabrication cost is an important issue. In the microwave regime of electromagnetic spectrum, the development of novel geometrical shapes of FSS structures is an attractive area for researchers. In addition to this, the miniaturization as well as angular and polarization stability of the structure are the potential issues. Therefore, it is required to design a FSS structure, which provides a stable bandpass/bandstop filtering characteristics over a wide range of AOIs and over different (perpendicular and parallel) polarization states.

However, in the wireless communication, the larger reflector antennas dimensions have been utilized to significantly enhance the signal received by antenna at the fixed operating frequency. The design and maintenance of such antennas are economically expensive as well its utilization for various applications is also a potential problem for research. Therefore, the demand of multiband FSS structures that allows the same reflector antenna to operate at two or more frequencies is increased. There are various techniques, which provide the multiband frequency characteristics such as layered/stacked, convoluted, perturbed and multi-resonant element technique. The layered/stacked planar FSS structure separated by a dielectric layer provides an added degree of freedom in designing a filter with multiple resonances in the desired frequency response. The layered/stacked FSS structures are difficult and costly to

construct, which increase its cost/complexity as compared to that of the single planar FSS structure. In addition to this, the numerical analysis of the layered/stacked FSS structure is very complicated due to the occurrence of coupling effects between the stacked FSS structures. The convoluted and perturbed FSS structures have required high degree of iterations, which are difficult to manufacture and the frequency response is sensitive to different polarization states of the incidence wave.

In this thesis, the state-of-the-art of FSS structure and its potential applications (mainly in wireless/satellite communication) are also overviewed. In addition to this, the FSS structures have been numerically analyzed using the equivalent circuit (EC) technique, which is further supported by using the commercial simulators such as CST Microwave Studio, Ansoft HFSS and Ansoft Designer. The EC technique is simple and has the potential of providing the better understanding of physical mechanism of the FSS structure and models the FSS structure in terms of energy storing inductive and capacitive components in series or parallel combination at the resonance frequency depending on the element shape. This thesis discusses the analytical, simulation and experimentally tested performance of the newly proposed FSS structure in the microwave regime, particularly S-, Ku- and Ka-band of the electromagnetic spectrum. Moreover, a generalized synthesis technique to obtain the geometrical parameters of single square loop FSS (SSLFSS) structure using its normalized mathematical expressions has been developed. However, the design of FSS structure becomes significantly easier with the knowledge of relationship between geometrical parameters (periodicity, shape, width (strip/slot) and size) of the FSS structure. The numerical analysis of the SSLFSS is extended to obtain the geometrical parameters of the novel modified circular patch/slot type FSS structure designs. In addition to this, the analysis and simulation of the circular ring FSS structure also has been explored to achieve the better angular stability than that of the SSLFSS.

With reference to the simple unit-cell geometry of FSS structure, the resonance mechanism and reflection/transmission characteristics of proposed modified circular ring single layer FSS geometries comprising patch/aperture element, which offer significantly better angular (up to 50^{o}) and polarization (perpendicular and parallel) stability as compared to that of the various reported FSS structures are examined in

detail. In this thesis, a novel (modified circular ring) FSS structure for the bandstop and bandpass filtering characteristics with significant miniaturization and angular/polarization stable frequency response is explored at 26 GHz and 13.5 GHz with approximately 15% fractional bandwidth (FBW). In order to demonstrate the practicality of the proposed modified circular ring FSS structure, we have experimentally measured the s-parameters of the proposed FSS structure at X-band, which provides the comparable frequency response as compared to that of the simulated response.

Further, two simplified and light weight multi-resonating FSS structures (patch/slot), which provide multiband frequency characteristics, have been discussed. A single layer multiband slot-type FSS, which consists of a modified circular ring loaded with concentric conventional circular ring, is discussed for the angular and polarization stability with reflection characteristics in S-band (2-4 GHz)/K_u (12-18 GHz) and transmission characteristics in X-band (8-12 GHz)/K_a-band (24-28 GHz). The resonance frequency of the slot-type multiband FSS structure downshifts with 0.093 % and 0.74 % in the 1^{st} and 2^{nd} transmission band, respectively for perpendicular polarized wave incidence. In addition to this, the resonance frequency downshifts with 0.096 % and 0.76 % in the 1^{st} and 2^{nd} transmission band, respectively for the parallel polarized wave incidence up to 50^{o} AOI with reference to the normal incidence. In addition to this, a patch-type multiband FSS structure, which consists of two concentric modified circular rings, is discussed for the angular and polarization stable frequency response at S/Ka and Ku-band of the electromagnetic spectrum. The resonance frequency of the patch-type multiband FSS structure downshifts with 0.367% and 0.93% in the 1^{st} and 2^{nd} transmission band, respectively for perpendicular polarized wave incidence. In addition to this, the resonance frequency downshifts with 0.234% and 0.673% in the 1^{st} and 2^{nd} transmission band, respectively for the parallel polarized wave incidence up to 50^{o} AOI with reference to the normal incidence.

Furthermore, an azimuthally periodic wedge shaped circular ring FSS structure for the bandstop and bandpass filtering characteristics with significant 3-dB/fractional bandwidth and angular/polarization stability at S-band, Ku-band and Ka-band is discussed. The azimuthally periodic wedge shaped circular ring bandstop FSS

structure provides the 0.4% downshift in the resonance frequency for wave incidence up to 50^{o} AOIs as compared to that of the normal wave incidence at Ku-band. In addition to this, an azimuthally periodic wedge shaped circular ring bandpass FSS structure provides 0.013% and 0.198% shift in the resonance frequency for the perpendicular and parallel polarized wave incidence up to 50^{o} AOI, respectively as compared to that of the normal wave incidence at Ku-band.

Finally, a generalized mathematical expression for the synthesis of geometrical parameters of SSLFSS structure is presented. In addition to this, a method to control the reflection coefficient of FSS structure at a given frequency is proposed. Moreover, in this thesis, novel geometrical shapes of FSS structures have been proposed, which provide single and multiband frequency response with significant angular and polarization stability in the microwave regime of the electromagnetic spectrum. The proposed modified circular ring FSS structure (for single-band frequency response) provide 1.09 % and 0.07 % downshift in the resonance frequency for perpendicular and parallel polarized wave incidence up to 50^{o} AOI as compared to that of the normal wave incidence as well as approximately 15% FBW. However, the multiband frequency response with significant angular and polarization stability is presented using the proposed FSS structure, which provides transmission in S-band and reflection in Ku/Ka-band for satellite communication.

The frequency response of the proposed modified circular ring bandpass FSS structure is measured for the normal wave incidence only, which will be extended to study the effect of the AOIs and polarization states of the incidence wave in future. In addition to this, the experimentally measurement of the scattering characteristics of the multiband FSS structure has also been considered for the future perspective. Moreover, the design issues of the conformal FSS structure and exploiting the bandpass/bandstop behaviour of the FSS structures at terahertz frequencies will be considered in future communication.

TABLE OF CONTENTS

CHAPTER-1

INTRODUCTION

1.1 OVERVIEW OF FREQUENCY SELECTIVE SURFACE

The frequency selective surface (FSS) structure is an array of periodically arranged metallic patches on a dielectric substrate or slots in the metallic screen, which behaves as a spatial filter to the electromagnetic waves and offer selectivity in frequency, angle-of-incidence (AOI) and polarization of the incident waves [1]. The FSS can be classified as high-pass, low-pass, bandpass and bandstop filter. These features make them suitable to control the propagation of electromagnetic energy and therefore, they can be employed in radomes, Cassegrain sub-reflector, diffraction gratings, frequency scanned antennas, microwave absorbers and recently in applications associated with security and efficiency of the wireless network communications [1-11]. As, Sinclair [12] has realized that the antennas placed on the aircraft provide significant scatterers, however, it is required to control the radar cross-section (RCS) of the antenna, which is significantly accomplished to an extent by using the FSS structure [13]. The basic principle underlying the physics of FSS structure is directly been evolved from the investigation of diffraction gratings in optics, which is used to decompose a beam of non-monochromatic light into its spectral orders. However, the study of FSS structures and their interaction with electromagnetic waves received potential attention in the mid-1960s. In addition to this, there are many literatures, which had been reported from 1919 to the famous Marconi and Franklin reflector for use in wireless telegraphy and telephony [1]. The patch- and slot-type FSS structures ideally exhibit total reflection and transmission, respectively, in the neighbourhood of the fundamental resonance frequency. The type of element geometry, size, inter-element spacing, dielectric substrate parameters and presence or absence of superstrate, which constitutes the unit-cell element, determines the overall resonance frequency, bandwidth and dependency on the AOI as well as polarization of the planar incoming wave. Therefore, in order to design a FSS structure for a desired frequency response, the appropriate selection of geometrical parameters is of prime importance because these parameters have potential to significantly vary the frequency response. The

unique characteristics and practical significances of FSS structures realized over many years have offered an extensive work both in academia and industrial sectors.

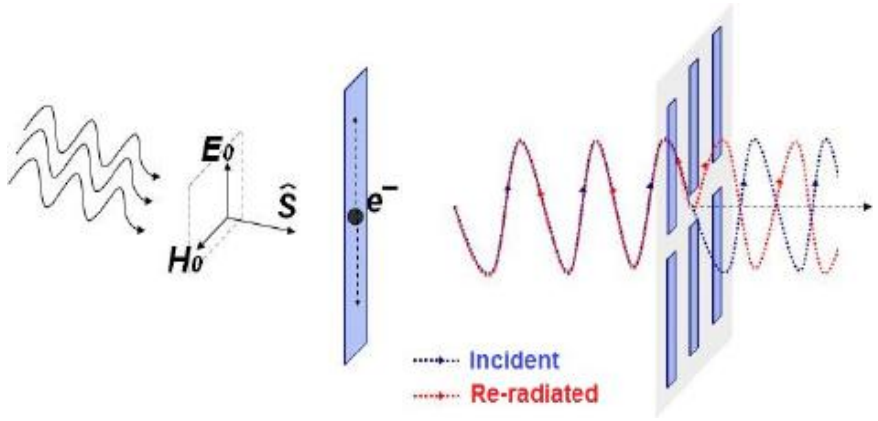

(a)

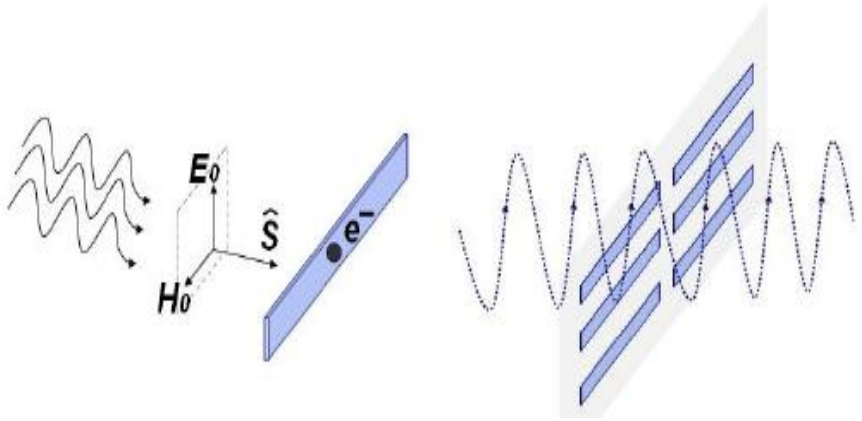

(b)

Fig.1.1 The basic filtering mechanism of FSS structure for E-vector (a) parallel and (b) orthogonal to the metallic dipole [14].

In order to understand the physical mechanism of the FSS filtering characteristics, two scenarios of the plane wave incidence on a metallic dipole FSS structure is presented as shown in Fig. 1.1. In the first scenario, a plane wave impinges on a metallic dipole FSS structure in such a way that the FSS structure is orthogonal to the Poynting vector and electric field vector is oriented along the length of the dipole as shown in Fig. 1.1(a) [14]. The electric field vector oscillates the electrons due to which a portion of incidence plane wave energy is transformed into kinetic energy and gives rise to re-radiated waves/energy. These re-radiated waves on the right side of the FSS structure results in the cancellation of the incidence plane wave, which are

on the left side of the FSS structure. In addition to this, the re-radiated waves on the left side of the FSS structure refer to as the reflected wave and this scenario result the low transmittance through the FSS filter [15]. In the second scenario, the electric field vector is orthogonal to the parallel metallic dipole FSS, which is shown in Fig. 1.1(b) [14]. In this case, the electrons do not re-radiate because of their inability to oscillate up and down. Therefore, the FSS structure remains invisible to the incidence plane wave and total transmission occurs or transmittance will be higher [15].

1.2 NUMERICAL TECHNIQUES FOR ANALYSIS OF FSS

In the computation of electromagnetic fields scattered by the FSS, several numerical methods are used. Various researchers have analyzed the reflection and transmission characteristics of different FSS structures through numerical techniques and validated the results through experimental measurements. However, all the numerical techniques are based on the well established Maxwell's equations and in general, these techniques are unable to provide exact solutions of the electromagnetic problem rather offer approximate solutions of sufficient accuracy. In the last five decades, various numerical techniques such as plane wave expansion method [16], spectral-domain Galerkin method [17, 18], method-of-moment (MoM) [19], finite methods (finite-difference-time-domain (FDTD) method [20, 21]/finite-element method (FEM) [22]) and equivalent circuit (EC) [23] method have been discussed to investigate the scattering characteristics of different FSS structures. Among the above mentioned numerical techniques, MoM, FDTD, FEM and EC technique are the most widely used numerical techniques. However, the MoM, FDTD and FEM are the computational intensive techniques and EC technique is comparatively simpler one. The selection of optimal technique for numerical modeling of FSS structure remains open. In this Section, we have discussed the state-of-the-art of different numerical techniques, which are available for the simulation of electromagnetic problems associated with the FSS structures.

The MoM technique investigated the scattering characteristics of the FSS structure in the frequency domain. The numerical modeling of FSS structure using MoM is initially discussed by Chen [24], which evaluates the current flowing on the metallic pattern by matching the tangential field at the surface of the unit-cell element and forms the integral equation for the unknown current. Further, the unknown electric

field depends upon the unknown current near the metallic pattern, which is expanded into a set of Floquet modes and by satisfying the boundary conditions on the surface of the metallic pattern, an integral equation for the unknown current is obtained. At the final stage, the MoM is used to reduce the integral equation into a set of linear algebraic equations. Earlier, the approach discussed by Chen [24], is referred as the integral equation approach. The generalized steps to solve the scattering problem using MoM method are:

1) Expand the unknown function in terms of a set of N basis function with unknown coefficient,
2) Enforce boundary conditions of the problems to generate a linear system of N equations, and
3) Solve the linear system of equations for unknown coefficients.

Thereafter, various researchers have discussed the different advancements in the MoM method to reduce its computational complexity [25-29]. The MoM approach has the potential to evaluate the scattering characteristics over a wide range of AOIs, however it is usually restricted up to periodic FSS structures, which have supported homogeneous dielectric substrate.

In order to investigate the complex FSS structure, which are backed with inhomogeneous dielectric substrate, the FDTD and FEM approach comes out to be an effective numerical tool [30]. These two methods come under the category of finite methods.

The FDTD technique investigates the scattering characteristics of FSS structure in time domain and covers a wide frequency range in a single simulation run. This technique is a direct solution of Maxwell's time dependent curl equations [31]. The steps to solve the scattering problem using FDTD are:

1) Breakdown the solution region into grid of nodes such as dividing the solution region into two different grids of nodes, one for the calculation of magnetic field and the other for the calculation of electric field,
2) Approximating the given differential equation by finite difference equivalent that relates the dependent variable at a point in the solution region to its values

at neighbouring point such as the value of magnetic field at an instant is calculated by the electric field at previous grid points, in other words, the electric field is solved at a given instant in time, then the magnetic field is solved at the next instant in time and so on [32], and

3) Solving the difference equations subjected to the prescribed boundary/initial conditions [33, 34]. In addition to this, various other scientists have discussed the numerical modeling of different FSS structures using the FDTD as discussed in [35-37].

The FEM technique investigates the scattering characteristics of different FSS structures in frequency domain and initialize with the partial differential equation form of Maxwell's equation. The generalized steps for the scattering problem using FEM technique are:

1) Discretize the solution region into finite number of sub regions and corner of each sub-region is called as node. In the first step, this method determine the field quantities at these nodes,

2) Derive governing equations for a typical sub region,

3) Integrating all sub-regions over the entire geometry, and

4) Solving the system of equations obtained from above steps.

The technical advancements in the FEM are discussed by various researchers as discussed in [38-40].

In comparison to the aforementioned numerical techniques, which are computationally intensive, the EC technique provides a simpler method to investigate the scattering characteristics of the different FSS structures. The EC technique is based on the transmission line analogy, where the EC parameters of a FSS structure is obtained due to the inductive and capacitive behavior of its geometrical parameters as discussed by Marcuvitz [41, 42]. This technique is a scalar technique due to which the modeling is limited upto linear polarizations and simple FSS geometries only. However, the dielectric substrates parameters and AOIs have been taken into account in the EC equations and the accuracy of the technique depends upon the assumptions made in the analysis. Various researchers have analyzed the different FSS structures

such as square loops [43-45], circular ring [46], dipoles [47-49] and Jerusalem cross [50] using EC technique. However, the EC technique provides the less precise analysis as compared to that of the other numerical methods rather offer better physical understanding of the filtering behaviour of the FSS structures, therefore, the EC technique is chosen as the analysis tool for this research. In addition to this, the EC technique provides the significantly accurate analytical response for this research, and most importantly it instantaneously characterizes the FSS structures with varying geometrical dimensions of the unit-cell element. Moreover, for the modeling of an infinite periodic FSS structure, the numerical methods such as MoM, FDTD and FEM require considerable computer resources and results complex computation, rather the EC technique require little computer resources and still offer an significantly accurate response. Due to these significances, the different FSS structures have been analyzed using EC technique in this thesis.

Earlier due to the lack of resources, a narrow range of electromagnetic problems associated with the FSS structures have been investigated by the researchers. However, the technical advancements in the computer techniques have revolutionized the way in which the electromagnetic problems have been analyzed. Therefore, majority of antenna and microwave engineers rely heavily on the computer methods to analyze and design the novel FSS structures. Various commercial electromagnetic simulators are available, out of which more commonly employed are CST Microwave Studio [51], Ansoft HFSS [52] and Ansoft Designer [53], which are based on finite integral technique, FEM and MoM, respectively. In this thesis, the numerical frequency responses have been validated through the simulation responses, which have been achieved CST Microwave Studio, Ansoft HFSS and Ansoft Designer. On the other hand, the experimental measurements offer the most realistic and reliable examinations of the scattering characteristics of FSS structure. However, the experimental measurements of the scattering characteristics require the prototyping of FSS structure, which is an expensive, time-consuming and inflexible method. Despite these issues, the experimental measurement of FSS structure is of significant importance because it offers the most realistic and reliable investigation of scattering characteristics of the FSS structure.

1.3 RELATED WORK

The FSS structures offer various applications in microwave, optical wave and terahertz regime of the electromagnetic spectrum [54-62]. The FSS structure is used to mitigate the interference, improve the gain/directivity of an antenna, and design the radome in the microwave regime of the electromagnetic spectrum. In addition to this, these structures provide potential applications in the satellite communication where it is required to maintain the purity of the signal in the specific band and to control the scattering characteristics of the signal to the desired level [63, 64]. The FSS structures have been used as polarizer, beam splitter and solar-energy collector in the optical wave regime and offer applications in imaging, sensing and communication in the terahertz regime of electromagnetic spectrum [65, 66]. However, for the significant functioning of FSS structures in microwave applications, these structures must provide a frequency response, which is close to the ideal filter's frequency response and must be stable to the wide range of AOIs and different polarizations of the incidence wave. However, the complete knowledge of reflection and transmission characteristics at the periodic array face is very essential to achieve the aforementioned frequency characteristics. Therefore, in this section, we have discussed the circuit parameter characterization to achieve the desired frequency response and the effect of AOIs/polarization of the incoming wave on the frequency response of FSS structure. Further, in the context of aforementioned performance requirements, the following sub-sections discuss the frequency characteristics of two dimensional FSS structure for single and multiband frequency characteristics through number of design examples.

1.3.1 CIRCUIT PARAMETER CHARACTERIZATION

There are various well established numerical techniques as discussed in Section 1.2 to analyze the different FSS structures. In this sub-section, we have discussed recent advanced numerical methods, which have been used for the analysis of different FSS structures. Kristensson et al in [67] have discussed the dielectric (bianisotropic material) backed FSS structure using the improved MoM, which also provide the integral representation of electromagnetic fields outside the dielectric slab. The MoM is used to obtain the unknown current on the FSS and from this current quantity, other parameters have been calculated. However, to design the FSS structure, the relevant

parameter selection process depends on the trial-error method and nature-inspired population based methods such as the genetic algorithm (GA) and particle swarm optimization (PSO), which demands the pattern of periodic structure and the parameters of the fixed pattern, need to be determined. In this view, Li et al [68] have integrated GA, used for optimization with fast full-wave numerical methods. In [69], the PSO has been used to adjust the geometrical parameters such as element size and spacing of the square loop FSS structure for the desired features and further the EC technique has been used for the analysis. For implementing PSO, first revisit the derivation of the EC formulation and then an objective function, which is based on the transmission coefficients at various frequencies at the pass/stop-bands, is defined. In PSO, instead of using a totally-chance oriented trial-error method, a multi-dimensional search operation is performed systematically by means of swarm intelligence. Dubrovka et al [70] have proposed a new general EC approach for a thin FSS, which is valid for any AOI and for any lattices, known as modal decomposition EC model (MDECM). This method is based on determining the admittances that relate the voltage and current intensity amplitudes for any incident Floquet mode and is achieved by studying the interaction of the plane waves of arbitrary AOI with the structure. Since, the general formulation of the method is very complex, so an approximate (testing) function for the aperture field is used to produce relatively simple circuits that can approximate the true admittance of the frequency selective surface and accuracy of the procedure depends upon the choice of the testing function. In order to validate the method, a theoretical study of the method has been considered using the ring slot and rectangular slot elements as test elements and the results of theoretical analysis are comparable with the computational electromagnetics (CEM) simulation. This method exhibits higher accuracy compared with conventional EC approaches and provides a better understanding of operation of FSS and potentially allows the synthesis by optimization of the circuit parameters, however, this method becomes rigorous for the highly complex structures such as Jerusalem cross. Sung et al [71] have implemented FSS-wall, which filter out undesired interference and accordingly improve the wireless system performance. Moreover, the scattering performance of FSS-wall is investigated using the EC modelling, which provides the comparable frequency response with the measured results. A dielectric backed FSS

structure, which provides compact (half of the original size) spatial band-pass filtering characteristics, is designed using GA and analyzed using the EC approach [72]. However, the designing approach discussed in [72] is only valid for normal wave incidences. In [73], a novel EC model using the GA is proposed to optimize the square loop FSS parameters for the desired transmission/reflection response effectively. The fitness function of GA is defined with the help of the EC model and a significantly short simulation time is achieved as compared to that of the GA without EC model. Various researchers have discussed different other novel numerical techniques such as Su et al [74] have analyzed the arbitrary shape patch/aperture FSS array using spectral domain integral equation method with Ewald transformation, which accelerates the computation. In order to further reduce the computation time, the lattice symmetry is introduced which reduce the number of unknown functions and linear equations [74]. The scale changing technique and finite element technique is compared for the analysis of finite size and thick FSS and reveals that the computation time in the scale changing technique significantly very less as compared to that of the FEM [75].

1.3.2 ANGULAR STABILITY

However, the resonance frequency of the FSS structure depends on the AOIs and polarization states of the incidence wave [76, 77] and there are various ways to reduce its dependency such as through the reactive loading of the dipoles, which is discussed in [78]. In [79], Xu et al have demonstrated angular insensitivity and narrow band transmission using capacitive loaded ring slot FSS structure, which is miniaturized to 0.082λ. The FSS structure discussed in [79] is placed in a Faraday cage structure created by a row of metallic substrate to eliminate the undesired coupling between the unit-cells. In order to improve the frequency response of the FSS structures in terms of the angular sensitivity, cross-polarization, reflection/transmission bandwidth and band-separation, several researchers have investigated the loaded (active/tunable, passive) FSS structures [80-83]. In addition to this, in [84], an active loaded FSS has been designed using PIN diodes between the FSS elements as well as DC magnetic biasing has been performed with ferrite substrate to ensure the loading effect, which tune the resonant frequency over a wide range and also switch the frequency response. In [85], the loading has been achieved through the varactor diodes which act as

capacitive loading in the ring and makes the FSS structure tunable. Mias [86] has been achieved loading through the surface mount reactive lumped element, which shifts the bandstop frequency from higher to lower value and vice-versa. However, these types of the structures are difficult to fabricate because of the complexity and cost of fabrication. In [87], the passively loaded slot elements have been discussed to achieve the dual band FSS structures, which significantly improve the bandwidth. In [88], a short-length (less than $\lambda/2$) loaded dipole FSS array, which provide unity reflection/transmission coefficient over a narrow bandwidth and is nearly independent up to 65^{o} AOI at desired frequency is achieved. The angular independence is achieved because the mutual impedance of short-length loaded dipole is less than the self impedance, which reduces the coupling effect between the scattering elements. Shaker and Shafai [89] have discussed the angular sensitivity of square patch elements surrounded by square short or open circuited conducting square rings. The angular sensitivity of the open and short square ring without the central square patch is discussed and demonstrated that the open ring is more angular stable [89]. In addition to this, loading of open and short square ring with the square patch further improves the angular stability. It is also been demonstrated that due to the asymmetrical geometry, the single layered open circuited square ring loaded with central square patch is not suitable for dual/circular polarization [89]. On the other hand, the short circuited square ring provides higher angular sensitivity while placed on a single layer substrate [89]. Further, a double-layer shorted ring FSS array, which provide an angular stable FSS structure for the certain separation of the dielectric layer is discussed [90]. Ghaffer et al [91] have discussed the angular stability of square loop FSS structure loaded with four PIN diodes across the aperture at 90^{o} intervals up to $\pm 45^{o}$ AOIs. Another tunable circular ring, split ring and convoluted ring FSS structures loaded with varactor diodes and surface mount resistors, which provide independent tuning for vertical and horizontal polarizations is discussed [92].

As discussed in section 1.2, there are various numerical techniques, which are discussed in reported literature however the synthesis technique, which is used to obtain the geometrical parameters of the FSS structure is also of significant importance. In view of this, we have discussed a generalized synthesis technique of single square loop FSS (SSLFSS), which provide the potential to meet the specific

resonance and bandwidth requirements. With the consideration of the angular and polarization stability taken into account, in this thesis, the novel FSS structures have been discussed, which are simple and provide significant angular and polarization stability.

1.3.3 MULTIBAND PERFORMANCE

Various researchers have discussed the different ways of achieving multiband characteristics in FSS structures, which accomplish these structures as the highly effective communication devices. However, to fulfil the increasing demand of multifunctional antennas/filters for the advanced communication systems, for example, the multi-functional sub-reflectors for satellite communication, there is need to develop multiband FSS structures [93-104]. FSS structures have widely used as sub-reflectors for the satellite communication in which a single main reflector share the different frequency bands and to increase the capabilities of multifunction and multi-frequency antennas, a subreflector equipped with FSS structure is required to operate at multi-frequency bands. In order to achieve the multiband frequency response, there are various available approaches such as layered/stacked FSS [105, 106], fractal/convoluted FSS [107-111], perturbation of a single-layered FSS [112], multi-resonant element FSS [113-116], and combination of these approaches [117, 118]. Initially, the layered/stacked FSS structures have been employed to provide the multiband frequency characteristics, which offer significant frequency response over a wide range of AOIs and different polarizations of the incidence wave. However these structures are complex, heavier, larger in volume and expensive, which are not suitable from practical perspectives [105, 106]. Further, the fractal/convoluted FSS structures have been explored, however these require high degree of iterations and are difficult to manufacture [107-111]. However, Werner and Lee [109] have discussed the three- stage design methodology to obtain the fractal crossbar tree based FSS structure, which provides the dual polarized (TE and TM) tri-band frequency response and may have further extended to achieve the multi-band frequency response. Ohira et al [110] have designed a single layer fractal FSS structure using micro-GA, which offer significant close reflection band separation and bandwidth as compared to that of the convoluted double square loop FSS structure. Further, Chiu and Wang [111] have presented a FSS structure with four symmetrical patterns of metallic meander

lines with a central patch, which is printed on only one surface of a substrate for the different polarization states and up to 60^{o} AOIs. The FSS structure discussed in [111] provides a dual-band frequency response, closely spaced bands of operation, miniaturization of ~ 8% of the free-space wavelength at the first resonance frequency and ~ 1.4 band separation. Hill and Munk [112] have designed a single layer dual-band FSS using the perturbation technique, whose frequency response is sensitive to different polarization states of the incidence wave. However, for the satellite communication applications, a simplified design, low profile, lighter in weight FSS structure is the prime demand, which is satisfied using the FSS structure with multi-resonant elements [113-116]. Parker et al [113] have discussed the concentric ring FSS, which is largely sensitive to the AOIs. Huang et al [114] have discussed a dual-layer (single and double screen) circular ring FSS structure has been discussed, which reflects X-band frequencies as well as transmits the S-band/Ku-band frequencies and results in a complex tri-band FSS structure. It has also been demonstrated that the double-screen panel of this FSS design that is backed with high dielectric constant material provides the lower transmission loss at S-band and wider reflection bandwidth at X-band than the single-screen panel [114]. Wu [115] has discussed a multiband (reflect Ka-band signal and transmit S-band/X-band/Ku-band signals) double square loop FSS with two dielectric layers, which are separated by a honey-comb and provides a complex FSS structure. Wu and Lee [116] have discussed a three layer FSS with circular concentric non-symmetric rings, which provide the similar frequency response as discussed in 115]. On the other hand, Delihacioglu et al [119] have discussed the angular and polarization behavior of dielectric backed L-shaped and one-turn helix shape FSS structure up to 60^{o} and 45^{o}, respectively for the perpendicular and parallel polarized wave using modal expansion method. The numerical frequency response of the FSS structure is comparable as compared to that of the measured frequency response. In [120], the scattering characteristics (reflection/transmission) of bandstop triangular FSS structure for the perpendicular and parallel polarized wave incidence up to 45^{o} are discussed. In addition to this, the results demonstrated in [120] reveal that the equilateral triangular conducting element/ isosceles triangular conducting elements exhibit same filtering properties as compared to that of the reported FSS structures.

With the consideration of aforementioned issues into account and to achieve simplified, low profile, lighter weight and spectral efficient multiband FSS in terms of angular and polarization (horizontal and vertical), we have proposed single layer novel multi-resonant FSS structure, which provide the bandstop and bandpass filtering characteristics as discussed in Chapter-5.

1.4 FACTORS AFFECTING THE FSS FREQUENCY RESPONSE

There are various factors, which govern the performance of the FSS structures, out of which the critical factors are:

A) Shape and parameters of element,
B) Dielectric substrate parameters,
C) AOIs and polarizations of the incidence wave, and
D) Element conductivity

1.4A SHAPE AND PARAMETER OF THE ELEMENT

The shape of FSS element has the potential of providing the desired frequency characteristics [121]. The FSS structure is composed of a metallic pattern, which is placed on a dielectric substrate and the choice of the metallic pattern depends upon the type of the application to which it has been used. The shape of the metallic pattern is unconstrained, however Munk [2], has categorized the shape of the metallic pattern of the FSS structures into four basic sections such as:

1) **Centre connected or N-pole type:** simple straight element, three legged element such as dipole, tri-pole, cross dipole, anchor element and Jerusalem cross.
2) **Loop type:** square, circular and hexagonal loop.
3) **Solid interior type:** also referred as patch type elements such as square meshes and circular patches.
4) **Combination type:** achieved through the combination of the aforementioned three types, this list is endless.

Fig. 1.2 shows some of FSS elements from these four categories. Each shape of the FSS element has its own merits and demerits depending upon the applications such as some of the geometrical shapes (dipole, cross-dipole and tri-pole) are more angular

sensitive, on the other hand allow a rapid transition between pass and stop bands. In addition to this, Jerusalem cross offer significantly wide operating bandwidth, on the other hand offer more polarization sensitivity. As, the different shapes of FSS structures have been reported in the literature, however, it is noted that the square loop and circular ring FSS structures are the potential candidates to be used as spatial filter in the satellite communication applications among the aforementioned shapes of the FSS structures [1] due to their structural simplicity and potential to offer better performance in terms of frequency selectivity, angular/polarization stability, bandwidth and band separation. Therefore, in this thesis, we have discussed the scattering characteristics of the SSLFSS structure. In addition to this, to achieve the specific frequency characteristics from the chosen shape of the FSS structure, the geometrical parameters such as periodicity (p), size (d), width of the patch/slot (w) and inter-element gap (g) of the FSS structure need to be well optimized. The reported studies have been suggested that the location of the resonance frequency of a FSS structure depends upon the size, periodicity and width of the conducting strip, in addition to this, the angular sensitivity depends upon the inter-element gap [2].

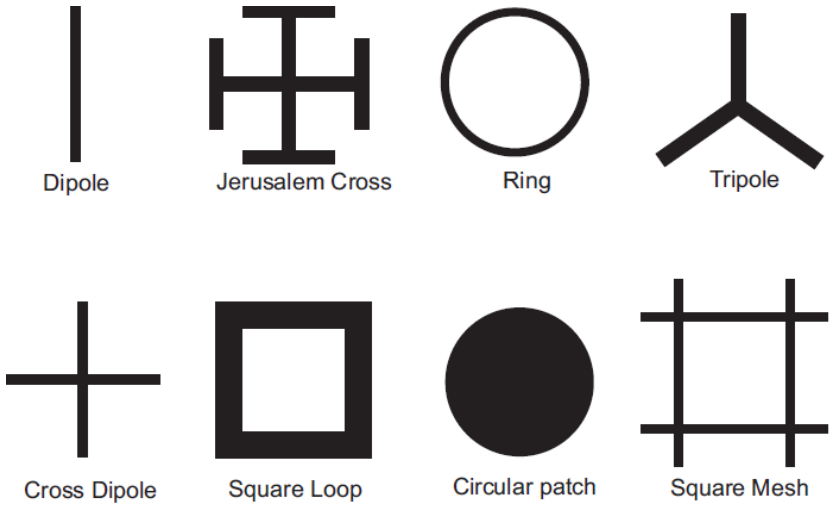

Fig. 1.2 The common FSS element shapes [2].

1.4B DIELECTRIC SUBSTRATE PARAMETERS

In the FSS structure design, the dielectric substrate not only provides the mechanical strength to the structure rather provide the angular stability [122-124]. The effect of

the dielectric permittivity and thickness of the dielectric substrate on the resonance frequency of FSS structure is interrelated. The dielectric substrate is categorized as:

1) Thick dielectric substrate

The substrate thickness is greater than the $0.05\times\lambda_o$, where λ_o is the operating wavelength. In this case, the resonance frequency (f_r) of the FSS structure downshifts by a factor of $\sqrt{\varepsilon_{eff}}$ from the original resonance frequency, where ε_{eff} is the effective dielectric permittivity of the FSS structure and is equal to the $(\varepsilon_r+1)/2$; if the FSS structure is attached to only one side of the dielectric substrate (in this case, dielectric permittivity of air is used, which is equal to 1) otherwise replaced by the dielectric permittivity of the other material (if FSS is sandwiched between the dielectrics).

2) Thin dielectric substrate

The substrate thickness is less than the $0.05\times\lambda_o$, where λ_o is the operating wavelength. In case of the thin dielectric FSS structure, the higher order evanescent modes, which are excited by the metallic pattern, remain significant at the air-dielectric boundary also. These higher order evanescent modes alter the storage energy near the FSS elements and vary the resultant resonance frequency, which results in a complicated modeling of the structure. In addition to this, the effect of the loss tangent is negligible on the resonance frequency of the FSS structure.

1.4C AOIs AND POLARIZATIONS OF THE INCIDENCE WAVE

1) EFFECT OF AOIs

When a plane wave impinges on the FSS structure at an oblique angle, the width of unit-cell metallic pattern and the inert-element gap between the unit-cells is reduced by a factor of $cos\theta$, where θ is the incidence angle as shown in Fig. 1.3 [125]. Therefore, the geometrical parameters of the FSS structure at the oblique incidence differ from the scenario of the normal incidence, which also varies the scattering characteristics of the FSS structure [126-128]. In this thesis, we have discussed the effect of different AOIs on the resonance frequency of SSLFSS structure by EC technique, which determine the equivalent inductive and capacitive behaviour of SSLFSS structure as a function of θ [42, 129]. For practical scenario, the plane waves are incidence on the FSS structure at different angles and the structure performance is

dependent on the angular sensitivity. Therefore, reducing the angular sensitivity of scattering characteristics of the FSS structure is being the current topic of research [130-132].

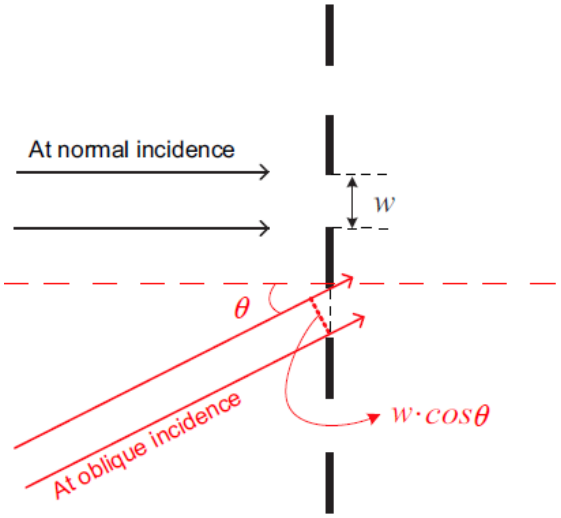

Fig. 1.3 The effect of oblique angle incidence on the geometrical parameters of FSS structure [125].

2) EEFECT OF POLARIZATION STATES

The scattering characteristics of FSS structure is also a function of polarization state of the incidence plane wave. In this thesis, we have mainly focused on the two polarization scenarios, such as perpendicular and parallel polarization. Considering the EC technique into account, we have demonstrated these two polarization state scenarios for the SSLFSS structure. As we have already discussed the basic filtering mechanism of the FSS structure, in this section, we will discuss the filtering mechanism of SSLFSS structure using the EC technique.

a) Perpendicular wave incidence

For the perpendicular polarized wave, the electric field is perpendicular to the plane of incidence as shown in Fig. 1.4(a) [125]. When perpendicular polarized wave incidence on the SSLFSS structure, the electric field vector, which is parallel to the vertical metallic strip, causes the electrons to oscillates due to which the surface current flows and results an inductor. In addition to this, the electric field vector, which is perpendicular to the horizontal metallic strip, represents a capacitor due to the separation of charges over the surface of the metallic conductor.

b) Parallel wave incidence

In parallel polarized wave, the electric field vector is parallel to the plane of incidence as shown in Fig. 1.4(b) [125]. When parallel polarized wave incidence on the SSLFSS structure, the electric field vector, which is parallel to the horizontal metallic strip, causes the electrons to oscillates due to which the surface current flows and results an inductor. In addition to this, the electric field vector, which is perpendicular to the vertical metallic strip, represents a capacitor due to the separation of charges over the surface of the metallic conductor. The patch type SSLFSS structure is represented as the single series LC circuit shunted across the transmission line of the characteristics impedance (Z_o). In both the polarization states, the electric field vector is polarized parallel to the conducting strip, which result an inductive component, however, the currents induced on the conducting strip due to the oscillations of electrons are different when plane wave incidence at oblique angles. This is because in the perpendicular-incidence wave scenario, the electric field vector is always parallel to the strip and excites the full length of each conducting strip irrespective of the incidence angle and in parallel-incidence wave scenario, the electric field vector arrives obliquely to the broadside of the strip, resulting in a shorter projected conducting strip length as the incident angle increases. The variations of the scattering characteristics of FSS structures with different AOIs and polarizations are undesirable and a FSS structure with significant angular as well as polarization stability is required for the various applications [133-136].

1.4D ELEMENT CONDUCTIVITY

When a FSS structure is illuminated by a plane wave, the surface current induced on the conducting metallic pattern. These induced currents reradiate the electromagnetic waves from the metallic pattern in the same way as the conductive strips inside a rectangular waveguide [137]. In case of the perfect electric conductor (PEC) metallic pattern, the SSLFSS structure is represented as series combination of inductor (L) and capacitor (C) using EC technique. On the other hand, for a lossy metallic pattern, the power dissipation occurs, which affect the overall frequency response of the FSS structure and alters the equivalent circuit representation of the SSLFSS structure, which has a resistor (R) in series with the L and C component. The resistive

component in the EC reduces the degree of attenuation in the bandstop FSS structure [138]. In this thesis, we have used aluminium (Al) and copper (Cu) as metallic patterns because these are easily available, economic and offer low conductor losses (high conductivity). However, the silver paint (95% silver) offers superior FSS performance with inexpensive production cost as compared to that of the other conducting materials (Al and Cu), however the silver paint itself is opaque and to ensure adequate transparency, the metallic pattern width must be kept very thin, which arises the fabrication issues [139].

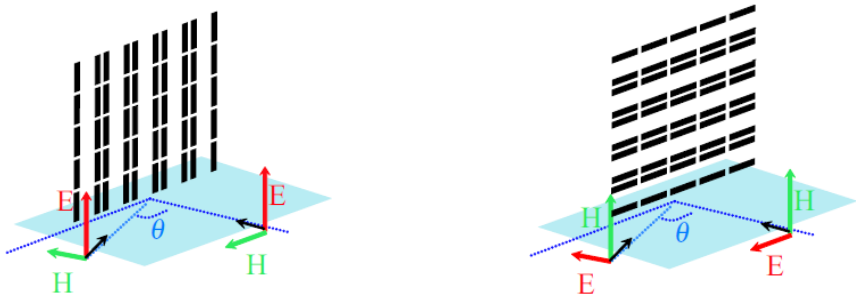

(a) (b)

Fig. 1.4 The inductive components of FSS structure with (a) perpendicular and (b) parallel polarized wave incidence [125].

1.5 MOTIVATION

The satellite communication is basically the communication of the satellite in space with large number of earth stations. The baseband signals are being generated by the users which are processed at the earth station and then transmitted to the satellite through the antennas. A satellite communication system operates in the microwave frequency band ranges from 1 GHz to 40 GHz. In the past decade, new and demanding satellite applications have been evolved, which leads to spectral congestion of the conventional frequency bands such as L (1-2GHz), S (2-4GHZ) and C (4-6GHz), allocated for satellite services [140]. There have been recent developments in the satellite industry including the provision of direct-to-home (DTH) services by Direct Broadcast Satellite (DBS) systems and the extension of satellite communications to non-geostationary (NGSO) orbit constellations [141-143]. All the above satellite communication systems, including the conventional geostationary (GSO) satellite systems, which belong to the Fixed Satellite Service,

gradually tend to employ higher frequency bands to satisfy the growing capacity requirements [144]. In addition to this, on operating above 10 GHz frequency, the atmospheric attenuations, which are mainly because of the humidity and oxygen, increases, therefore one have to choose the selected frequency bands, where the atmospheric attenuation is low. Therefore, the research has been focused on the investigation of the satellite communication systems at the Ku band (12-18 GHz), Ka band (26.5-40 GHz) and even at higher frequency bands. Moreover, the volume and weight constraints imposed by the launch vehicle generally demand a satellite communication antenna design using a single reflector to operate over multi-frequency bands. One possible way is to design a feed, which operate at different frequency bands, which results an inefficient solution. The researchers come up with a more desirable way, which is the designing of a FSS structure to a reflector system, which create different focal points and allow separate placement of feeds optimally designed for each frequency band. The FSS structures have the essential characteristics, which is transparent for one band of frequencies and reflective at other frequency band. However, various researchers have discussed physical insight and electromagnetic behaviour of variety of FSS structures using different numerical techniques as reported in [16-22]. In satellite communication applications, the frequency response of the FSS structures undergoes polarization variation in the direction of electric field due to the Faraday rotation effect as wave propagates in the ionosphere [23]. However, in realistic world, the electromagnetic waves propagating through space exhibit different AOIs and polarizations, therefore, in order to design a potential FSS structure in these respects, the structure must have a stable frequency response with respect to transmission and reflection characteristics for different AOIs and polarizations. The existing literatures in the microwave regime of the electromagnetic spectrum discuss only about the investigation of the FSS structures using different numerical techniques but not its synthesis, which is very important aspect to find the values of the geometrical parameters of FSS structure in order to meet the specific scattering characteristics. The motivation for the realization of this thesis lies in the need for developing a simple synthesis technique to obtain the geometrical parameters of SSLFSS structure. In addition to this, we have proposed novel geometrical shapes of FSS structures, which provide significantly much better

scattering characteristics as compared to that of the various reported FSS structures. In this thesis, the proposed geometrical shapes have provided the significant single-band and multiband scattering characteristics in microwave regime of the electromagnetic spectrum.

1.6 PROBLEM FORMULATION

The FSS structures have been investigated in the microwave regime of the electromagnetic spectrum since past five decades. In the microwave regime, the researchers have focused to develop the novel geometrical shapes of FSS structures, which have the potential to provide significant frequency response as compared to that of the reported FSS structures. In this regard, initially the focus was to design and analyze the novel FSS structures, which exhibits single resonance (bandstop and bandpass). Various simple geometries such as discussed in [43-50] have been explored to provide the single-band frequency characteristics. Thereafter, several researchers have investigated the loaded FSS structures [145-154], which have been classified as active loaded and passive loaded FSS structures. An active loaded FSS has been designed by implementing a tuning circuit as a part of FSS pattern to switch the frequency response (reflections and transmission) from transmission to reflection and vice-versa over the chosen frequency range [146-150]. However, these types of the structures are difficult to fabricate because of the complexity and cost of fabrication. On the other hand, the passive loaded FSS structures are of significant importance because the reflection/ transmission bandwidth and the resonant frequency is less sensitive to the angle of plane wave incidence. In addition to this, the fabrication of passive loaded FSS structures is easier due to the reduced complexity and cost of fabrication as compared to that of the active loaded FSS structure. Therefore, various researchers [151-154] have studied the passive element loaded FSS structures.

However, for the satellite communication applications, the FSS structure must be simple, low profile, and provide the significant angular/polarization stability for wide range of AOIs and different polarizations. With these aspects taken into consideration, we have proposed simple passive loaded FSS structures, which provide the significant scattering characteristics as compared to that of the other reported FSS structures in

the microwave regime of the electromagnetic spectrum. Moreover, in order to design the multiband FSS structure for the satellite communication applications, a simplified design, low profile and light weight FSS structure is the prime demand, therefore, in this thesis, we have discussed multi-resonant element FSS structure, which provide the multi-band frequency characteristics with significantly stable angular and polarization response. Moreover, the following design issues have been taken into consideration in order to propose the novel FSS structures.

- Design, analysis and control of behavior of flat-screen FSS in S (2-4 GHz)-band, and Ku (12-15 GHz)/Ka (24-28 GHz)-band,
- Parametric optimization of FSS structure for significant reflection and transmission characteristics in S, Ku and Ka-band,
- Analysis to enhance approximately 10% bandwidth,
- Prediction of the reflection and transmission characteristics with varying incident angle of plane wave in the range of $\pm 50^{o}$,
- Prediction of reflection and transmission characteristics with the variations in the polarization (perpendicular and parallel) states, and
- Validation of frequency responses using commercial simulators.

With the aforementioned design issues taken into consideration, we have discussed the SSLFSS as well as proposed novel unit-cell FSS structures such as modified circular ring FSS with four pairs of parallel straight conductors/slots and azimuthally periodic wedge shaped metallic vane, which have been achieved through the passive loading of the classical circular ring FSS structure. With the further geometrical modifications in the proposed FSS structures, we have discussed single layer multiband FSS structures (patch/aperture), which provide significant angular (up to 50^{o}) and polarization (horizontal and vertical) insensitive response using multiresonant approach.

1.7 THESIS ORGANIZATION

The remainder of thesis is organized as follows. **Chapter 2** discusses the synthesis technique of bandstop SSLFSS structure (without the dielectric substrate) and find

suitable applications in the fast analysis as well as fabrication of FSS structure. Moreover, a way to control the reflection at any frequency is discussed, which find an application in controlling the reflection level at any frequency. In addition to this, the two simple, cheaper and lightweight FSS structures for satellite communications have been investigated.

The **Chapter 3** provides a detailed description of the issues related to the structural transformation from SSLFSS to circular ring FSS structure. Further, the need to develop a modified circular ring FSS from the geometrical variations in the classical circular ring FSS structure has been discussed. In this Chapter, the effect of the supporting dielectric to proposed FSS structure is also investigated.

Chapter 4 presents the extension of proposed synthesis technique for the bandpass FSS, which is backed with the dielectric substrate and investigate the scattering characteristics of the proposed bandpass FSS structure at S, K_u/K_a and X-band. At each frequency of interest, the angular and polarization stability of proposed bandpass FSS is also discussed. In addition to this, the frequency response of proposed bandpass FSS structure is experimentally measured at X-band.

Chapter 5 explores the scattering characteristics such as resonance frequency and bandwidth of proposed planar multiband FSS structures (slot-and patch-type) in the microwave regime of the electromagnetic spectrum. The angular/polarization stability and electric field distribution of the planar multiband FSS structure has been discussed in the microwave regime of the electromagnetic spectrum.

Chapter 6 discusses the structure for bandstop and bandpass filtering characteristics. It includes the radial optimization and performance evaluation of the structure with respect to the wide range of AOIs and different polarization states. Finally, **Chapter 7** concludes the thesis and recommends the possible future directions.

CHAPTER-2

SYNTHESIS OF SINGLE-SQUARE-LOOP FSS STRUCTURE

2.1 INTRODUCTION

Various FSS structures such as dipole [155, 156], cross-dipole [157], circular ring [158], Jerusalem cross [159], and square loop [160] have been developed to reduce the adjacent channel interference in the communication systems, which occur due to the congestion in the electromagnetic spectrum. However, the square loop and circular ring in aforementioned FSS structures have regarded as the potential candidates, which offer significant frequency response in terms of the angular stability, cross polarization, bandwidth and band-separation [2, 161]. However, the square loop FSS structure has thoroughly been investigated and expressed in terms of the normalized mathematical-expressions (inductive and capacitive) using an EC technique [43]. There are various numerical techniques, which have been discussed in Section 1.2 to analyze different FSS structures, where each one is associated with its own merits and demerits. The EC technique is very popular due to its simplicity (where the equivalent lumped parameters of a FSS are obtained from the inductive and capacitive behaviour of the loop arms and the inter-element gap, respectively) and potential to provide the better understanding of its physical mechanism. Due to these reasons, we have selected SSLFSS structure as FSS geometry and EC technique for the numerical analysis. To design a SSLFSS structure (patch-type), which resonates at a specific frequency, it is desired to obtain its geometrical parameters such as periodicity (p), size (d), conducting strip-width (w), and inter-element gap (g).

However, the existing literatures on the SSLFSS structure discuss only about the evaluation of scattering characteristics using different numerical techniques but not its synthesis, which is significantly very important to meet the specific resonance frequency and bandwidth requirement. In this Chapter, a simple synthesis technique of a SSLFSS structure is developed. The remainder of Chapter is organized as follows. Section 2.2 discusses the generalized mathematical expression to obtain the geometrical parameters of the SSLFSS structure. Section 2.3 discusses the frequency

responses obtained numerically and using simulation tool (CST Microwave Studio). Section 2.4 demonstrates the effect of a wide range of AOIs on the scattering parameters of the FSS structure. Section 2.5 presents a method to control the reflection coefficient of the structure. Section 2.6 discusses the bandwidth control technique of SSLFSS structure. Section 2.7 illustrates two inexpensive SSLFSS structures, which find applications in satellite communication system. Section 2.8 implements the Babinet principle to justify the utility of the proposed synthesis for the bandstop and bandpass FSS structures (without backed dielectric). Finally, Section 2.9 concludes the Chapter.

2.2 THEORY OF OPERATION

The EC technique of SSLFSS structure is developed by Marcuvitz as discussed in detail in [42] and further used by several researchers to extract the circuit lumped parameters such as inductance (L) and capacitance (C) associated with the structure [43, 162]. The unit-cell configuration of SSLFSS structure along with its geometrical parameters such as periodicity, size, conducting strip-width and inter-element gap is shown in Fig. 2.1. In order to design a SSLFSS, it is required to yield its geometrical parameters, which resonates at a specific frequency with the desired bandwidth. The existing methods only provide the knowledge about the value of L and C for a chosen square loop FSS structure but the accurate synthesis of the SSLFSS from the knowledge of the resonance frequency is a challenging task and has not been dealt adequately. Therefore, a simple and novel mathematical expression to compute its geometrical parameters with certain accuracy has been developed. For perpendicular polarized wave, the EC elements are obtained by the following mathematical expressions as given in [69]:

$$\frac{\omega_r L}{Z_o} = \frac{d}{p}\cos\theta \times F(p, w, \lambda, \theta) \tag{2.1}$$

where, $F(p, w, \lambda, \theta) = \frac{p}{\lambda}\left[\ln \csc\left(\frac{\pi w}{2p}\right) + G(p, w, \lambda, \theta)\right]$ (2.2)

$$\frac{\omega_r C}{Y_o} = 4\,\frac{d}{\lambda}\sec\theta \times F(p, g, \lambda, \theta) \times \varepsilon_{eff} \tag{2.3}$$

where, $F(p, g, \lambda, \theta) = \frac{p}{\lambda}\left[\ln \csc\left(\frac{\pi g}{2p}\right) + G(p, g, \lambda, \theta)\right]$ (2.4)

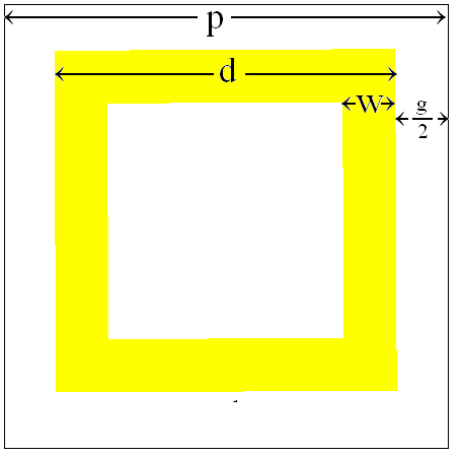

Fig. 2.1 The unit-cell configuration of SSLFSS structure.

In Equations (2.1) - (2.4), ε_{eff}, Z_o, Y_o, θ, $G(p,w,\lambda,\theta)$ and $G(p,g,\lambda,\theta)$ are the effective dielectric permittivity of the medium, characteristic impedance in free-space, characteristic admittance in free-space, AOI, the correction factors for associated inductance and capacitance, respectively. However, at the cost of minor sacrifice in the accuracy, Equation (2.1) and (2.3) may be re-written as following.

$$\frac{\omega_r L}{Z_o} = \frac{d}{p}\cos\theta \,.\frac{p}{\lambda}\ln\csc\left(\frac{\pi w}{2p}\right) \tag{2.5}$$

and,

$$\frac{\omega_r C}{Y_o} = \frac{d}{p}\sec\theta \,.\frac{p}{\lambda}\ln\csc\left(\frac{\pi g}{2p}\right) \times \varepsilon_{eff} \tag{2.6}$$

Considering the air as a dielectric substrate and on multiplying the Equation (2.5) and (2.6), we yield the following relationship.

$$\omega_r^2 LC = 4\left(\frac{d}{p}\right)^2\left(\frac{p}{\lambda}\right)^2 \times \ln\csc\left(\frac{\pi w}{2p}\right) \times \ln\csc\left(\frac{\pi g}{2p}\right) \tag{2.7}$$

In (2.7), the left hand side of the equation indicates the resonance/anti-resonance condition. At resonance, for the ideal reflective FSS, its value must be 1.0 ($\omega_r^2 = 1/LC$). Therefore, the expression (2.7) is modified as follows.

$$1 = 4\left(\frac{d}{p}\right)^2\left(\frac{p}{\lambda}\right)^2 \times \ln\csc\left(\frac{\pi w}{2p}\right) \times \ln\csc\left(\frac{\pi g}{2p}\right) \tag{2.8}$$

Further, Equation (2.8) is simplified as:

$$1 = 4\left(\frac{d}{p}\right)^2\left(\frac{p}{\lambda}\right)^2 \times \ln\left(\frac{1}{\sin\left(\frac{\pi w}{2p}\right)}\right) \times \ln\left(\frac{1}{\sin\left(\frac{\pi g}{2p}\right)}\right) \tag{2.9}$$

For the case of $w << 2p$ and $g << 2p$ and by applying the small angle approximation, Equation (2.9) is modified as follows.

$$1 = 4\left(\frac{d}{p}\right)^2\left(\frac{p}{\lambda}\right)^2 \times \ln\left(\frac{2p}{\pi w}\right) \times \ln\left(\frac{2p}{\pi g}\right) \tag{2.10}$$

In case of the loosely packed FSS, the value of g is quite greater than w and the ratio of $2p/\pi w$ dominates over the ratio of $2p/\pi g$ and with the minor sacrifice in the accuracy, the Equation (2.10) is simplified as.

$$1 = 4\left(\frac{d}{\lambda}\right)^2 \times \ln\left(\frac{2p}{\pi w}\right) \tag{2.11}$$

For a given FSS structure, the resonance response varies with the AOI and periodicity of the FSS structure, therefore in order to avoid the grating lobes to occur, the periodicity is related to the wavelength as follows [163].

$$p(1 + \sin\theta) < \lambda \tag{2.12}$$

From Equation (2.12), it is observed that for a given maximum incidence angle, a mathematical relation between the periodicity and wavelength is established as long as the inequality is satisfied. To understand the concept, we take the case that FSS structure must operate satisfactorily over the angle θ_1. Then we can select the value of $\theta = \theta_2$ in Equation (2.12), where $\theta_2 > \theta_1$. On this way, it is revealed that the inequality of Equation (2.12) is satisfied and the value of p is fixed as.

$$p = M\lambda \tag{2.13}$$

In Equation (2.13), M is a constant and varies between 0 to 1. The substitution of Equation (2.13) in Equation (2.11) gives the following expression.

$$1 = 4\left(\frac{d}{\lambda}\right)^2 \times \ln\left(\frac{2M\lambda}{\pi w}\right) \tag{2.14}$$

The Equations (2.12) and (2.14) have demonstrated that with the knowledge of the operating frequency, the desired strip-width as the fraction of wavelength, the maximum expected AOI of plane wave and size of the square loop have been computed and further optimized. In general, the procedure is equally-suitable for the parallel polarized wave because the square loop FSS structure is polarization independent. Therefore, the synthesis technique developed for the perpendicular polarization is also applicable to parallel polarization mode of operation. Further, Equation (2.14) also provides a way to control the value of the reflection at any

specific frequency. In Equation (2.7), the left hand side of the equation has been set as 1.0 for the resonance condition. Ideally, the value of $|S_{11}|$ is equal to 1.0 at the resonance frequency. When the left hand side of Equation (2.7) is replaced by some other value (lesser than 1.0), that results in an off-resonance condition, which is used to govern the amount of the reflection at that particular frequency.

2.3 NUMERICAL RESULTS

In order to validate the theory proposed in Section 2.2, the geometrical parameters of the SSLFSS structure at 3 GHz, 15 GHz and 26 GHz have been computed and its correctness has been checked using CST Microwave Studio, which is based on the finite integral technique. In the first case, the geometrical parameters of SSLFSS structure are analyzed for the normal wave incidence ($\theta = 0^o$). In order to calculate the value of p while avoiding the occurrence of grating lobe at the intended frequency, the value of p is calculated by meeting the condition described in Equation (2.12), therefore, the value of θ must be greater than 0^o. On this way, to fulfill the synthesis constraint, the value of $\theta = 10^o$ has been selected, which results the value of M is 0.8520. Once the value of M is fixed for different values of w/λ, the value of d is computed using the Equation (2.14), which has been discussed in Tables 2.1, Table 2.2 and Table 2.3, for 3 GHz, 15 GHz, and 26 GHz, respectively. Further, to support the numerical analysis, the SSLFSS structure has been simulated at 3 GHz, 15 GHz and 26 GHz using the CST Microwave Studio and frequency responses at each frequency of interest are demonstrated in Fig. 2.2. The value of the resonance frequency obtained by the simulation is shown in 5^{th} column of these tables (Table 2.1, Table 2.2 and Table 2.3) and in the last column of these tables, the relative error with respect to the intended frequencies are presented. Table 2.1, Table 2.2 and Table 2.3 have explored that for the fixed value of p, with the increase in the value of w/λ, the relative percentage deviation from the intended frequency is reduced in spite of the normal incidence of the electromagnetic wave as the structure has been simulated in the Transient Solver which supports only the normal incidence. Further, the resonance frequency response is saturated and the effect of increase in the strip-width on the f_r (resonance frequency) is insignificant.

Table 2.1 The loop parameters at 3 GHz for 10° AOI.

w/λ	p (mm)	d (mm)	w (mm)	f_r (GHz) (CST MWS)	% deviation of f_r
0.01	85.20	25.02	1	3.30	10
0.02	85.20	27.52	2	3.22	7.3
0.03	85.20	29.38	3	3.18	6.0
0.04	85.20	30.96	4	3.16	5.3
0.05	85.20	32.38	5	3.15	5.0
0.06	85.20	33.69	6	3.15	5.0

Table 2.2 The loop parameters at 15 GHz for 10° AOI.

w/λ	p (mm)	d (mm)	w (mm)	f_r (GHz) (CST MWS)	% deviation of f_r
0.01	17.04	5.00	0.2	16.56	10.4
0.02	17.04	5.50	0.4	16.09	7.2
0.03	17.04	5.87	0.6	15.91	6.0
0.04	17.04	6.19	0.8	15.81	5.4
0.05	17.04	6.47	1.0	15.75	5.0
0.06	17.04	6.73	1.2	15.75	5.0

Table 2.3 The loop parameters at 26 GHz for 10° AOI.

w/λ	p (mm)	d (mm)	w (mm)	f_r (GHz) (CST MWS)	% deviation of f_r
0.01	9.83	2.88	0.11	28.65	10.1
0.02	9.83	3.17	0.23	27.92	7.3
0.03	9.83	3.39	0.34	27.56	6.0
0.04	9.83	3.57	0.46	27.40	5.3
0.05	9.83	3.73	0.57	27.32	5.0
0.06	9.83	3.88	0.69	27.13	4.3

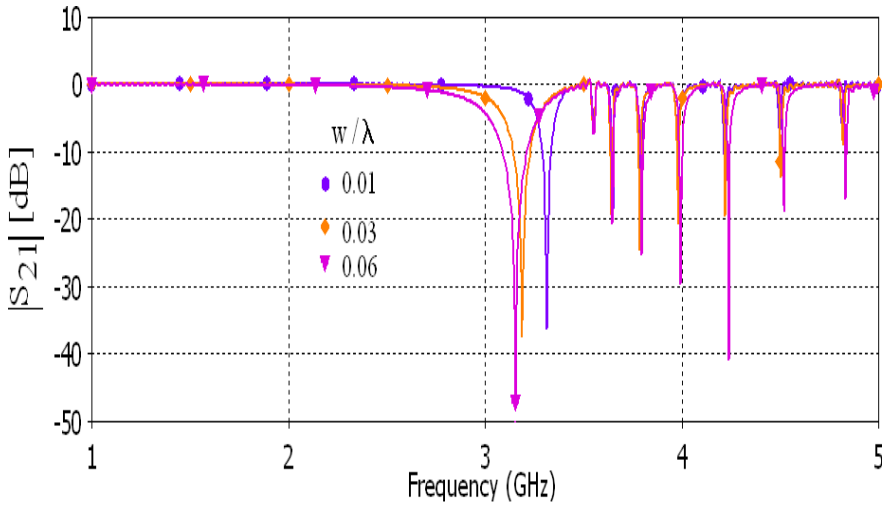

(a)

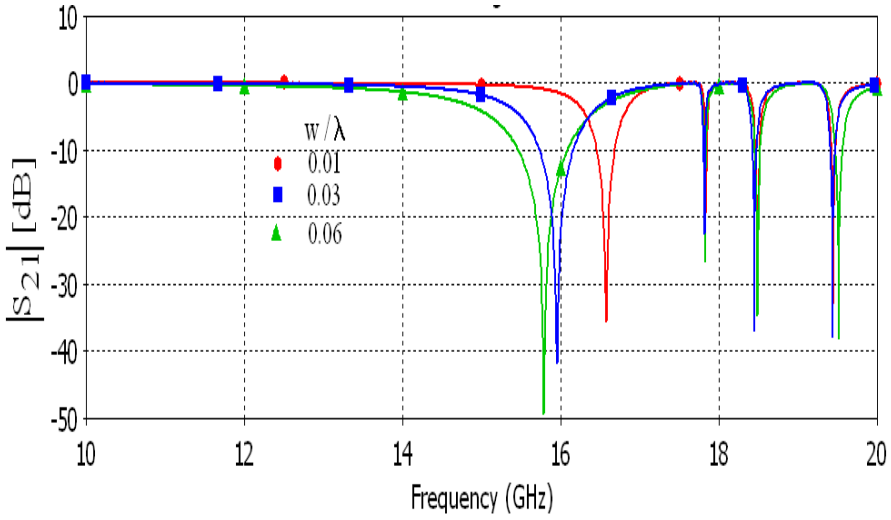

(b)

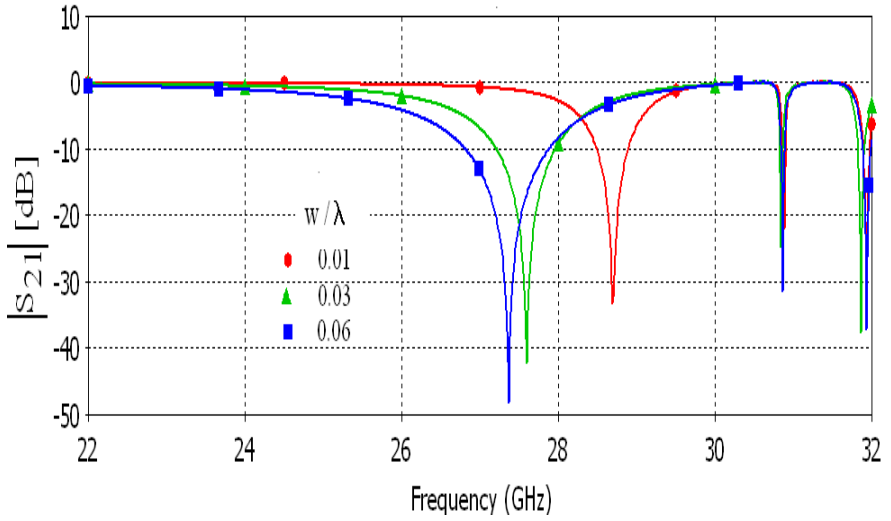

(c)

Fig. 2.2 The effect of w/λ on the resonance frequency on (a) 1-5 GHz (b) 12-18 GHz and (c) 22-32 GHz frequency range.

The deviation is significantly reduced with the strip-width but the small percentage error still exists as to simplify the synthesis process, the value of the correction factor and the gap between the two loops has been neglected. The simulated value of the S_{21} parameter in 1-5 GHz, 10-20 GHz and 22-32 GHz are demonstrated in Fig. 2.2(a), Fig. 2.2(b) and Fig. 2.2(c), respectively which show different transmission-null points as mentioned in Tables 2.1, Table 2.2 and Table 2.3. Fig. 2.2(a), Fig. 2.2(b) and Fig. 2.2(c) have demonstrated that at a given incidence angle (10^o in this case), with the increase in the *w/λ*, the transmission-null point downshifts and the transmission-null bandwidth is increased. In other words, with the increase in the value of the width of

strip, the inductive effect of SSLFSS structure is reduced, which causes the width of scattering parameter to increase. In the lossless condition, $|S_{21}|^2 + |S_{11}|^2 = 1$, which indicates that when S_{21} is minimum, S_{11} reaches to maximum and the flatness of the reflective property of the SSLFSS structure is increased. From this numerical analysis, it is also clear that by varying the value of w/λ, the desired band of rejection of the signal is achievable.

2.4 EFFECT OF ANGLE-OF-INCIDENCE

Fig. 2.2(a), Fig. 2.2(b) and Fig. 2.2(c) have demonstrated that the maximum relative error between the intended and achieved operating frequency is about 10% which can be further reduced by reducing the value of θ in Equation (2.12). When θ is set equal to zero, the value of $p = \lambda$ and Equation (2.12) is not satisfied which calls for the addition of the correction factor in the Marcuvitz Equation [42].

Table 2.4 The effect of AOI on SSLFSS structure designed at 3 GHz with 0.06 w/λ.

AOI	p (mm)	d (mm)	w (mm)	'f_r' (GHz) (CST MWS)
0^o	100	32.5346	6	2.87
5^o	91.9831	33.1259	6	3.03
10^o	85.2000	33.6969	6	3.15
15^o	79.4395	34.2461	6	3.23
20^o	74.8145	34.7721	6	3.30
25^o	70.2929	35.7475	6	3.32
30^o	66.6667	35.7475	6	3.33
35^o	63.5495	36.1932	6	3.35
40^o	60.8721	36.6083	6	3.36
45^o	58.5786	36.9911	6	3.32
50^o	56.6237	37.3396	6	3.32
55^o	54.9707	37.6520	6	3.30
60^o	53.5898	37.9265	6	3.27
65^o	52.4574	38.1617	6	3.24
70^o	51.5546	38.3562	6	3.21
75^o	50.8666	38.3562	6	3.18
80^o	50.3827	38.6183	6	3.17
85^o	50.0953	38.6844	6	3.15
90^o	50.0000	38.7065	6	3.14

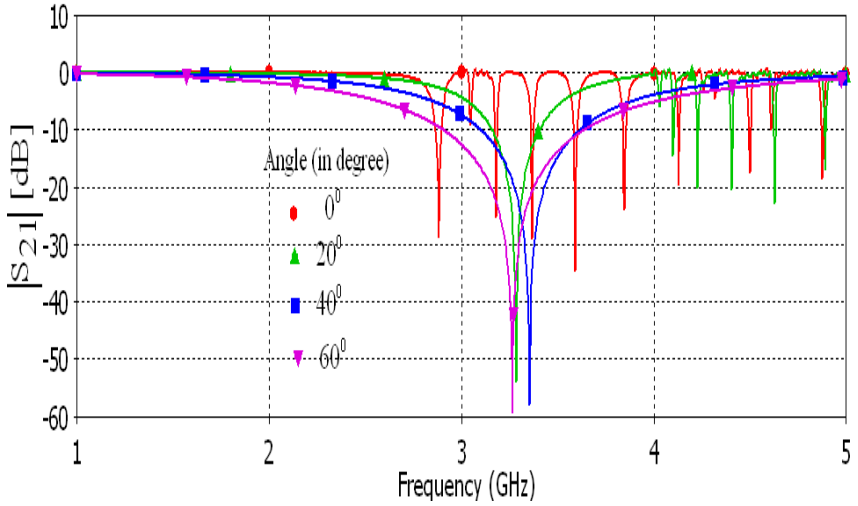

Fig. 2.3 The frequency response on the S_{21} (magnitude in dB) parameter for different AOIs.

Table 2.5 The effect of AOI on SSLFSS at 15 GHz with 0.06 *w/λ*.

AOI	*p* (mm)	*d* (mm)	*w* (mm)	'f_r' (GHz) (CST MWS)
30°	13.3333	7.1495	1.2	16.70
35°	12.7099	7.2386	1.2	16.83
40°	12.1744	7.3217	1.2	16.82
45°	11.7157	7.3982	1.2	16.78
50°	11.3247	7.4679	1.2	16.68
55°	10.9941	7.5304	1.2	16.56
60°	10.7180	7.5853	1.2	16.41

Table 2.6 The effect of AOI on SSLFSS designed at 26 GHz with 0.06 *w/λ*.

AOI	*p* (mm)	*d* (mm)	*w* (mm)	'f_r' (GHz) (CST MWS)
30°	7.6923	4.1247	0.6923	29.137
35°	7.3326	4.1761	0.6923	29.224
40°	7.0237	4.2240	0.6923	29.229
45°	6.7591	4.2682	0.6923	29.153
50°	6.5335	4.3084	0.6923	28.990
55°	6.3428	4.3445	0.6923	28.79
60°	6.1834	4.3761	0.6923	28.42

However, to design a SSLFSS structure, we set the θ close to 0° for the normal wave incidence and in this case the error is reduced significantly. In order to illustrate this effect, the geometrical parameters of SSLFSS structure have been calculated at 3 GHz for $0^o \leq \theta^o \leq 90^o$ as demonstrated in Table 2.4. However, for the fixed value of w/λ = 0.06, with the increase in the AOI, the difference between the intended and

simulated resonance frequency increases initially and then reduced as illustrated in Table 2.4. In addition to this, the maximum deviation is achieved at $\theta = 40^o$, which is about 12%. Theoretically, with the increase in AOI, the value of p is reduced and the array becomes densely packed and at lower incidence angle, the FSS array is loosely packed. On this way, it is seen that with the certain relaxation in the accuracy, the mathematical expression is used for loosely as well as densely packed FSS array. Fig. 2.3 has shown the effect of variation in AOI on the normally incidence wave simulation in the range of $\theta^o \leq 60^o$, which revealed that at every wave incidence angle used in this computation, (except for $\theta = 0^o$), the SSLFSS structure resonates between 3 to 3.5 GHz and it shows the convergence of the result. In the case of $\theta = 0^o$, the resonance occurs at 2.87 GHz which is lower than that of the intended frequency (3 GHz) as it does not satisfy Equation (2.12). Further, from Fig. 2.3, it is observed that with different values of the incidence angles, the periodicity, size and the strip-width of the FSS structure changes, which causes the shift in the resonance frequency and bandwidth. In addition to this, to validate the theory, the resonance response has been computed for 15 GHz and 26 GHz and the similar behaviour has been observed. The observation in the range of $30^o \leq \theta^o \leq 60^o$ at these two frequencies is demonstrated in Table 2.5 and Table 2.6, respectively.

2.5 CONTROLLING THE REFLECTION COEFFICIENT

However, there is no any direct method to compute or anticipate about the dimension of the loop size which satisfies the desired refection coefficient condition. In this section, we have developed a relationship between the S_{11} parameter and resonance frequency, and explored that the desired level of reflection coefficient has been obtained by simply manipulating the design of loop. To understand the design method, we have simulated the SSLFSS structure with the geometrical parameters shown in the last row of Table 2.4, which corresponds to 90^o incidence angle and resonate at 3.14 GHz (as shown in Fig. 2.4). In addition to this, Fig. 2.4 also demonstrates that S_{11} is 0 dB at 3.14 GHz and in the range of 2.6 GHz-3.7 GHz, the value of S_{21} is less than -10 dB, which shows the strong reflection of the normal incidence signal. On the linear scale, it is clear that the maximum reflection corresponds to $S_{11} = 1$ at 3.14 GHz, which is equal to 100% reflection. Further, we

assume a condition in which it is required to maintain the value of reflection coefficient less than 100% at 3.14 GHz.

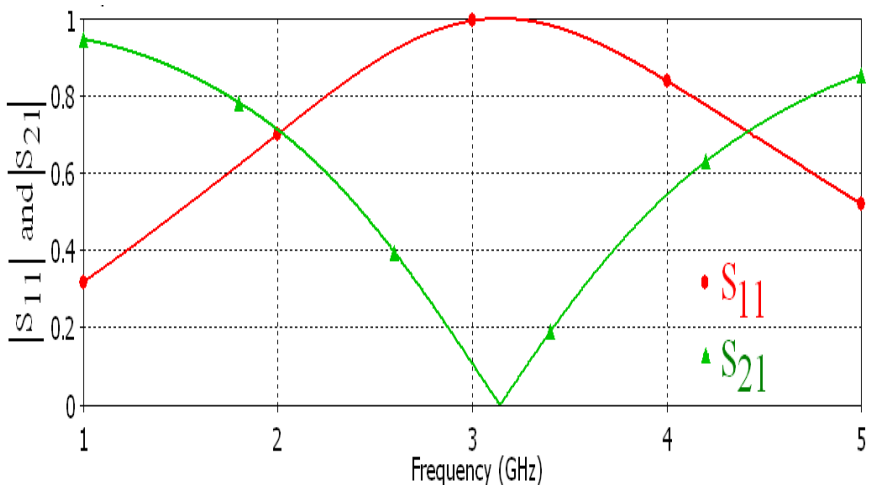

Fig. 2.4 The scattering parameters of SSLFSS structure with d = 38.7065 mm, p = 50 mm, and w = 6 mm at 3 GHz.

In order to achieve this value, the geometrical parameters of the SSLFSS structure must be changed and the amount of the change depends on the flatness and roll-off factor of S_{11} curve. When p and d of the SSLFSS is increased and w is decreased, the stop-band bandwidth is reduced and S_{11} parameter falls sharply, which does not maintain the linearity. However, in the present case as shown in Fig. 2.4, with the wider strip-width, the change in the S_{11} parameter on either side of the resonance frequency is linear, which indicates that for the wider strip-width and smaller size, a linear relationship between the $|S_{11}|$ and operating frequency exists. It further illustrates that to reduce the reflection coefficient to x% at frequency the resonance frequency (f_r), the S_{11} must be multiplied by x=100 and correspondingly.

$$|S_{21}| = \sqrt{1 - \left(\frac{x}{100}\right)^2} \qquad \text{for } |S_{11}|^2 = 1 \tag{2.15}$$

To explore the concept of linearly increase/decrease in the maximum reflection frequency point, we look at the fundamental relationship between impedance (Z) and scattering (S) parameters of the SSLFSS structure [164].

$$\begin{bmatrix} Z_{11} & Z_{12} \\ Z_{21} & Z_{22} \end{bmatrix} = Z_o \begin{bmatrix} \frac{(1+S_{11})(1-S_{22})+S_{12}S_{21}}{(1-S_{11})(1-S_{22})-S_{12}S_{21}} & \frac{2S_{12}}{(1-S_{11})(1-S_{22})-S_{12}S_{21}} \\ \frac{2S_{21}}{(1-S_{11})(1-S_{22})-S_{12}S_{21}} & \frac{(1-S_{11})(1+S_{22})+S_{12}S_{21}}{(1-S_{11})(1-S_{22})-S_{12}S_{21}} \end{bmatrix} \tag{2.16}$$

The *Z*-parameter is converted into its equivalent T-Network as demonstrated in Fig. 2.5, where Z_1 and Z_2 are equal to zero [71]. In Fig. 2.5, the value of normalized impedance Z_3 is related to the equivalent circuit model by the following formula.

$$Z_3 = j\left(\frac{\omega_r L}{Z_o} - \frac{Y_o}{\omega_r C}\right) \tag{2.17}$$

where, $Y_o = 1/Z_o$ and L and C are the equivalent inductance and capacitance at ω_r as mentioned Equation (2.5) and Equation (2.6). From Equation (2.17), it is revealed that the impedance (Z_3) is directly proportional to the inductance and operating frequency as well as inversely proportional to the capacitance. In the case of loosely packed FSS, the value of capacitance is negligible in comparison to the inductance. Under this condition, Z_3 is proportional to ω_r. It states that for loosely packed FSS, the scattering parameter is proportional to the impedance of FSS and the proportional change in the value of scattering parameter at the resonance frequency has been achieved by the change in the impedance level. To make this change, the resonance frequency of the square loop must be increased by the same factor. On this way, a complete control on the scattering parameter is possible.

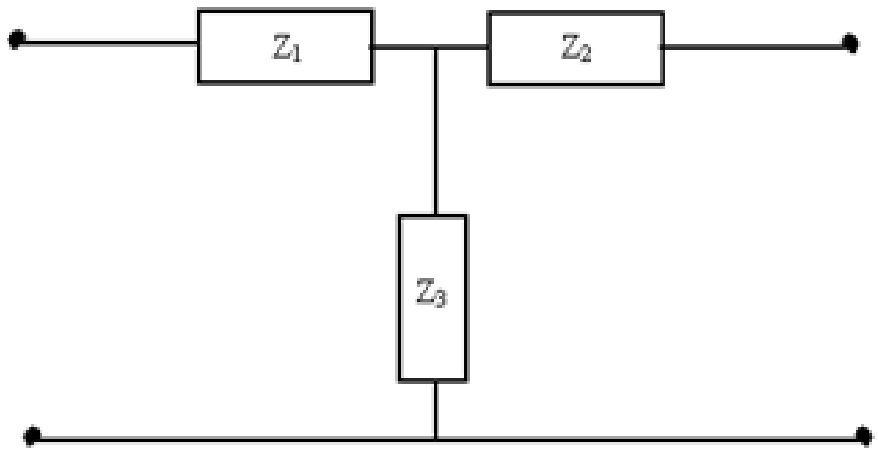

Fig. 2.5 The EC representation of SSLFSS structure.

For example, when we need the S_{11} = 10% at 3 GHz, it indicates that the FSS structure corresponding to the resonance of 30 GHz to be designed as 3 GHz must be scaled up by 3 GHz/0.1. In order to obtain the various values of the reflection level for the geometrical parameters of SSLFSS structure as demonstrated in last row of Table 2.4, the outcome of this process to control the reflection is shown in Table 2.7. From the first and the last column of Table 2.7, it is clear that for the wider strip and loosely

packed SSLFSS structure, the required value of the reflection is achievable by simply scaling up the resonance frequency by that factor. Further, the first significant figure of the last column is very close to the required magnitude of reflection coefficient. The simulated result of $|S_{11}|$ against the frequency is shown in Fig. 2.6. From Fig. 2.6, it is clear that the resonance frequency obtained for different geometrical parameters of the SSLFSS structure as mentioned in column 5, 6, and 7 of Table 2.7 is comparable to the required resonance frequency as described in column 2 of Table 2.7. Since, the resonance condition is satisfied, $|S_{11}|$ is also satisfied at 3 GHz.

Table 2.7 The control of reflection coefficient by varying the loop size.

Required S_{11} at 3 GHz	SSLFSS designed to resonate at (GHz)	The loop parameter for w/ λ=0.06				Simulated (CST MWS) value of S_{11} at 3 GHz (in fraction)
		λ (mm)	*p* (mm)	*d* (mm)	*w* (mm)	
0.1	30.0	10	5	3.8706	0.6	0.0971
0.2	15.0	20	10	7.7413	1.2	0.1963
0.3	10.0	30	15	11.6119	1.8	0.3325
0.4	7.50	40	20	15.4826	2.4	0.4078
0.5	6.00	50	25	19.3532	3	0.5223
0.6	5.00	60	30	23.2239	3.6	0.6443
0.7	4.28	70.09	35.04	27.1307	4.2	0.7696
0.8	3.75	80	40	30.9652	4.8	0.8823
0.9	3.33	90.09	45.04	34.8707	5.4	0.9658
1.0	3.00	100	50	38.7065	6	0.9993

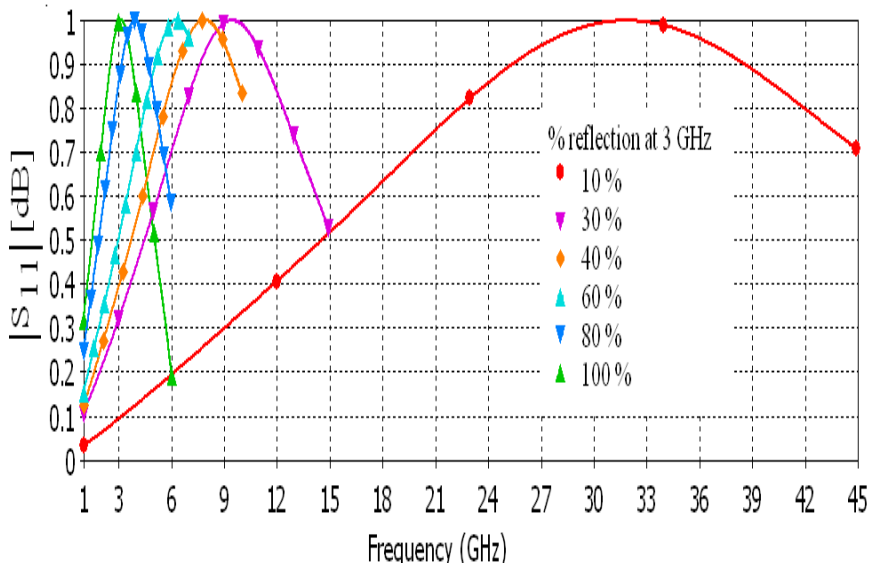

Fig. 2.6 The controlled reflection coefficient at 3 GHz.

Table 2.8 The control of reflection coefficient by varying the loop size at 15 GHz.

Required S_{11} at 15 GHz	SSLFSS designed to resonate at (GHz)	The loop parameter for w/ λ=0.06				Simulated (CST MWS) value of S_{11} at 15 GHz (in fraction)
		λ (mm)	p (mm)	d (mm)	w (mm)	
0.1	150	2	1	0.77	0.12	0.104
0.2	75	4	2	1.54	0.24	0.200
0.3	50	6	3	2.32	0.36	0.298
0.4	37.5	8	4	3.09	0.48	0.403
0.5	30	10	5	3.87	0.60	0.511
0.6	25	12	6	4.64	0.72	0.621
0.7	21.43	13.98	6.99	5.41	0.83	0.745
0.8	18.75	16	8	6.19	0.96	0.855
0.9	16.66	17.98	8.99	6.96	1.08	0.944
1.0	15	20	10	7.74	1.2	0.993

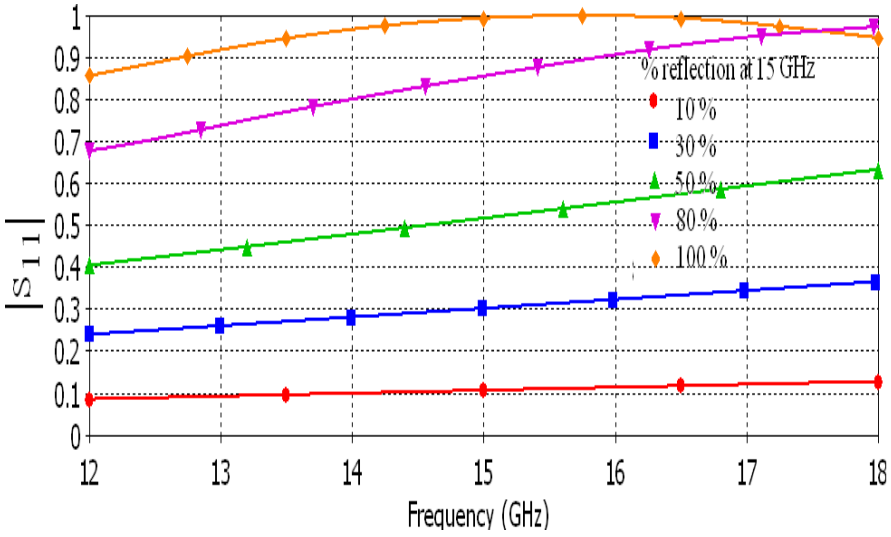

Fig. 2.7 The value of controlled reflection coefficient in the range of 12-18 GHz.

Further, to validate the proposed method of analysis of the reflection coefficient at a given frequency, the procedure has been repeated at 15 GHz and similar result has been obtained. The required geometrical parameters to achieve the desired reflection coefficient at 15 GHz are shown in Table 2.8 and in the last column, the value of the achieved reflection coefficient at 15 GHz is shown. Further, the structures have been simulated in the 12-18 GHz frequency window as shown in Fig. 2.7 and the observed reflection coefficient at 15 GHz is comparable to that of the desired one. On this way, it is concluded that to achieve the desired refection coefficient at any frequency, the

frequency is to be divided by that fraction of the reflection coefficient and the new frequency serves as the resonance frequency of the structure.

2.6 BANDWIDTH CONTROL

The band of operation of SSLFSS structure is largely affected by its size and strip-width. When the size of square loop is reduced and strip-width is increased, the rejection bandwidth of structure is also increased and with the enhancement in the loop size, the bandwidth is decreased. It indicates that the bandwidth is inversely related to the *d* and *p*. In case of the larger loop, the bandwidth may further be controlled by varying the *w*. To show the effect of loop size and its strip-width on the transmission/reflection bandwidth of SSLFSS structure, we have discussed five structures with different parameters at 3 GHz such as: a) p = 85.20 mm, d = 29.38 mm, w = 3 mm, b) p = 85.20 mm, d = 29.38 mm, w = 6 mm, c) p = 85.20 mm, d = 33.69 mm, w = 6 mm, d) p = 66.6667 mm, d = 35.7475 mm, w = 6 mm, and e) p = 50 mm, d = 38.7065 mm, and w = 6mm. However, the parameters mentioned in (a) and (c) are taken from Table 2.1 and parameters mentioned in (d) and (e) from Table 2.4. The S_{21} parameter of the structures is demonstrated in Fig. 2.8. From Fig. 2.8, it is revealed that for the case (a) and (b) and (c) where the periodicity is close to the wavelength, the rejection bandwidth is narrow. Further, in the case (a) strip width is 3 mm in comparison to (b) where the strip width is equal to 6 mm. Due to the change in only the strip-width the resonance frequency shifts to 3.24 GHz from 3.14 GHz in the case of (a). The half power bandwidth in the case of (a) an (b) are 7.64% and 5%, respectively. It indicates that for the narrow bandwidth, the strip-width is to be increased but the structure resonates at higher frequency. Now in the case (c), while keeping the same *p* and *w* as of (b), and increasing the value of *d*, the resonance frequency downshifts and it is due to the reduction in the quality factor, which reduces due to the change in the inductance value where the inductance is associated with *w*. In the case (c), the f_r and -3 dB fractional bandwidth (FBW) are 3.11 GHz and 8.66%, respectively. In the case of (d) and (e), the *p* and *d* have been reduced and increased, respectively, while keeping the strip-width constant equal to 6 mm. With the reduction in the *p*, the rejection bandwidth is increased which is evident from Fig. 2.8. On this way, the smaller loop size is used to increase the band-rejection limit which would be a wide band rejection. In addition to this, another important

phenomenon is the effect of *p* on the resonance condition of the structure. If the *p* is close to the wavelength, the multiple resonances have been achieved and used in the design of multi-resonance FSS structure [165, 166]. In addition to this, for the wide rejection band, the smaller loop size is required.

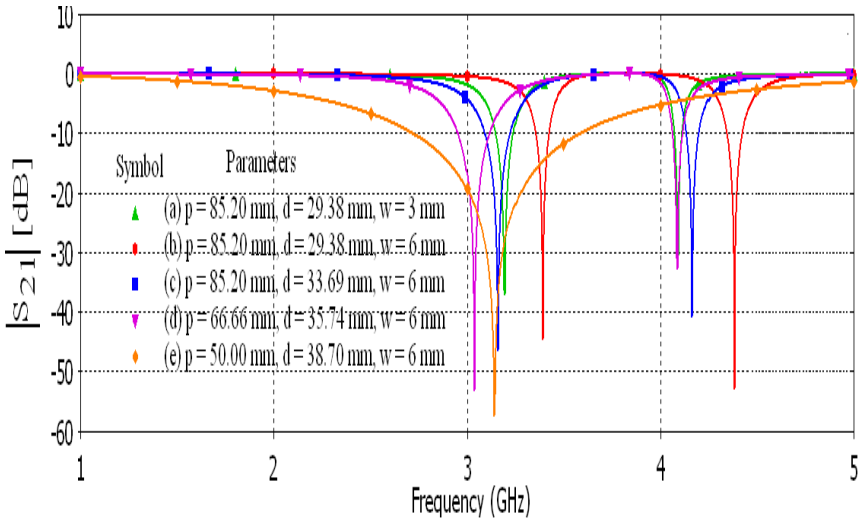

Fig. 2.8 The effect of geometrical parameters of SSLFSS structure on $|S_{21}|$ parameter.

2.7 DESIGN OF A LOW COST INEXPENSIVE SSLFSS STRUCTURE FOR SATELLITE COMMUNICATION

As, for the practical purpose, it is necessary to design the FSS structure on a dielectric material. However, the use of the dielectric material changes the performance of the structure [167] as the characteristic impedance above and below the structure is changed and resonance frequency downshifts as $f_r/\sqrt{\varepsilon_{eff}}$ [1, 2]. However, we have considered a dielectric support of Thermocol, which has relative dielectric permittivity (ε_r) is equal to 1.05 because the selection of this kind of material reduces the separate analytical treatment of the structure as its ε_r is close to the free-space and the dependence of the performance of FSS structure on the substrate is alleviated. However, two SSLFSS structures at 3 GHz and 22 GHz with about 10% bandwidth for the satellite communication are designed. These FSS structures are similar to the structure shown in Fig. 2.1 except backed dielectric support of Thermocol (relative dielectric permittivity ε_r = 1.05 and thickness h =10 mm). The dimensions of structure has been parametrically tuned to resonate near 3 GHz and in this case the values of *p*, *d*, *w*, and conductor thickness (*t*) are 85.20 mm, 33.69 mm, 6mm and 0.01 mm, respectively. The response of structure is shown in Fig. 2.9 where it is noted that the

structure resonates at 3.1 GHz and 9.2% FBW. From Table 2.2 and Table 2.3, it is observed that with the increase in the operating frequency, for narrow strip-width and larger periodicity, the bandwidth narrows but relative error is increased, which is quite significant for the precise application of the spectrum. To overcome this constraint, we have designed a structure with f_r = 20 GHz, w/λ = 0.02, $\theta = 20^o$ and corresponding values of *p*, *d* and *w* are 11.1772 mm, 4.21149 mm and 0.3 mm, respectively. The thickness of conducting material and dielectric substrate are 0.01mm and 10 mm, respectively. The response of the structure is shown in Fig. 2.10, which reveals that the FBW is 10.9% and the structure resonates at 21.96 GHz which is in close agreement to the requirement.

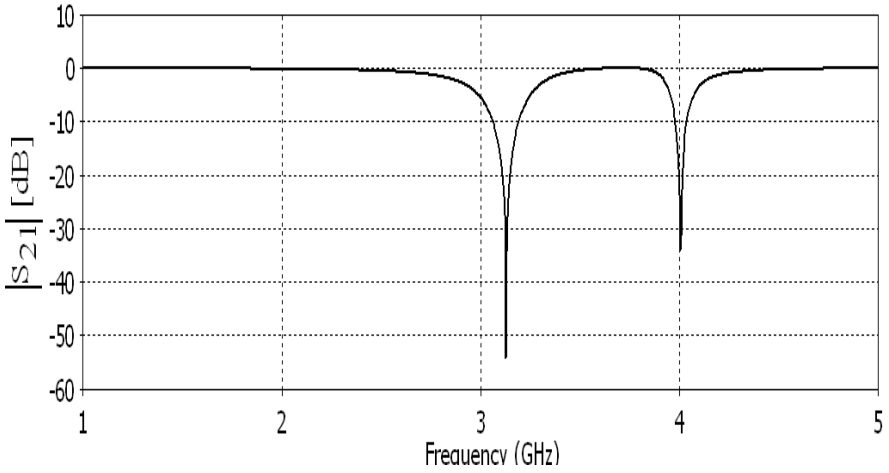

Fig. 2.9 The transmission parameter of the SSLFSS structure with Thermocol dielectric support.

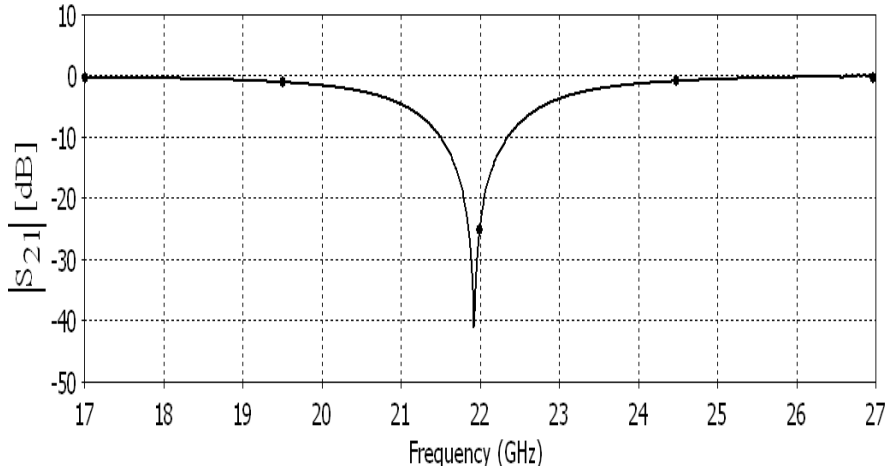

Fig. 2.10 The transmission response of SSLFSS structure with *p* = 11.1772 mm, *d* = 4.21149 mm and *w* =0.3 mm.

2.8 EXTENSION OF PROCEDURE FOR BANDPASS FSS STRUCTURE

It is known fact that the bandpass and bandstop FSS structure are complementary to each other when the FSS structure satisfies following conditions [168, 169].

1) The metallic sheet of FSS structure must be perfect electric conductor (PEC).
2) FSS must be free-standing.
3) The electric field must be of complimentary polarization.

With the above issues taken into consideration, a bandstop FSS structure has been converted into bandpass by replacing the conducting material part by the slot and the vacant part of the FSS structure by the conductor. In this case, the *p* remains same, *w* is replaced by the slot-width and *d* becomes the size/length of the slot. To demonstrate the resonance behaviour of the bandstop and bandpass SSLFSS structure for the same values of the geometrical parameters, we have simulated these structures in two different frequency bands. In the first case, the value of *p*, *d*, and *w* are 50 mm, 38.70 mm, and 6 mm, respectively, which are shown in the last row of Table 2.4 and expected resonance frequency in bandpass as well as in the bandstop FSS structure is 3.14 GHz. The bandstop and bandpass SSLFSS structure are shown in Fig. 2.11(a) and Fig. 2.11(b), respectively and their corresponding simulated resonance behaviour are shown in Fig. 2.12(a) and Fig. 2.12(b). Fig. 2.12(a) and Fig. 2.12(b) demonstrate that the resonance frequency in both the cases remains same, which is 3.14 GHz. The only difference is the interchange of S_{21} and S_{11} parameter, which indicates that the synthesis technique (in its present form) has the potential to realize both bandstop and bandpass SSLFSS only if the value of ε_r of the dielectric substrate used is close to ε_r of the air. To verify the consistency of approach, the similar structure as shown in Fig. 2.11(a) and Fig. 2.11(b) have been simulated in the frequency range of 22-30 GHz with parameters such as p = 9.83 mm, d = 3.39 mm and w = 0.34 mm, respectively (taken from the 3rd row of the Table 2.3). The scattering characteristics of bandstop (shown in Fig. 2.13(a)) and bandpass (shown in Fig. 2.13(b)) SSLFSS structures in the frequency range of 22-30 GHz have been demonstrated in Fig. 2.14(a) and Fig. 2.14(b), respectively. The frequency responses shown in Fig. 2.14(a) and Fig. 2.14(b) have demonstrated that both structures resonate near 27.5 GHz and they have similar graph pattern except the interchange in the S_{11} and S_{21} parameters.

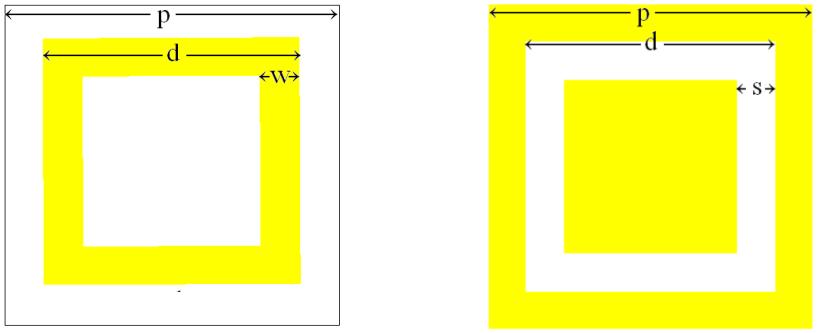

(a) (b)

Fig. 2.11 The unit-cell configuration of SSLFSS structure (a) bandstop and (b) bandpass.

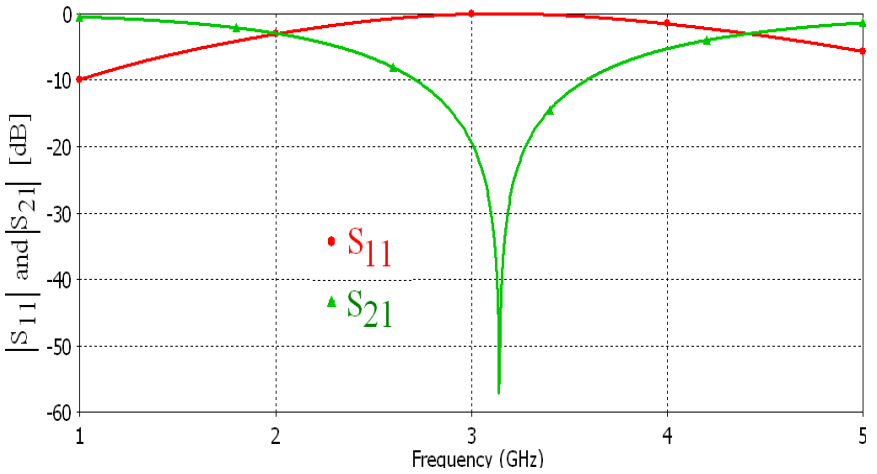

(a)

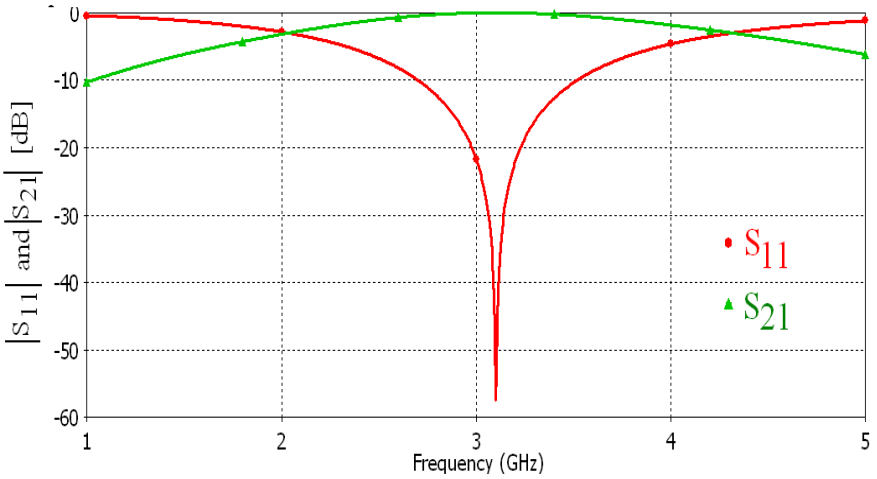

(b)

Fig. 2.12 The scattering characteristics of the (a) bandstop and (b) bandpass SSLFSS structure in 1-5 GHz band.

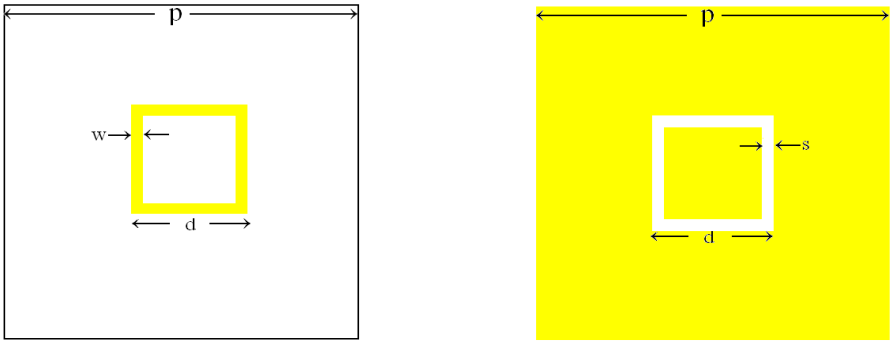

(a) (b)

Fig. 2.13 The frequency selective surface (a) bandstop and (b) bandpass at 22-30 GHz range.

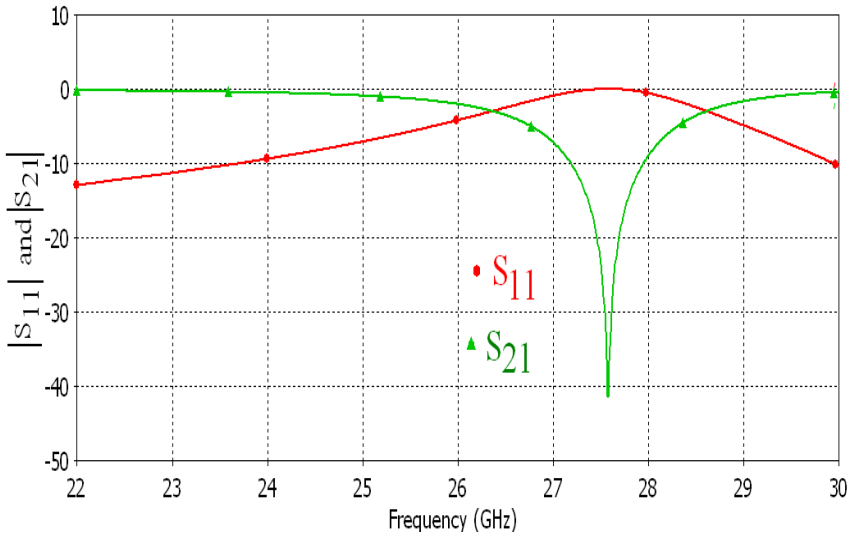

(a)

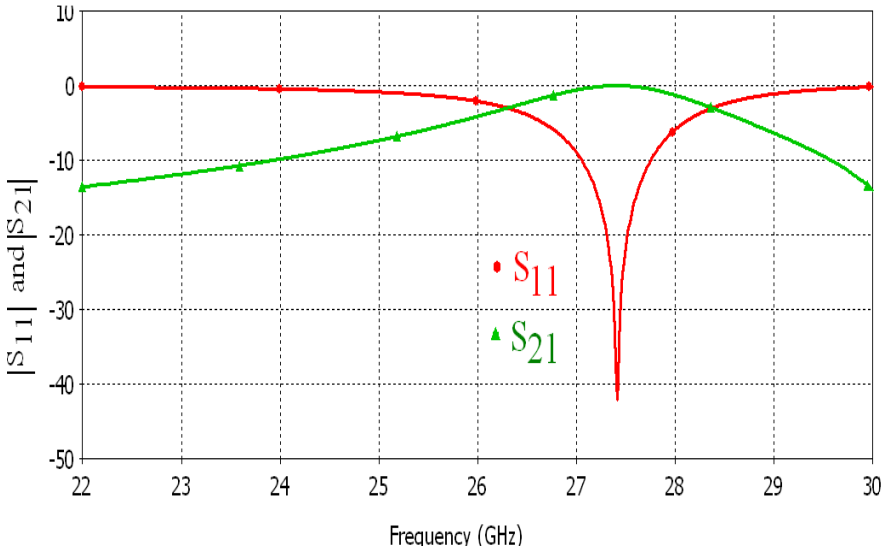

(b)

Fig. 2.14 The response of (a) bandstop and (b) bandpass FSS at 22-30 GHz band.

2.9 CONCLUSION

In this Chapter, a simple synthesis technique to obtain the geometrical parameters such as periodicity, size, width of strip and inter-element gap of SSLFSS structure is discussed. The process of computation of various parameters is discussed using the equivalent circuit technique, which is supported by the commercial simulator results. In addition to this, the method to control the reflection at any frequency is also explored, which find application in interference control. Further, this method has been used to design SSLFSS structures at 3 GHz and 22 GHz with the controlled bandwidth, which find suitable applications in satellite communication. Moreover, the process has been extended to the synthesis of bandpass FSS structure and the desired results have been obtained which indicates the application of the process for both types of the FSS.

CHAPTER-3

ANALYSIS OF BANDSTOP MODIFIED CIRCULAR RING FSS STRUCTURE

3.1 INTRODUCTION

In the microwave regime of electromagnetic spectrum, the main emphasis of the researchers is to develop new geometrical shapes of FSS structures, which provide significant improvement in terms of the angular/polarization stability and reflection as well as transmission bandwidth. As the synthesis technique of the SSLFSS is discussed in Chapter-2 for the free-standing FSS structure, however the supported dielectric substrate provides the significant influence on the resonant behaviour of the structure. Therefore, in this chapter, the synthesis technique of the SSLFSS structure is modified to be used for dielectric backed SSLFSS structure. The angular/polarization stability of a FSS structure are the important aspects from the communication perspective, which need to be considered while designing the FSS because without addressing this issues, the FSS design remains incomplete. As, it has been discussed in [2] that the circular ring FSS structure is more angular stable as compared to that of the SSLFSS due to its rotational symmetry.

In view of this, the synthesis technique of dielectric backed SSLFSS is implemented on the circular ring FSS structure, which reveals that for same values of periodicity, loop size and strip-width, the circular ring FSS resonate at higher frequency as compared to that of the SSLFSS. On the other hand, for the significant implementation of synthesis technique of SSLFSS on the circular ring FSS, both (single square loop and circular ring) the structures must resonate at the same frequency, which has been achieved by enhancing its size and periodicity. However, this enlargement deteriorates the angular stability of the circular ring FSS structure and results the larger size [170-172].

In order to overcome this limitation and to achieve better angular/polarization stability, the four pairs of parallel straight conductors of length (l) have been inserted in the circular ring FSS structure. The remainder of the chapter is organized as follows. Section 3.2 discusses the generalized synthesis technique to obtain the

geometrical parameters of the dielectric backed SSLFSS. Section 3.3 explores the issues associated with the structural transformation i.e. from SSLFSS to circular ring and further to the modified circular ring FSS structure. Section 3.4 discusses numerical analysis of the proposed modified circular ring FSS structure. Section 3.5 discusses the angular and polarization stability of the proposed modified circular ring FSS structure at 3 GHz, 13.5 GHz and 26 GHz for the perpendicular and parallel polarized wave incidence up to 50^o. Finally, the work concludes in Section 3.6.

3.2 GENERALIZED SYNTHESIS TECHNIQUE FOR DIELECTRIC BACKED SSLFSS

Among the several numerical techniques, we have used EC technique because it provides simpler, rapid and accurate frequency response. The synthesis technique to compute the geometrical parameters of the dielectric backed SSLFSS structure is discussed in Fig. 3.1. In this synthesis approach, the width of the conducting strip (w) and inter-element gap (g) has been interpreted in terms of its EC and provide the normalized mathematical expressions of its associated inductance and capacitance. On the multiplication of these two normalized mathematical equations, we have achieved the resonance criteria. Ideally for the reflective FSS structure, the value of $\omega_r^2 LC$ must be equal to unity at the resonance frequency such that $\omega_r^2 = 1/LC$, therefore, the expression for the resonant criteria has been modified as shown in Fig. 3.1. Further, in order to simplify the synthesis technique of the FSS structure, we have considered the loosely packed array of FSS structure with negligible width of the conducting patch of the unit-cell element and inter-element gap between the unit-cell elements as compared to twice of the periodicity (p). Moreover, the periodicity of the bandpass SSLFSS structure has been given as [2]:

$$p(1 + \sin\theta) < \lambda/2 \tag{3.1}$$

where, θ and λ is the AOI and wavelength corresponding to the operating frequency, respectively. In order to satisfy the Equation (3.1), we have considered AOI, $\theta = 10^o$ for normal wave incidence, therefore, Equation (3.1) is modified as follows: $p(1 + \sin\theta) = \lambda/2$.

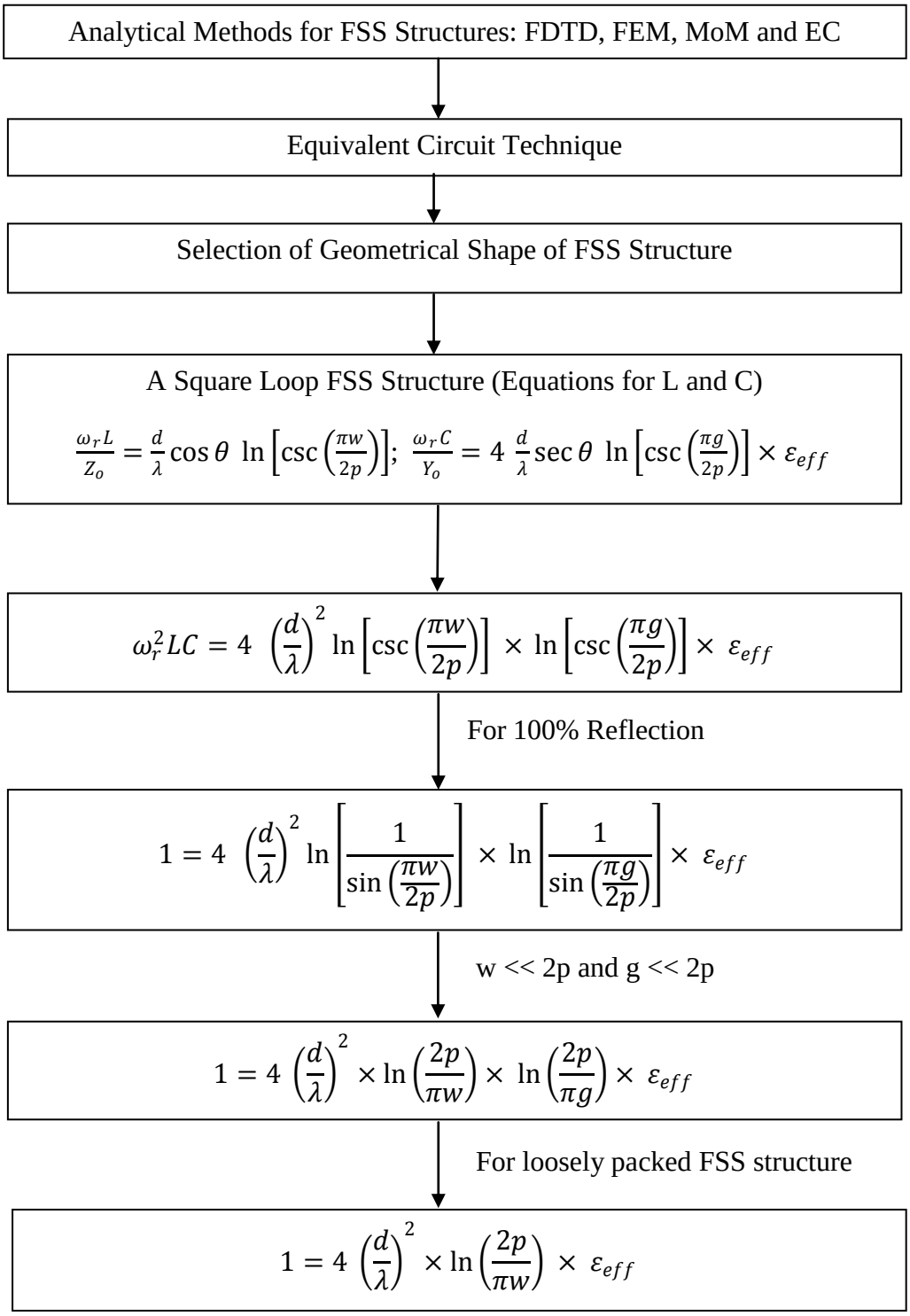

Fig. 3.1 The generalized synthesis approach for the dielectric backed SSLFSS structure.

The geometrical parameters of the dielectric backed SSLFSS structure at 3 GHz, 13.5 GHz and 26 GHz have been computed using the generalized synthesis technique (discussed in Fig. 3.1), which are given in Table 3.1.

Table 3.1 The geometrical parameters of SSLFSS structure at 3 GHz, 13.5 GHz and 26 GHz.

Frequency (GHz)	*p* (mm)	*d* (mm)	*w* (mm)
3	42.51	25.02	1
13.5	9.465	5.5594	0.2222
26	6.25	3.3598	0.125

3.3 STRUCTURE TRANSFORMATION

We have transformed the synthesis technique of the SSLFSS structure on the circular ring FSS because the circular ring FSS structure is more angular stable as compared to that of the square loop FSS. From the mode matching technique as reported in [172, 173], it is illustrated that for the same values of *p*, *w* and *d*, the ratio of perimeter of the square loop (P_{SL}) to the circumference of circular ring (C_{Cir}) is equal to the ratio of the resonance frequency of the circular ring (f_{r2}) to that of the resonance frequency of the square loop (f_{r1}). In other words, the P_{SL}, C_{Cir}, f_{r1} and f_{r2} are related as follows.

$$P_{SL}/C_{Cir} \cong f_{r2}/f_{r1} \cong K \tag{3.2}$$

From Equation (3.2), it is revealed that the $K > 1$ for the same value of *p*, *d* and *w*. In addition to this, the Equation (3.2) illustrated that the resonance frequency of circular ring FSS structure is greater than that of the square loop FSS structure and the value of *K* is approximately equal to 1.273. To validate this concept, this ratio is computed using CST Microwave Studio for various loosely coupled FSS structures with arbitrarily selected dimensions such as *p*, *d*, and *w* as shown in Table 3.2.

Further, the resonance frequencies obtained from the simulation have been represented in Fig. 3.2, which demonstrates several resonance frequencies placed in Table 3.2. In Fig. 3.2, the annotation I and II indicate the resonance frequency of the square loop and circular ring FSS structure, respectively for the dimensions mentioned in the second row of Table 3.2. Similarly, the responses of square loop and circular ring FSS structure of third row of the Table 3.2 are indicated by annotation III and IV, respectively. Further, for last two rows, the responses of the square loop and circular ring FSS structure are indicated by V and VI, VII, and VIII, respectively. From Table 3.2 and Fig. 3.2, it is illustrated that for the same dimensions, the circular ring FSS structure resonance frequency may be obtained from the knowledge of the

SSLFSS structure's geometrical parameters.

Table 3.2 The comparison of the resonance frequency of square loop and circular ring FSS structure.

p (mm)	d (mm)	w (mm)	$4\times d$ (square loop) (mm)	$\pi \times d$ (circular ring) (mm)	f_{r1} (GHz) (CST MWS)	f_{r2} (GHz) (CST MWS)	f_{r2}/f_{r1}
50	40	4.0	160	125.663	2.5600	3.2200	1.25
30	20	1.0	80.0	62.8310	4.7940	5.8440	1.21
8.0	5.0	0.2	20.0	15.7070	19.692	23.844	1.21
5.0	3.0	0.1	12.0	9.42400	31.097	37.877	1.21

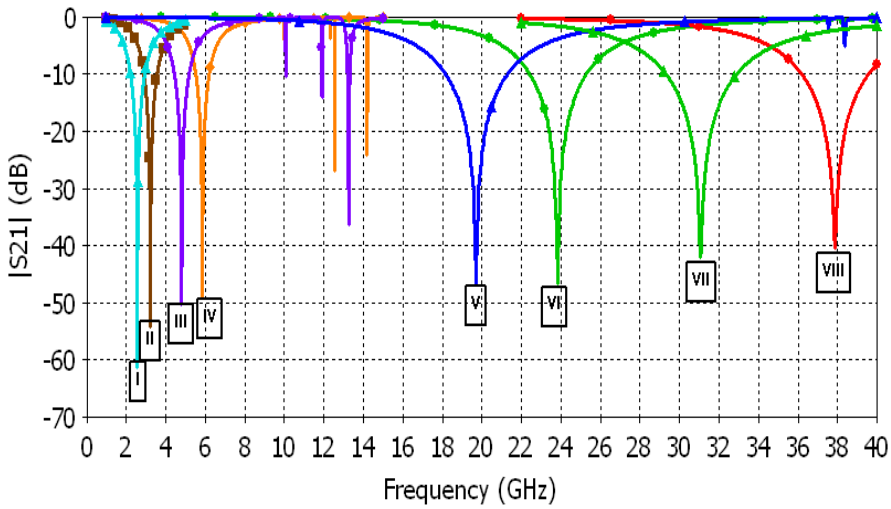

Fig. 3.2 The comparison of the frequency response of square loop and circular ring FSS structure.

However, for the square loop FSS array, the effect of inter-element gap capacitance is more significant in comparison to that of the circular ring FSS as the distance between the adjacent unit-cells (m=g) is always fixed as shown in Fig. 3.3(a) whereas in the circular ring FSS array, the distance between adjacent unit-cells (m=g) varies when moves between ± 90^o with respect to the line crossing the 0^o through the centre as shown in Fig. 3.3(b). Therefore, in the circular ring FSS structure, the resonance frequency mainly depends upon its inductance. However, for the significant implementation of the synthesis technique of the SSLFSS on the circular ring, we need to reduce the resonance frequency of a circular ring FSS structure up to the desired value, which is equal to that of the SSLFSS structure and is achieved by increasing the size of circular ring FSS structure. However, with the increase in the

effective size of the circular ring FSS, the value of p is increased, which reduces the angular stability of the structure and affects its miniaturization [1, 171]. To overcome this limitation and to achieve better angular stability, the four pairs of parallel straight conductors of length (l) have been inserted in the circular ring FSS structure, which modified the circular ring FSS (shown in Fig. 3.4(a)) into the proposed FSS structure (shown in Fig. 3.4(b)). The proposed modified circular ring FSS structure (shown in Fig. 3.4(b)) consists of metallic patch of the Aluminium foil with electrical conductivity σ = 3.8×10^{7} S/m, magnetic permeability μ = 1.2566×10^{-6} H/m and is placed on the Teflon substrate with relative dielectric permittivity ε_r = 2.1 and loss tangent 0.002.

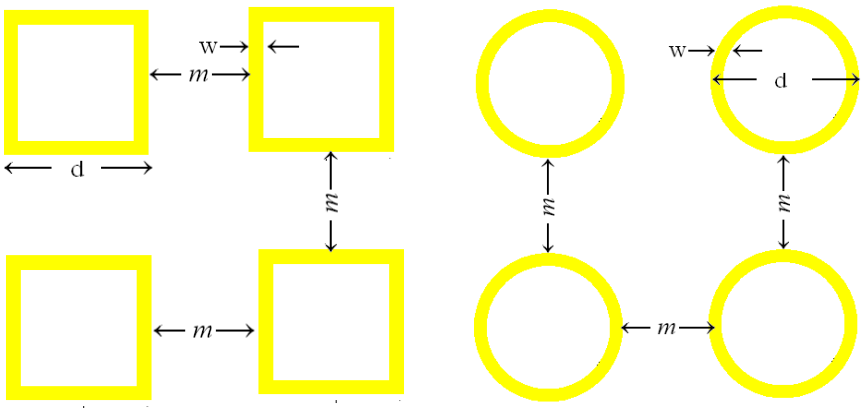

(a) (b)

Fig. 3.3 The array of (a) single square loop and (b) circular ring FSS structure.

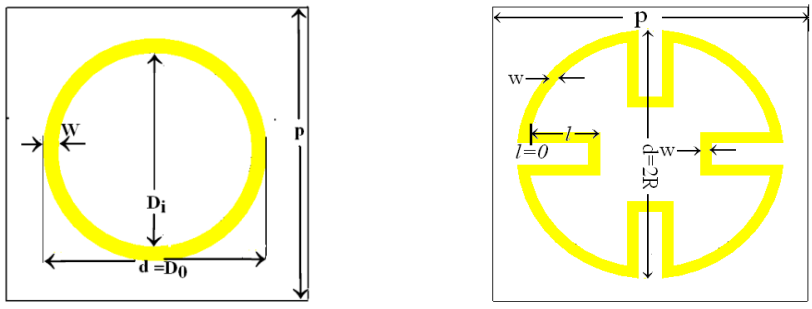

(a) (b)

Fig. 3.4 The unit-cell configuration of (a) circular ring and (b) proposed modified circular ring FSS structure.

3.4 NUMERICAL ANALYSIS

For the circular ring FSS structure, the value of inductance is given as [174].

$$L_1(nH) = 1.257 \times 10^{-6}.a\left[\ln\left(\frac{a}{w+t}\right) + 0.078\right].K_g \quad (3.3)$$

where $a = \frac{D_o+D_i}{4}$ and

$K_g = 0.57 - 0.145\ln\left(\frac{w}{h}\right)$; for $\frac{w}{h} > 0.05$

In Equation (3.3), a, D_o, D_i, h, w, t and K_g are the mean radius, outer diameter, inner diameter, substrate thickness, width of the conducting strip, thickness of metallic strip and correction factor (indicates the height of the substrate from the ground plane), respectively. In general, Equation (3.3) is used to obtain the value of the microstrip inductance above the grounded substrate and on the other hand, in FSS structures, the ground plane beneath the substrate is not used. Therefore, the correction factor K_g which provides the effect of electric field between the microstrip structure and the ground plane, is set equal to the unity [174]. In addition to this, the capacitance of the circular ring FSS structure is given as:

$$C = \frac{1}{(2\pi f_{r2})^2 L_1} \quad (3.4)$$

In Equation (3.4), C is the capacitance of the unit-cell of circular ring FSS structure. For a circular ring FSS structure, the value of f_{r2} is obtained using Equation (3.2) and the value of C is extracted by substituting the value of L_1 from Equation (3.3) into (3.4). Keeping the value of p, w and d same in both FSS structures (circular ring and proposed modified circular ring) indicates that the inter-element gap capacitance is approximately same and the value of C obtained by using Equation (3.4) has also been used as the inter-element gap capacitance of the proposed modified circular ring FSS structure (shown in Fig. 3.4(b)). Further, the downshift in the resonance frequency of the proposed modified circular ring FSS structure is controlled by varying the value of l, which influence the total inductance of the proposed FSS structure with its associated inductance L_2 and is given as:

$$L_2(nH) = 4 \times 10^{-4} l[\ln\left(\frac{l}{w+t}\right) + 1.193 + 0.333\left(\frac{w+t}{l}\right)]K_g \quad (3.5)$$

Therefore, the total inductance (L) of the proposed modified circular ring FSS structure is the sum of L_1 and L_2. For any value of l except zero, $L > L_1$ and the

resonance frequency of the proposed modified circular ring FSS structure (f_{MR}) is decreased without affecting the other parameters, which is given as [164]:

$$f_{MR} = \frac{1}{2\pi\sqrt{LC}} \tag{3.6}$$

where $L = L_1 + L_2$. With the decrease in resonance frequency, the wavelength (λ) in comparison to $l = 0$ is increased and due to this the ratio of period-to-the wavelength (p/λ) is decreased and the angular stability of the FSS has been increased [1].

3.5 FREQUENCY RESPONSE OF MODIFIED CIRCULAR RING FSS STRUCTURE

3.5.1 FREQUENCY RESPONSE AT 3 GHz

As demonstrated in Table 3.1, the geometrical parameters of dielectric backed SSLFSS at 3 GHz are: p = 42.51 mm, d = 25.02 mm and w = 1 mm. In addition to this, the thickness of dielectric substrate (h) and metallic conductor (t) for S-band is computed as: 10.00 mm and 0.01 mm, respectively. Using these geometrical parameters, the circular ring FSS structure resonate at 3.69 GHz, 3.672 GHz and 3.70 GHz analytically, CST Microwave Studio and Ansoft HFSS, respectively. It has already been discussed that the resonance frequency of the circular ring FSS structure mainly depends upon the inductance, therefore to resonate the circular ring FSS structure at lower frequency that is at 3 GHz without changing p and d, there is need to increase the value of inductance, which is achieved through the proposed modified circular ring FSS structure as shown in Fig. 3.4(b). When l = 0, the proposed modified circular ring FSS structure represents a circular ring FSS and in this case, the associated inductance L_1 and capacitance C is obtained by using Equation (3.3) and (3.4), respectively as well as the value of resonance frequency has been computed through Equation (3.2). In this case, the analytical value of the resonance frequency is 3.69 GHz and the corresponding value of the inductance L_1 and capacitance C is 38.49 *nH* and 48.38 *fF*, respectively. For any other values (except zero) of l, the inductance L_2 associated with the internally extended length of the four pairs of parallel straight conductors is obtained by using Equation (3.5) and on this way the total inductance L is the sum of L_1 and L_2, and the resonance frequency is obtained by Equation (3.6).

Table 3.3 The effect of *l* on the resonance frequency at 3 GHz.

l (mm)	*L* (*n*H)	*C* (*f*F)	f_{MR} (GHz) Analytical	f_{MR} (GHz) CST MWS	f_{MR} (GHz) Ansoft HFSS
0	38.49	48.38	3.69	3.672	3.70
3.2	45.13	48.38	3.41	3.384	3.40
4.0	48.76	48.38	3.27	3.252	3.30
4.8	51.75	48.38	3.18	3.132	3.20
5.6	55.45	48.38	3.07	3.000	3.00
6.0	56.89	48.38	3.05	2.940	3.00

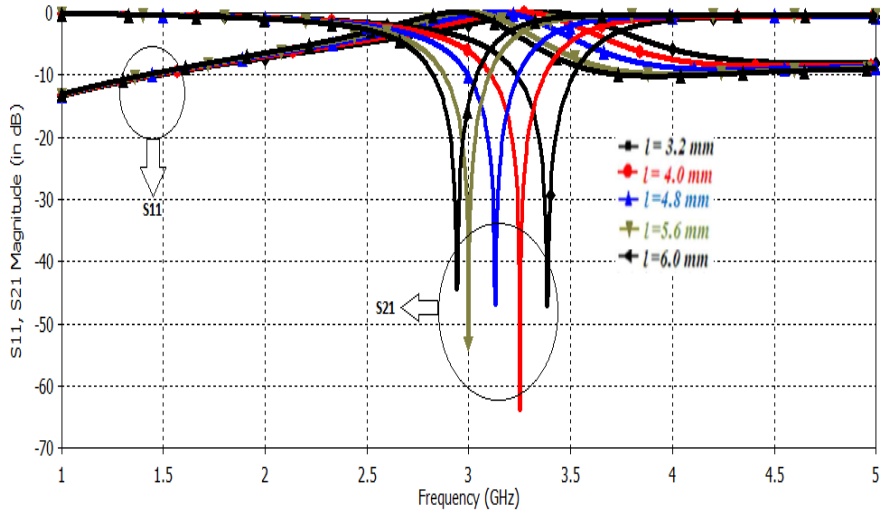

(a)

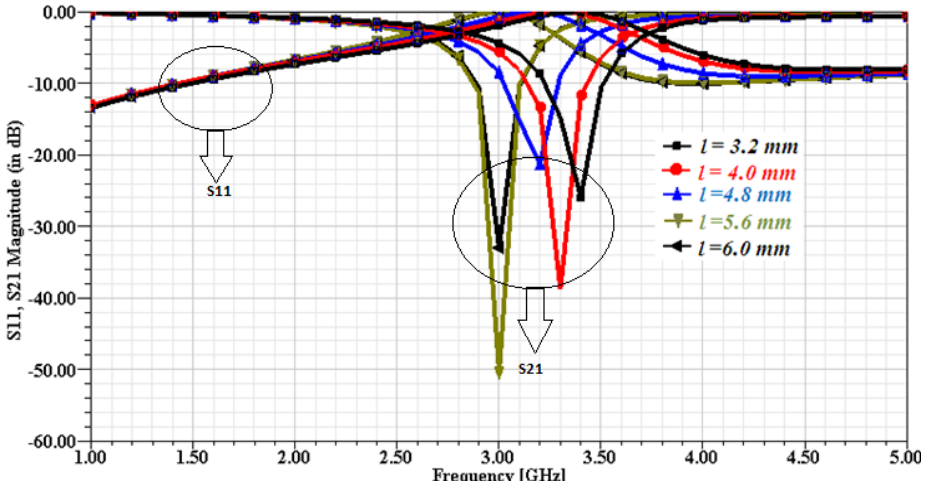

(b)

Fig. 3.5 The simulated frequency response of proposed structure as predicted in Fig. 3.4(b) over the transmission and reflection coefficients for various values of *l* using the (a) CST Microwave Studio and (b) Ansoft HFSS.

For different values of *l*, the analytically computed values of total inductance *L* and *C* are shown in Table 3.3. Further, with the increase of *l*, the resonance frequency shifts towards the intended frequency. The proposed FSS structure has been simulated for the different values of *l* using CST Microwave Studio and Ansoft HFSS to support the analytical frequency response at normal wave incidence as shown in Fig. 3.5(a) and Fig. 3.5(b), respectively. Table 3.3 and Fig. 3.5 have demonstrated that the proposed modified circular ring FSS structure with internally extended length l = 5.6 mm provides close agreement with the intended frequency in terms of the reflection/transmission frequency response. Therefore, the geometrical parameters of the proposed modified circular ring FSS structure at 3 GHz are obtained as: p = 42.51 mm, d = 25.02 mm, w = 1 mm and l = 5.6 mm.

3.5.2 ANGULAR AND POLARIZATION STABILITY AT 3 GHz

Due to the internal elongation of length in the proposed FSS structure as shown in Fig. 3.4(b), the resonance frequency and p/λ is reduced, which significantly enhance the angular stability. In order to demonstrate this effect, the proposed modified circular ring FSS structure with l = 5.6 mm is simulated for the perpendicular and parallel polarized wave incidence up to 50^{o}AOI.

For the perpendicular polarized wave incidence up to 50^{o}, the f_{MR} downshift with 3.30 % and 3.00 % with respect to the normal incidence, which has been obtained using CST Microwave Studio (shown in Fig. 3.6(a)) and Ansoft HFSS (shown in Fig. 3.6(b)), respectively. This angular stability has been achieved by considering the smaller value of the periodicity (p) as well as appropriate dielectric profile for the FSS structure, which provide the significant effect on the associated *L* and *C*. In addition to this, the percentage decrease in 3-dB reflection/transmission bandwidth for perpendicular polarized wave incidence up to 50^{o} is 3.15 % (shown in Fig. 3.6(a)) and 3.28 % (shown in Fig. 3.6(b)) using CST Microwave Studio and Ansoft HFSS, respectively as compared to that of the normal incidence. Further, the FBW of the proposed FSS structure for 0^{o}, 10^{o}, 30^{o} and 50^{o} are 28.87%, 28.47%, 28.45% and 28.91%, respectively, through CST Microwave Studio and 29%, 28.95%, 28.79% and 28.94%, respectively, through the Ansoft HFSS. It is important to note that the FBW is greater than 28% even at the 50^{o} of AOI.

Moreover, for the parallel polarized wave incidence up to 50^{o}, the 1.07 % and 0.66 % downshift in the resonance frequency has been achieved using CST Microwave Studio (shown in Fig. 3.7(a)) and Ansoft HFSS (shown in Fig. 3.7(b)), respectively as compared to that of the normal incidence. However, the percentage decrease in 3-dB reflection/transmission bandwidth for parallel polarized wave incidence up to 50^{o} AOI is 3.21 % and 2.64 % using CST Microwave Studio Ansoft HFSS as compared to the normal incidence. Further, the FBW of the proposed FSS structure for 0^{o}, 10^{o}, 30^{o} and 50^{o} are 23.73%, 23.41%, 23.00% and 23.24%, respectively, using CST Microwave Studio and 23.98%, 24.0%, 23.82% and 23.52%, respectively, using Ansoft HFSS.

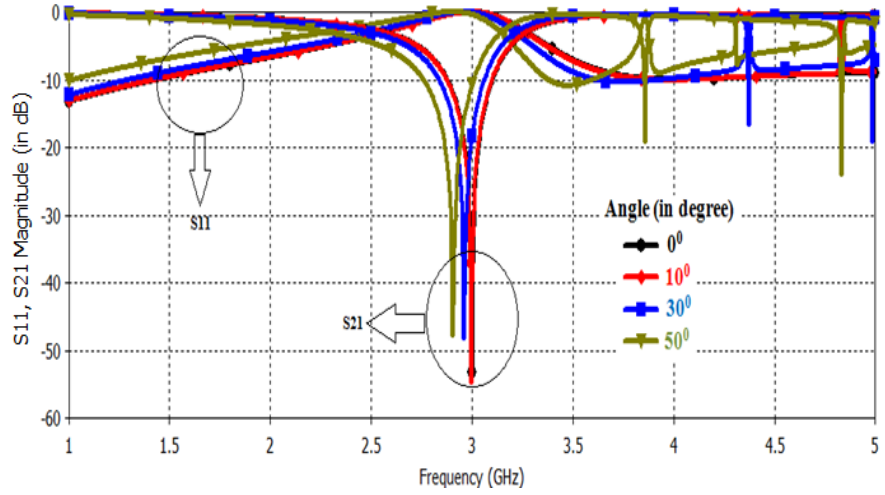

(a)

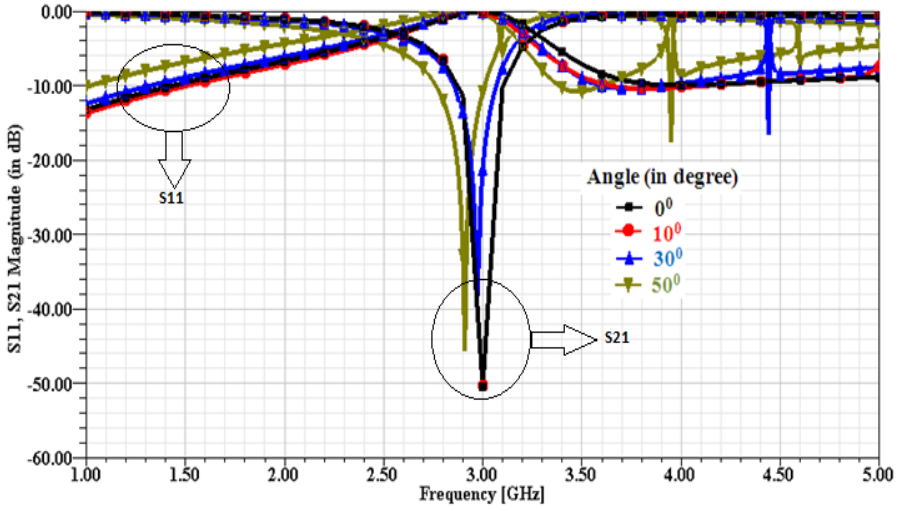

(b)

Fig. 3.6 The effect of AOI on the resonance frequency of proposed FSS structure at S-band for the perpendicular polarized wave using the (a) CST Microwave Studio and (b) Ansoft HFSS.

From the EC point of view, the proposed modified circular ring FSS structure has been represented by a single series LC circuit, which is shunted across a transmission line of impedance Z_o, where Z_o is the characteristic impedance of free-space and is equal to the 377Ω. However, with increasing the AOI as 0^o, 10^o, 30^o and 50^o, the value of inductance decreases as 55.45 *nH*, 54.60 *nH*, 48.02 *nH* and 35.64 *nH*, respectively due to increase in the value of Z_o which results the increase in the out-of-band rejection level and decreases the 3-dB reflection/transmission bandwidth, and provides the narrow bandwidth as shown in Fig. 3.6 and Fig. 3.7.

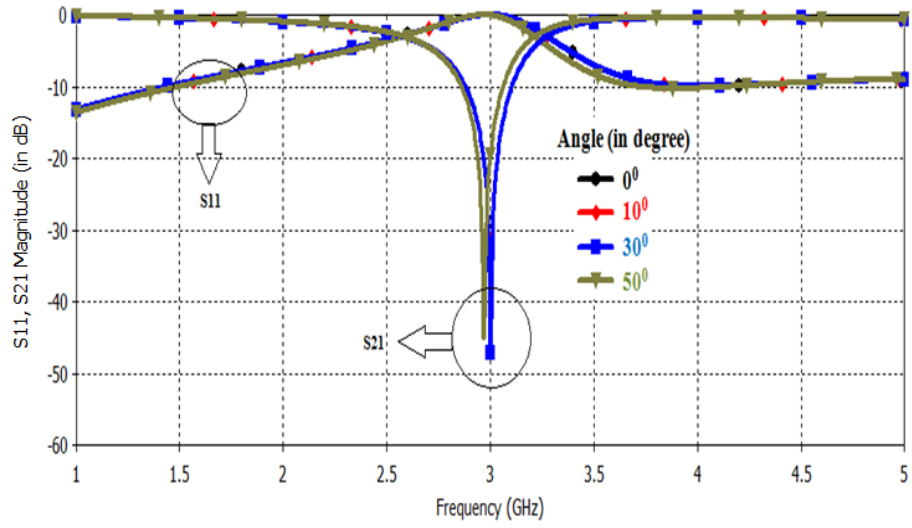

(a)

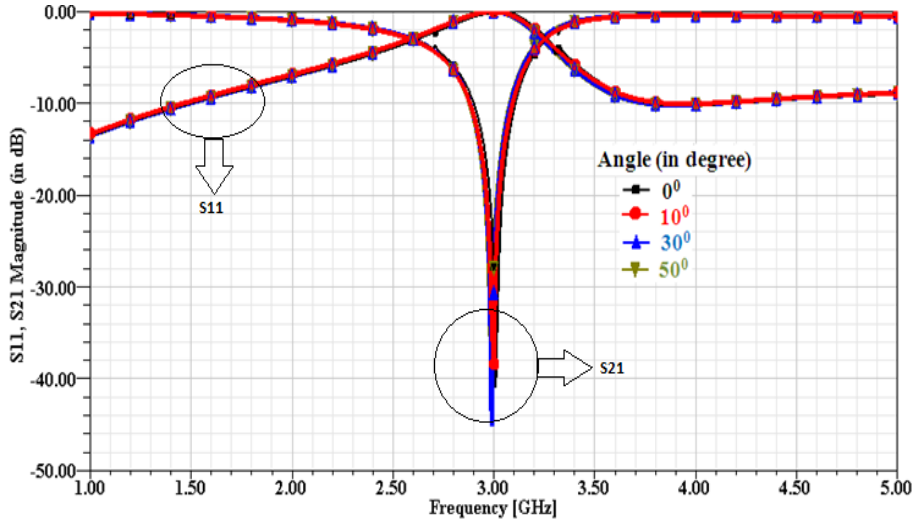

(b)

Fig. 3.7 The effect of AOI on resonance frequency of the proposed FSS structure at S-band for parallel polarized wave using (a) CST Microwave Studio and (b) Ansoft HFSS.

In addition to this, Fig. 3.6 and Fig. 3.7 demonstrate that the perpendicular polarization offers significantly small variations in the frequency response characteristics as compared to that of the parallel polarization because it lies on the symmetrical configuration of the FSS structure. Moreover, in order to discuss the generic nature of the proposed modified circular ring FSS structure, the proposed structure is also discussed at 26 GHz and 13.5 GHz for the perpendicular and parallel polarized wave incidence up to 50^{o} AOI. The geometrical parameters of the dielectric backed SSLFSS structure at 26 GHz and 13.5 GHz are discussed in Table 3.1, which are computed using the generalized synthesis approach discussed in Fig. 3.1. From the structural transformation discussed in section 3.3, the geometrical parameters of the proposed modified circular ring FSS structure are computed at 26 GHz and 13.5 GHz.

3.5.3 FREQUENCY RESPONSE AT 26 GHz

Using the geometrical parameters that is *p*, *w* and *d* discussed in Table 3.1 for 26 GHz, the dielectric backed SSLFSS structure resonate at 26 GHz with CST Microwave Studio, which is shown in Fig. 3.8. When the same value of *p*, *d*, and *w* are used to design a circular ring FSS structure, the simulated resonance frequency of the structure is 33.68 GHz as shown in Fig. 3.8, which is 1.29 times greater than that of the square loop FSS structure.

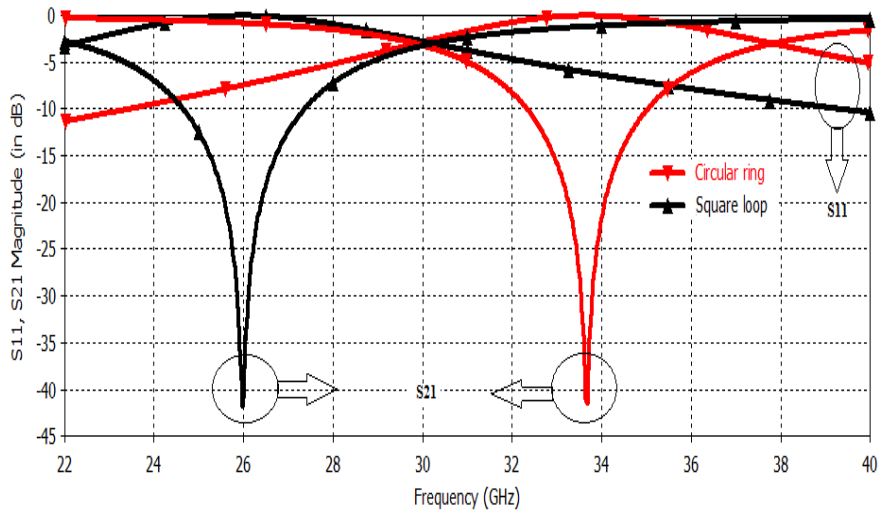

Fig. 3.8 The reflection and transmission parameters frequency response of the SSLFSS and circular ring FSS structure at 26 GHz.

Table 3.4 The effect of the *l* on the resonance frequency at 26 GHz.

l (mm)	L (nH)	C (fF)	f_{MR} (GHz) (Analytically)	f_{MR} (GHz) (Ansoft Designer)	f_{MR} (GHz) (CST MWS)
0	7.7115	2.996	33.11	33.115	33.38
0.5	10.2360	2.996	28.73	28.74	29.61
0.6	10.9115	2.996	27.83	27.83	28.48
0.7	11.6131	2.996	26.98	26.91	27.34
0.8	12.3377	2.996	26.17	26.18	26.21
0.9	13.0824	2.996	25.42	25.42	25.11
1.0	13.8448	2.996	24.71	24.72	24.10

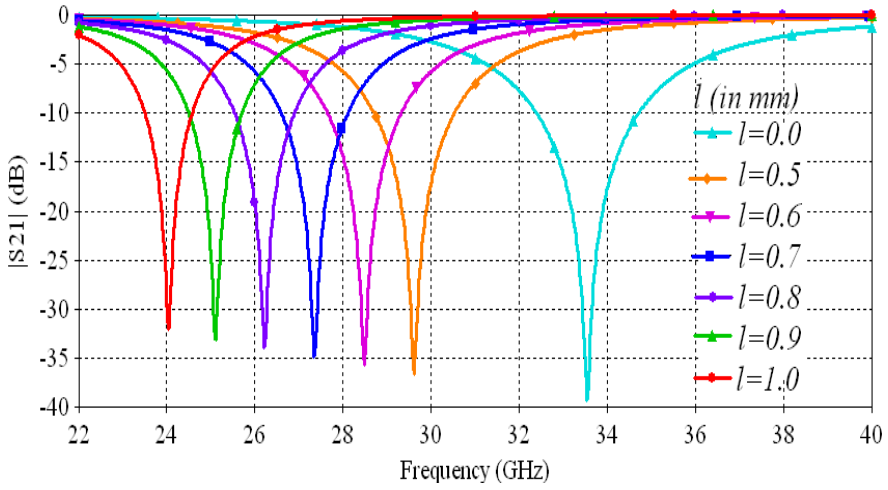

Fig. 3.9 The effect of *l* on the frequency response of the proposed modified circular ring FSS structure for various values of *l* (mm) using CST Microwave Studio.

Table 3.5 The geometrical parameters of proposed modified circular ring FSS structure at 26 GHz and 13.5 GHz.

Structure Parameters	Dimension at 26 GHz (mm)	Dimension at 13.5 GHz (mm)
Periodicity (*p*)	6.25	9.465
Size (*d*)	3.398	5.5594
Strip-width (*w*)	0.25	0.2222
Screen thickness (*t*)	0.02	0.02
Length (*l*)	0.8	1.0
Substrate Thickness (*h*)	0.5	0.5

For the significant implementation of the proposed synthesis technique on the circular ring FSS, it is required to resonate the circular ring FSS structure at the same resonance frequency as that of the square loop FSS structure that is at 26 GHz, which may be obtained by increasing the values of *p* and *d*. However, increasing the values

of p and d affects the miniaturization and angular stability of circular ring FSS structure. Therefore, the circular ring FSS (shown in Fig. 3.4(a)) is modified to the structure shown in Fig. 3.4(b). The effect of l of the proposed modified circular ring FSS structure on the resonance response at 26 GHz is demonstrated in Table 3.4, which reveals that the resonance frequency response computed numerically and using EC model nearly close to each other but the response deviate a bit in CST Microwave simulation as it takes into account the parameters such as the effect of conductor thickness, the port effect and computational domain of the simulator. However, these frequency responses are still found comparable.

The effect of variation in the length l on the resonance frequency obtained by using CST Microwave Studio is shown in Fig. 3.9 which clearly reveals that the resonance frequency deceases with the increasing value of l due to increase in L_2. As shown in Table 3.4 and Fig. 3.9, at l = 0.8 mm, the proposed modified circular ring FSS structure resonate close to the desired resonance frequency, which is 26 GHz. On this way, the geometrical parameters of proposed modified circular ring FSS structure are calculated at 26 GHz and 13.5 GHz, which are demonstrated in Table 3.5.

3.5.4 ANGULAR AND POLARIZATION STABILITY AT 13.5 GHz AND 26 GHz

The frequency response of the proposed modified circular ring FSS structure for perpendicular and parallel polarized wave incidence up to 50^o is analyzed at 26 GHz and 13.5 GHz, which has been shown in Fig. 3.10 and Fig. 3.11, respectively. The performance of the proposed modified circular ring FSS structure in terms of the reflection/transmission characteristics at 26 GHz simulated using CST Microwave Studio for the perpendicular and parallel polarized wave incidence up to 50^o AOI have been demonstrated in Fig. 3.10(a) and Fig. 3.10(b), respectively. For the perpendicular and parallel polarization wave incidence up to 50^o AOI, the shift in the resonance frequency is 1.97 % and 1.07 %, respectively with reference to the normal wave incidence. As, in Fig. 3.10(a), it has been shown that for perpendicular polarized wave incidence at 50^o, the grating lobes approaches the resonance frequency in the operating band, which reduces the 3-dB bandwidth. The grating lobes have been moved away from the resonance frequency by further reducing the value of

periodicity [2], which further improves the angular stability and its miniaturization. However, theoretically, for the symmetric structure, in both modes of propagation that is perpendicular and parallel there should be the same resonance frequency.

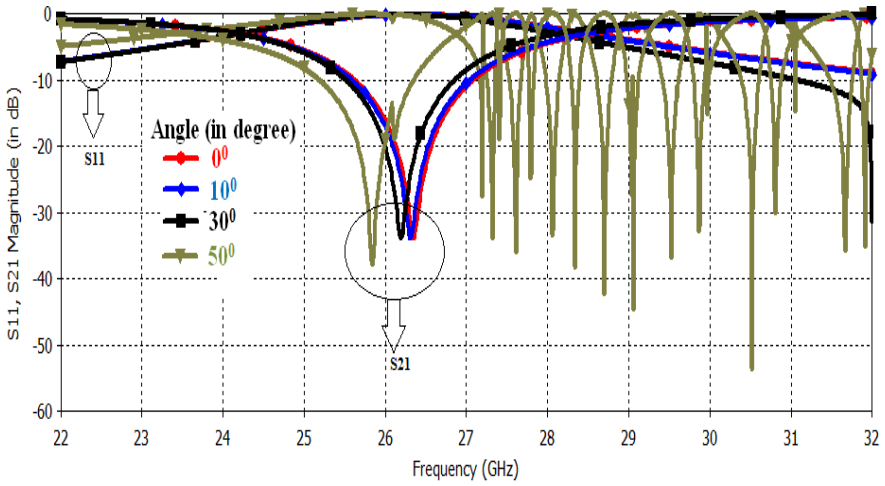

(a)

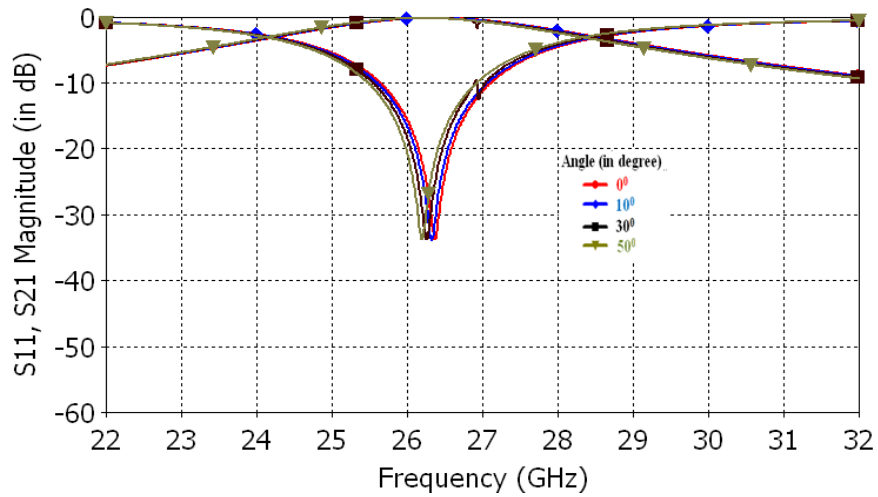

(b)

Fig. 3.10 The effect of AOI on the resonance frequency of the proposed modified circular ring FSS structure at 26 GHz for (a) perpendicular and (b) parallel polarized wave incidence up to 50^{o} AOI through CST Microwave Studio.

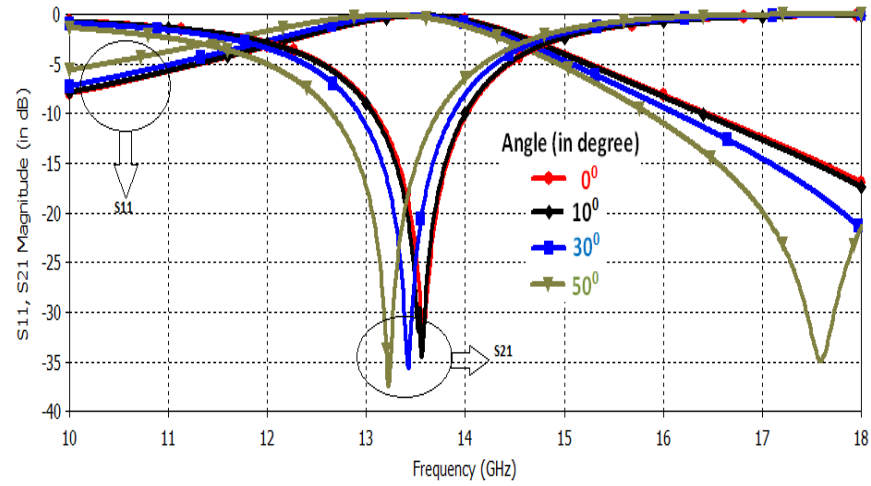

(a)

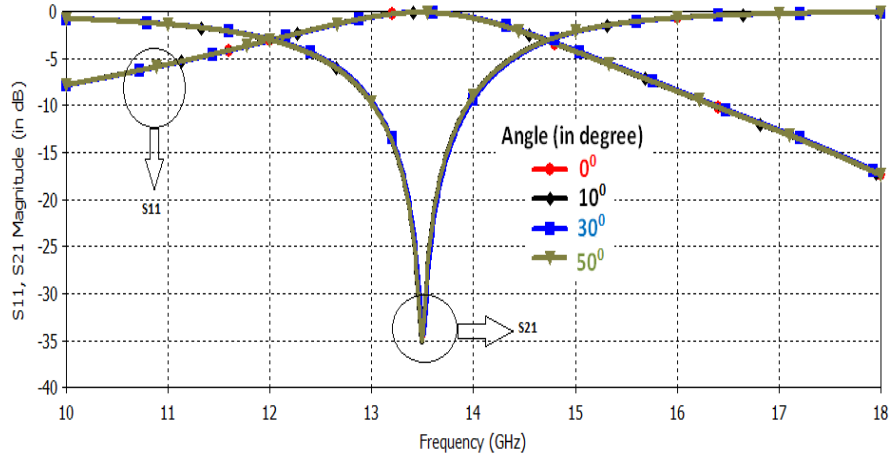

(b)

Fig. 3.11 Effect of AOI on the resonant frequency of the proposed bandstop FSS structure at 13.5 GHz for (a) perpendicular and (b) parallel polarized wave incidence up to 50^{o} AOI through CST Microwave Studio.

On the other hand, Fig. 3.11(a) demonstrates that the proposed structure resonates at 13.57 GHz for the perpendicular polarized wave and Fig. 3.11(b) demonstrates that the structure resonates at 13.50 GHz for the parallel polarized wave incidence at 0^{o}, which results a discrepancy of about 0.7 GHz. This kind of deviation in the simulation response is attributed to the simulation problem mainly due to the meshing. As, the number of mesh cells needed for two differently polarized waves is different for the same adaptive meshing criteria in CST Microwave Studio, hence the deviation is attributed to the simulation set-up and meshing of structure.

For the perpendicular and parallel polarized wave incidence up to 50^o AOI, the shift in the resonance frequency is 1.89 % and 0.12 %, respectively at 13.5 GHz as shown in Fig 3.11. The FBW at 13.5 GHz and 26 GHz for the perpendicular and parallel polarized wave incidence up to 50^o AOI is discussed in Table 3.6. From these two designs, it is observed that the FBW is greater than 16% even at the 50^o AOI, which is significantly high.

Table 3.6 The FBW of proposed FSS structure at 13.5 GHz and 26 GHz for perpendicular and parallel polarized wave incidence up to 50^o AOI.

AOI	% FBW (at 26 GHz)		% FBW (at 13.5 GHz)	
	Perpendicular Polarization	Parallel Polarization	Perpendicular Polarization	Parallel Polarization
0^o	16.5	16.17	23	19.94
10^o	16.41	16	20.22	19.84
30^o	15.16	16.12	20.1	19.7
50^o	15.04	15.87	19.92	19.67

Table 3.7 Results of comparison of the frequency deviation of the proposed FSS structure to other FSS structures.

AOI	Reported Literature	FSS structure	% deviation of f_r
45^o	Lee and Langley [162]	Gridded and	7
45^o	Reed [163]	Rectangular	16.6
45^o	Sung et al [175]	Square Loop	10
45^o	Yan et al [176]	Spiral Meander	5
45^o	Parker and Hamdy [177]	Circular Ring	5.95
45^o	Hosseinipanah et al. [178]	Square Loop	5.45
50	Structure shown in Fig. 3.4(b)		1.97 (TE), 1.07 (TM) - 26 GHz 1.89 (TE), 0.12 (TM) - 13.5 GHz 3.12 (TE), 0 .66 (TM)- 3 GHz

Moreover, for the comparison of frequency deviation of the proposed modified circular ring FSS structure with the other FSS structures, which have been reported in literature are listed in Table 3.7. However, Lee and Langley [162] have presented an improved EC model to analyze the gridded-square and double-square FSS structure at oblique angle for perpendicular and parallel polarization states, which provide frequency response comparable with the measured response. In [163], a thin, planar

and perfectly conducting rectangular FSS is analyzed using modal method, which offers comparable frequency response that of the measured response. Sung et al [175] have discussed the angular behaviour of a bandstop square loop FSS up to 45^{o} using EC model, which provides a downshift in the resonance frequency as compared to that of the normal wave incidence with at least 30-dB attenuation. In [176], a bandpass miniaturized FSS, which consists of four symmetrical spiral patterns of metallic meander lines printed on one side of a substrate, is discussed for the different polarizations and incidence angles. Moreover, the main focus is on the miniaturization, which is also compared with various existing literatures [176]. In [177], the angular sensitivity of the circular ring FSS structure up to 45^{o} is discussed on the closely packed square and triangular lattices, which offer maximum deviation of 5.95 % in the resonance frequency as compared to that of the normal incidence, ~ 26 % reflection bandwidth and 3:1 transmission/reflection band ratios. Hosseinipanah et al [178] have discussed the angular stability of the bandpass square loop FSS structure at 2 GHz using simulation (CST Microwave Studio) and EC technique, which reduces the specific absorption rate (SAR) of staff/people working in indoor environment near to radar antenna and the possibility of interference in wireless local area network (WLAN) system.

3.6 CONCLUSION

In this Chapter, the generalized synthesis technique of dielectric backed SSLFSS structure is discussed, which is further used to compute the geometrical parameters such as periodicity, diameter, extension length and width of the conducting strip of the bandstop modified circular ring FSS structure at 3 GHz, 13.5 GHz and 26 GHz. The proposed synthesis technique reduces the number of iterations to determine the geometrical parameters of FSS structure. The analytical and simulation results have revealed that the proposed modified circular ring FSS structure is highly angular and polarization stable with maximum deviation of 3.12 % and 0.66 % in the resonance frequency for the perpendicular and parallel polarized incidence up to 50^{o}, respectively. In addition to this, the proposed modified circular ring FSS structure is simple in terms of the fabrication and provides ~ 28 % (at 3GHz) and ~ 16 % (at 26 GHz and 13.5 GHz) FBW up to 50^{o} AOI.

CHAPTER-4

DESIGN AND ANALYSIS OF BANDPASS MODIFIED CIRCULAR RING FSS STRUCTURE

4.1 INTRODUCTION

FSS structures have potential to impart the bandstop and bandpass spatial filtering characteristics depending upon their application requirements [2]. Ideally, the bandstop and bandpass FSS structures provide the total reflection and transmission characteristics at the resonance frequency, respectively [163]. However, various researchers have discussed different geometrical shapes of the bandstop FSS structures, which allow the propagation of direct current signals through it, which are not suitable for various applications as discussed in [2]. Therefore, the demand of designing the bandpass FSS structures has been increased and are very much significant for the modification of electromagnetic (EM) architecture of the buildings, which is essential in order to accommodate the advanced and imminent wireless technologies [179, 180]. As discussed in Chapter-3 that the angular and polarization stability are the important aspect of FSS structure design, which has to be explored in order to enhance the spectral performance of FSS structures. In view of designing the novel FSS structures, dual-band bandpass FSS with four symmetrical spiral patterns of metallic meander line printed on FR4 dielectric substrate as demonstrated in [111] and, the actively loaded (with varactor diode and surface mount capacitor) circular ring FSS structure as demonstrated in [92] has been discussed. Kiani et al. [129] have explored two-layer absorb/transmit FSS structure in which the first layer consists of conducting cross-dipole with a circular aperture in the centre and second layer uses resistive cross- dipole element for perpendicular and parallel polarized wave, respectively, up to 45^{o} of AOI. Further, the, the single-band bandpass FSS [176] and a single-band bandpass FSS with four spiral rectangles connected to a cross-line element in the middle [181], have been explored for both the perpendicular and parallel polarized wave incident up to 60^{o} AOI.

In this Chapter, the proposed modified circular ring FSS structure, which is backed with a dielectric substrate, is explored for the bandpass filtering characteristics. As,

the effect of the dielectric substrate on the resonance frequency of bandstop and bandpass FSS structure are different, therefore the synthesis technique of bandpass SSLFSS, which is backed with dielectric substrate is discussed. The synthesis technique of bandpass SSLFSS structure is further used to compute the geometrical parameters (*p*, *w* and *d*) of the bandpass modified circular ring FSS structure in the same way as it is discussed for the bandstop FSS structure (in Chapter-3). The unit-cell configuration of the modified circular ring bandpass FSS structure is shown in Fig. 4.1(a) along with its EC, which is shown in Fig. 4.1(b).

In this Chapter, a single-layer bandpass modified circular ring FSS structure, which provides very significant results in terms of the angular and polarization stability as compared to that of the reported tunable circular ring [92], cross-dipole with an aperture in the centre [129] and other several novel bandpass FSS structures as discussed in [111, 176, 181]. In addition to this, the proposed bandpass FSS also provides the significant angular and polarization stable frequency response as compared to that of the classical geometrical shapes (square loop and circular ring) of the FSS structure as discussed in [162, 163, 175, 177, 178]. The simple geometry of proposed bandpass FSS structure provides the ease of fabrication as compared to that of the tunable and fractal FSS structures. The proposed bandpass FSS results an angular stable structure up to 50^{o} of AOI for two principal orientations (perpendicular and parallel polarizations) relative to the incident plane wave in X-band regime of the electromagnetic spectrum. The proposed bandpass structure has been simulated using 3D electromagnetic commercially available simulators such as CST Microwave Studio and Ansoft HFSS. A prototype of the proposed bandpass FSS is fabricated and experimentally tested for s-parameters.

The remainder of chapter is organized as follows. Section 4.2 describes the approach that is the transformation of bandpass SSLFSS structure synthesis technique to obtain the geometrical parameters of the proposed bandpass modified circular ring FSS along with its material specifications. Section 4.3 discusses the frequency response at two different frequencies (26 GHz and 13.5 GHz), which includes the miniaturization at 26 GHz, and angular/polarization stability of the proposed modified circular ring bandpass FSS structure for the perpendicular and parallel polarized waves incidence up to 50^{o} AOI at these two frequencies. Section 4.4 discusses the prototype of

proposed modified circular ring bandpass FSS structure at 10.50 GHz and also presented its electric field distribution, angular and polarization stability of the structures. Finally, Section 4.5 concludes the work.

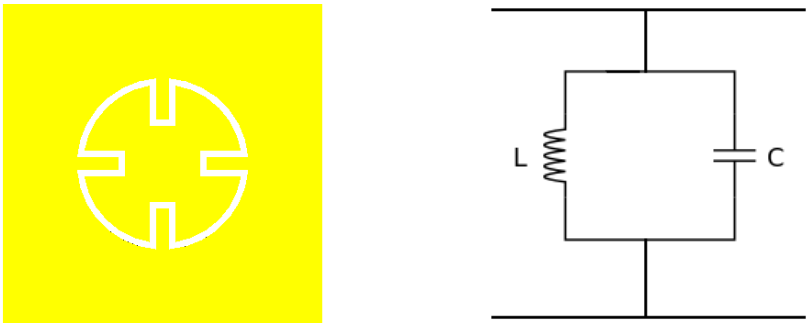

(a) (b)

Fig. 4.1 The proposed bandpass modified circular ring FSS structure (a) unit-cell configuration and (b) its equivalent circuit.

4.2 GENERALIZED SYNTHESIS TECHNIQUE

4.2.1 SINGLE-SQUARE-LOOP BANDPASS FSS STRUCTURE

It is very significant to study the unit-cell element of planar bandpass and bandstop FSS array because according to the Floquet theorem, a single unit-cell efficiently describes the field through the FSS array [163]. However, it is not suitable to compute the geometrical parameters of the bandpass FSS structure using the bandstop synthesis technique. Due to this reason, a synthesis technique of dielectric backed bandpass SSLFSS structure is discussed using the EC technique. According to EC approach, slot-width (w) and the inter-element conducting gap (g) in case of array of bandpass SSLFSS structure is responsible for the presence of capacitance (C) and inductance (L), respectively, which has been expressed in terms of the normalized mathematical expressions as shown in Fig. 4.2. On the multiplication of these normalized mathematical expressions, we have achieved the resonance criteria. Ideally, for achieving 100% transmission for bandpass FSS structure, the $\omega_r^2 LC$ in the achieved mathematical equation is replaced by unity, which is shown in Fig. 4.2. Moreover, in order to simplify the analysis of the bandpass SSLFSS structure, we have considered the loosely packed array of FSS structure with negligible slot-width (w) and inter-element conducting gap (g) as compared to twice of the periodicity (p).

In addition to this, the periodicity (p) of the bandpass SSLFSS structure is computed using Equation (3.1).

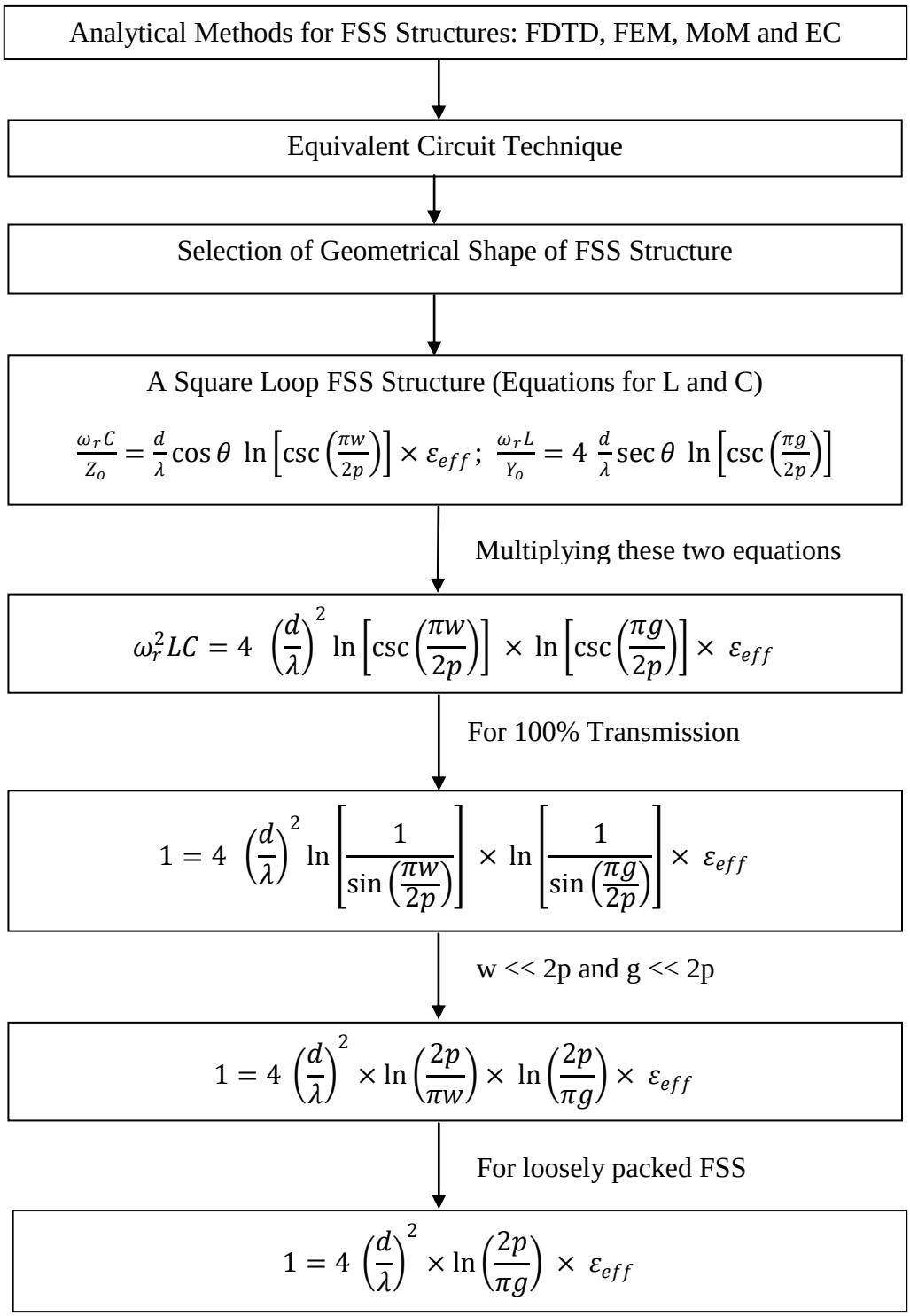

Fig. 4.2 A simple synthesis technique of bandpass SSLFSS structure.

By using the synthesis technique discussed in Fig. 4.2, we have computed the values of *p*, *w* and *d* of bandpass SSLFSS structure at 26 GHz and 13.5 GHz, which are presented in Table 4.1.

Table 4.1 The geometrical parameters of the proposed modified circular ring bandpass FSS structure.

Frequency (GHz)	*p* (mm)	*d* (mm)	*w* (mm)
26	9.83	2.88	0.11
13.50	18.93	5.77	0.2222

4.2.2 MODIFIED CIRCULAR RING BANDPASS FSS STRUCTURE

However, after computing the geometrical parameters of bandpass SSLFSS structure at three different frequencies, which are discussed in Section 4.2.1 and then using the structural transformation discussed in Section 3.3, we have computed the geometrical parameters of the bandpass modified circular ring FSS structure. The unit-cell element of proposed modified circular ring bandpass FSS structure, has a metallic sheet of copper with thickness, t = 0.02 mm and electrical conductivity, $\sigma = 5.8\times10^7$ S/m through which a modified circular ring is etched out and backed with commercially available dielectric substrate of certain thickness, relative dielectric permittivity and loss tangent. However, on simulating the bandpass SSLFSS and circular ring for the same values of the *p*, *w* and *d*, the bandpass circular ring also resonate at a higher frequency as compared to that of the SSLFSS. Further, the effect of four pairs of parallel straight slots of length (*l*) on the resonance response of bandpass modified circular ring FSS structure at 26 GHz is demonstrated in Fig. 4.3. Fig. 4.3 revealed that with increase in *l*, the resonance frequency downshifts and on this way, at *l = 0.450* mm, the proposed structure resonate at 26.04 GHz, which is close to the intended frequency, therefore the value of *l* (*mm*) has been selected as 0.450 for 26 GHz. For practical applications, various desired operating frequencies have been obtained by adjusting the *l* and ε_r. Theoretically, the longer *l* means the larger perimeter of the slot, which downshift the resonance frequency. In the similar way, the computed values of *p, w* and *d* of proposed modified circular ring bandpass FSS structure at 26 GHz and 13.50 GHz are shown in Table 4.2.

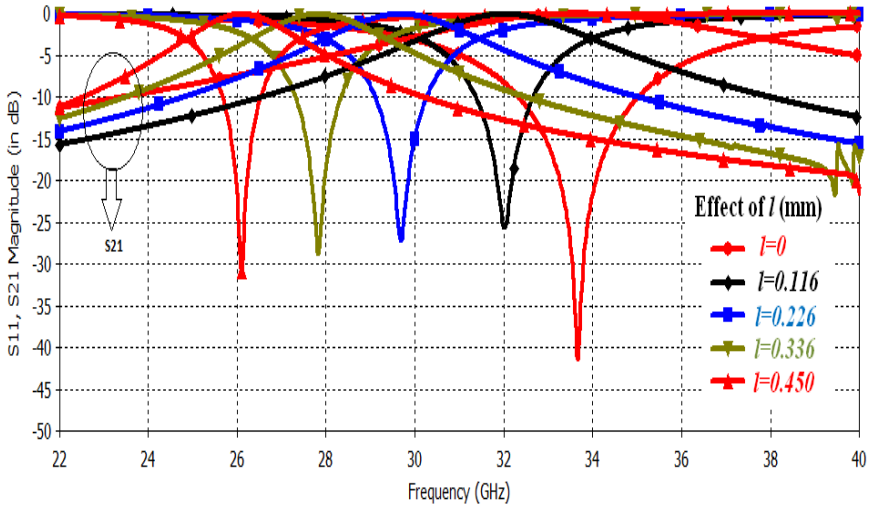

Fig. 4.3 The effect of *l* on the resonance frequency of the proposed bandpass FSS structure at 26 GHz.

Table 4.2 The geometrical parameters of proposed bandpass FSS structure at 26 GHz and 13.5 GHz.

Structure Parameters	Dimensions (mm) at 26 GHz	Dimensions (mm) at 13.5 GHz
Periodicity (*p*)	4.6	8.5
Slot diameter (*d*)	2.7998	5.3757
Slot width (*w*)	0.1042	0.20
Screen thickness (*t*)	0.02	0.02
Slot length (*l*)	0.450	0.950
Substrate thickness (*h*)	0.5	0.5

4.3 FREQUENCY RESPONSE AT 26 GHz and 13.5 GHz

4.3.1 MINIATURIZATION

For comparing the size of classical SSLFSS and proposed modified circular ring FSS structure, which have been operating at the same resonance frequency (26 GHz), the geometrical parameters are demonstrated in Table 4.3.

Table 4.3 The geometrical structure size comparison between the modified circular ring FSS and SSLFSS structure.

Element Type	*w* (*mm*)	*p* (*mm*)	Element Area (mm^2)	Resonance Frequency (GHz)
Proposed FSS	0.1042	4.6	21.16	26
SSLFSS	0.1042	9.83	96.62	26.04

For approximately same resonance frequency as demonstrated in Table 4.3, the proposed modified circular ring FSS structure has p = 4.6 mm as compared to p = 9.83 mm of classical SSLFSS structure, therefore, the size reduction is approximately 78%.

4.3.2 ANGULAR AND POLARIZATION STABILTY

We have discussed the angular and polarization stability of the proposed modified circular ring bandpass FSS structure for the perpendicular and parallel polarized wave incidence up to 50^{o} AOI at two different frequencies using CST Microwave Studio.

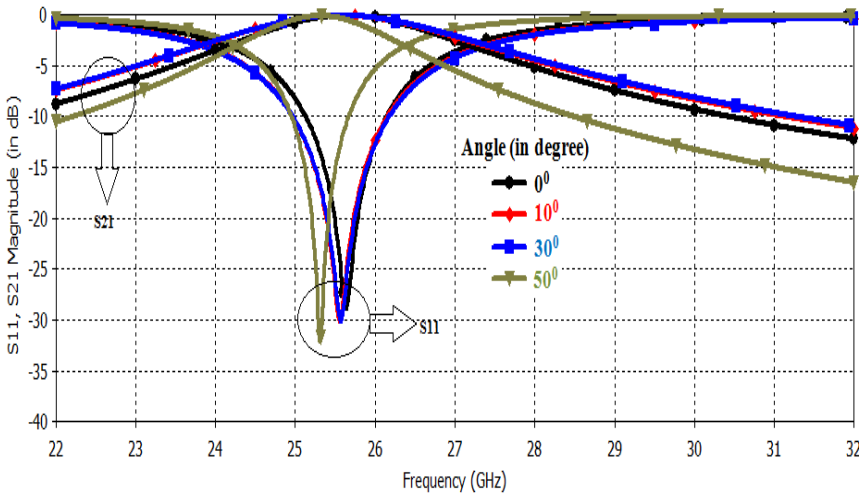

(a)

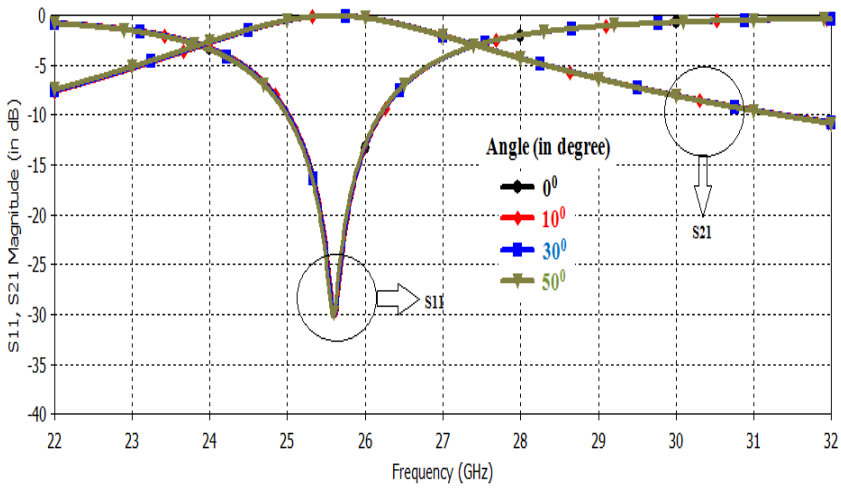

(b)

Fig. 4.4 The effect of AOI on the frequency response of proposed FSS structure by simulation using CST Microwave Studio at 26 GHz for (a) perpendicular and (b) parallel polarized incidence wave.

Fig. 4.4(a) and Fig. 4.4(b) demonstrate that the downshift in the resonance frequency is 1.30 % and 0.078 % at 26 GHz for the perpendicular and parallel polarized wave incidence up to 50^{o} AOI, respectively as compared to the normal incidence. In addition to this, Fig. 4.5(a) and Fig. 4.5(b) have demonstrated that the resonance frequency downshift with 1.09 % and 0.07 % at 13.5 GHz for the perpendicular and parallel polarized wave incidence up to 50^{o}, respectively as compared to the normal incidence. The FBW at 26 GHz and 13.5 GHz for the perpendicular and parallel polarized wave incidence up to 50^{o} AOI has been discussed in Table 4.4.

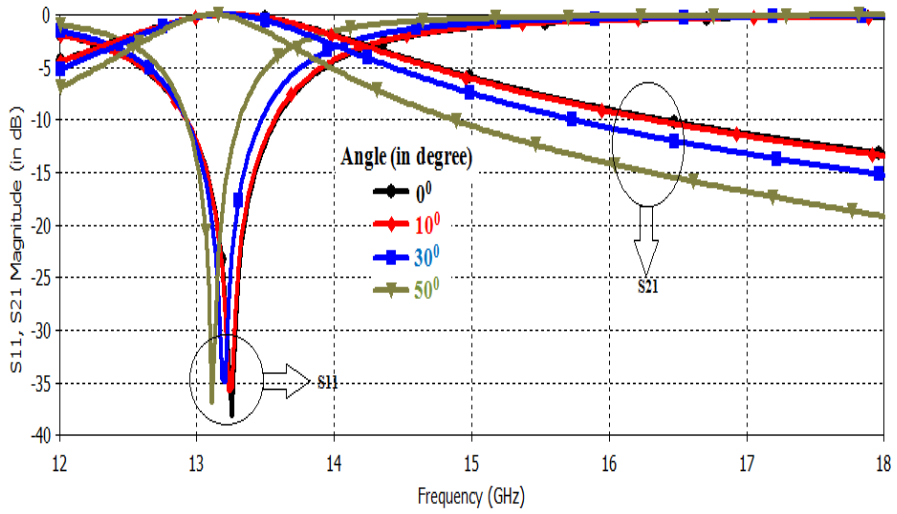

(a)

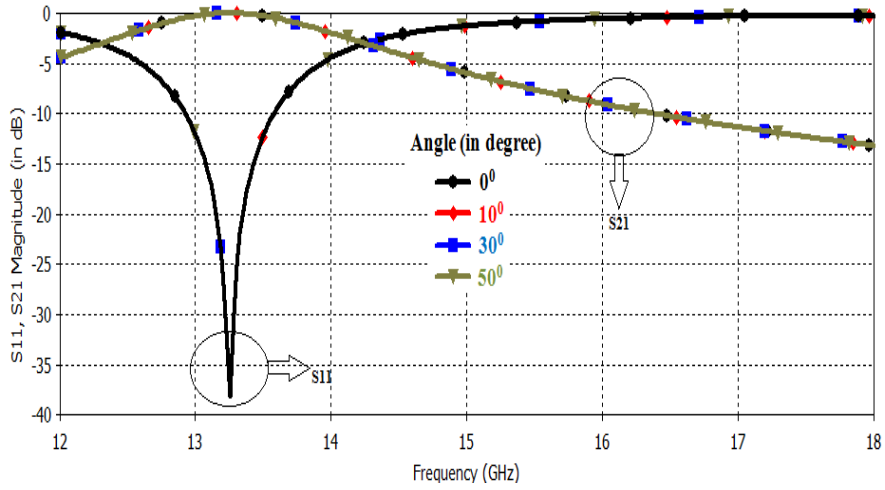

(b)

Fig. 4.5 The effect of AOI on the frequency response of proposed FSS structure by simulation using CST Microwave Studio at 13.5 GHz for (a) perpendicular and (b) parallel polarized incidence wave.

Table 4.4 The FBW of proposed FSS structure at 26 GHz and 13.5 GHz for perpendicular and parallel polarized wave incidence up to 50^o AOI.

AOI	% FBW (26 GHz)		% FBW (13.5 GHz)	
	Perpendicular Polarization	Parallel Polarization	Perpendicular Polarization	Parallel Polarization
0^o	15.10	15.24	15.04	14.95
10^o	15.06	15.23	15	14.95
30^o	15.05	15.23	14.99	14.94
50^o	14.83	15.20	14.94	14.93

4.4 FREQUENRESPONSE AT 10.50 GHz

However, the modified circular ring bandpass FSS structure in X-band has been fabricated and tested based on the available infrastructure. Using the generalized synthesis technique discussed in Fig. 4.2, we have computed the values of *p*, *w* and *d* as 9 mm, 6.10 mm and 0.40 mm, respectively of bandpass SSLFSS structure at 10.50 GHz. Further using the theory discussed in Section 4.2, the geometrical parameters (*p*, *w* and *d*) of the proposed bandpass modified circular ring FSS structure are computed, which are presented in Table 4.5.

Table 4.5 The geometrical parameters of proposed modified circular ring bandpass FSS structure at 10.50 GHz.

p (mm)	*d* (mm)	*w* (mm)	*t* (mm)	*l* (mm)	ε_r	Tanδ	*h* (*mm*)
9	6.9	0.46	0.02	1.08	3.2	0.0038	0.762

4.4.1 Electric field distribution, angular and polarization stability

Moreover, we have discussed the electric field distribution, angular and polarization stability of proposed modified circular ring bandpass FSS for the perpendicular and parallel polarized wave incidence up to 50^o at X-band (8-12.5 GHz). We have simulated the proposed modified circular ring bandpass FSS structure at 10.50 GHz using commercially available simulators such as CST Microwave Studio and Ansoft HFSS. The simulation has been performed through implementing the unit-cell boundary conditions along the *x* as well as *y*-axis and open boundary condition along the *z*-axis in CST Microwave Studio [182] and master/slave boundary along *x* as well as *y*-axis and Floquet boundary condition along *z*-axis in Ansoft HFSS [183] for the

proposed modified circular ring bandpass FSS. The proposed modified circular ring bandpass FSS structure provides the resonance pole transmission at 10.691 GHz, for both the normally incidence perpendicular and parallel polarized wave.

In order to clarify the bandpass resonance, we have provided the electric field distribution diagrams at 10.691 GHz for normal incident perpendicular and parallel polarized wave, which are shown in Fig. 4.6(a) and Fig. 4.6(b), respectively. In addition to this, Fig. 4.6(a) has demonstrated that for the perpendicular polarized wave, the electric field distribution for the component parallel to the direction of wave propagation is weak. Moreover, the Fig. 4.6(b) has demonstrated that for the parallel polarized wave, the electric field distribution for the component perpendicular to the direction of the wave propagation is weak. Further, the electric field values are very weak outside the proposed bandpass FSS structure, and the passband arise from enhanced transmission assisted by the slot resonance for the normally incidence perpendicular and parallel polarized wave in the proposed bandpass FSS structure. Fig. 4.7(a) and Fig. 4.7(b) have depicted that for the perpendicular polarized wave, the resonant frequency of the proposed bandpass FSS downshifts with 0.85% and 0.84% through CST Microwave Studio and Ansoft HFSS, respectively up to 50^{o} AOI. In addition to this, the effect of parallel polarized waves, which are incident normally and at oblique angle up to 50^{o} and the performance of the proposed modified circular ring bandpass FSS has also been discussed. Fig. 4.8(a) and Fig. 4.8(b) have demonstrated that for the parallel polarized wave, the resonant frequency of the proposed modified circular ring bandpass FSS downshifts with 0.76% and 0.65% through CST Microwave Studio and Ansoft HFSS, respectively up to 50^{o} AOI.

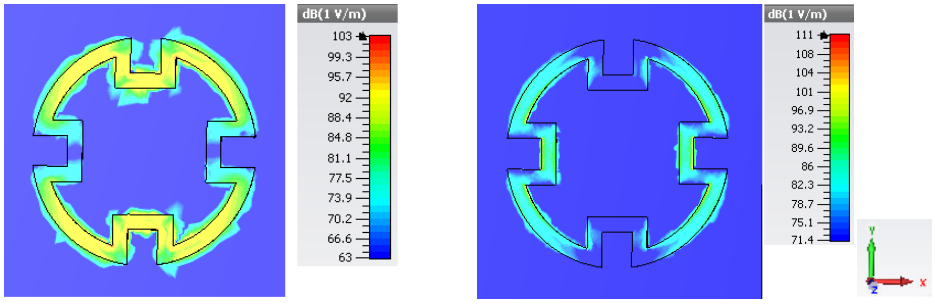

(a) (b)

Fig. 4.6 The electric field distribution in the proposed FSS structure at 10.691 GHz for normally incidence (a) perpendicular (b) parallel polarized wave.

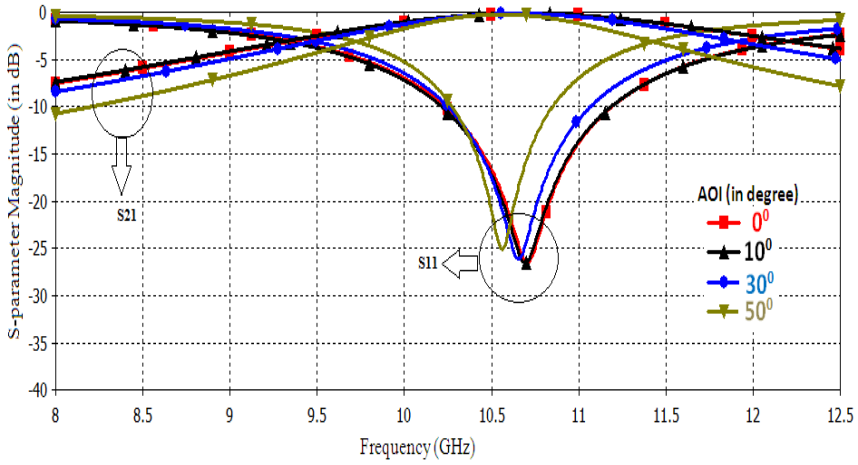

(a)

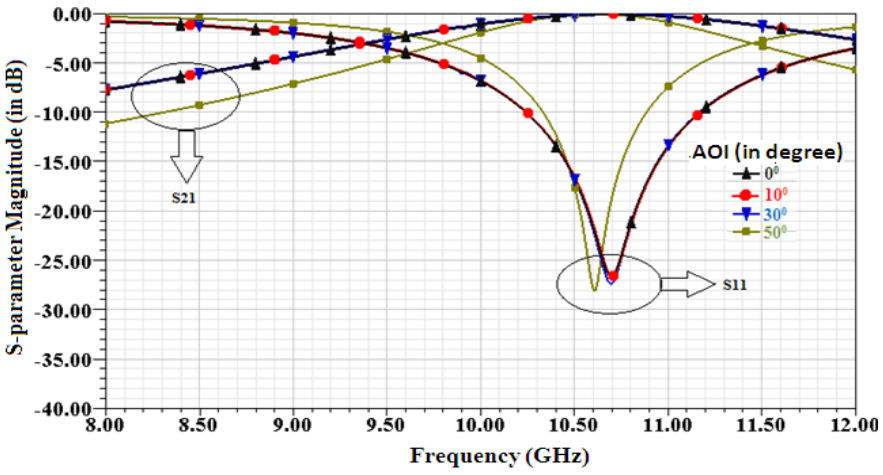

(b)

Fig. 4.7 The effect of perpendicular polarized wave incidence up to 50^{o} AOI on the resonance frequency of the proposed modified circular ring FSS structure at X-band using (a) CST Microwave Studio and (b) Ansoft HFSS.

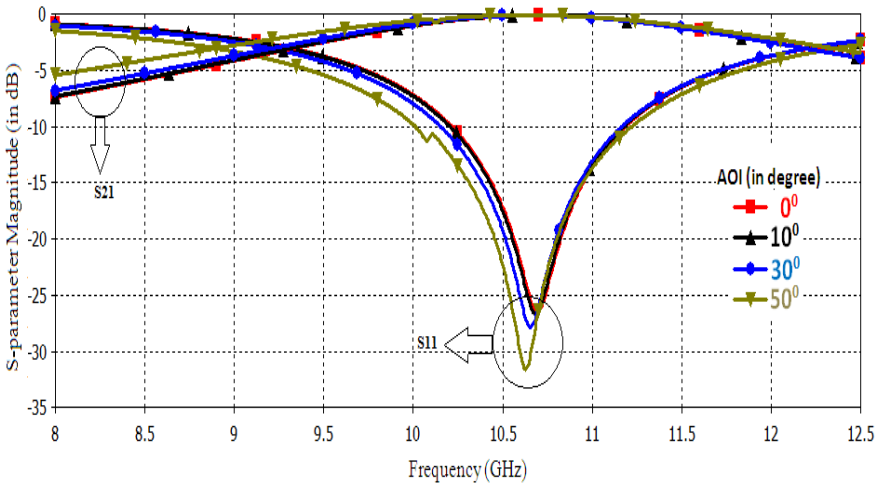

(a)

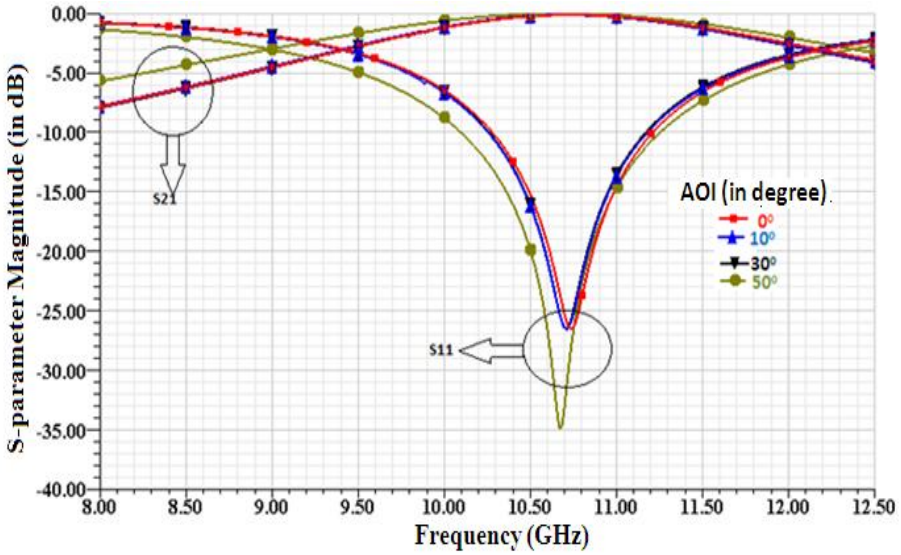

(b)

Fig. 4.8 The effect of AOI on the resonant frequency of the proposed FSS structure at X-band for parallel polarized wave using (a) CST Microwave Studio and (b) Ansoft HFSS.

4.4.2 EXPERIMENTAL VALIDATION

The FSS structure fabricated on a single sided copper clad substrate of 18x18 cm^2 using the conventional chemical processing is placed between the two horn antennas and illuminated by the plane waves generated by the transmitting horn antenna, which is incident normally to the FSS structure [169]. In addition to this, the transmitted waves through FSS structure have been collected by the receiving horn antenna and vector network analyzer is used to observe the frequency response [184]. The structure parameters are given in Table 4.5 and the scheme of measurement setup is shown in Fig. 4.9. The frequency response of the proposed modified circular ring bandpass FSS structure is demonstrated in Fig. 4.10, which signifies that the proposed bandpass modified circular ring FSS structure resonate at 10.69 GHz and 10.70 GHz through CST Microwave Studio and Ansoft HFSS, respectively, where as in the measured result it resonates at 10.69 GHz. Therefore, the deviation in the resonant frequency achieved through CST Microwave Studio and Ansoft HFSS is 0.009% and 0.09%, respectively as compared to the measured results, which demonstrate the practicality of the proposed FSS structure. Fig. 4.10 also demonstrates that -10 dB impedance bandwidth extends from 10.09 to 11.08 GHz and 10.22 to 11.18 GHz through CST Microwave Studio and Ansoft HFSS, respectively against the measured

value of 10.37 GHz to 10.96 GHz. The significant discrepancy is that the measured bandwidth is narrow than the simulated one, which is due to the following factors: (a) diffractions from the edge of the finite FSS panel, (b) machining precision and (c) the measured conditions. At resonance, S_{11} in measured result is -24.15 dB against simulated value is -26.33 dB and -26.85 dB through CST microwave Studio and Ansoft HFSS, respectively.

Moreover, for the comparison of angular and polarization stability of the proposed FSS structure with the other FSS structures in reported literature are listed in Table 4.6.

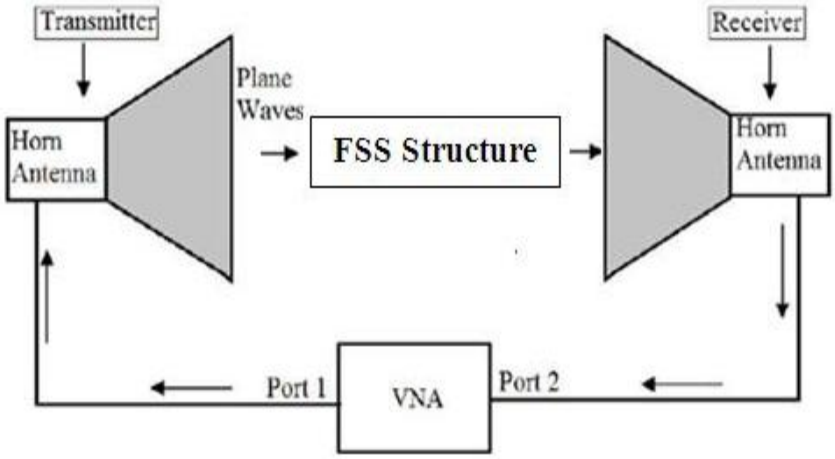

Fig. 4.9 The scheme of measurement setup.

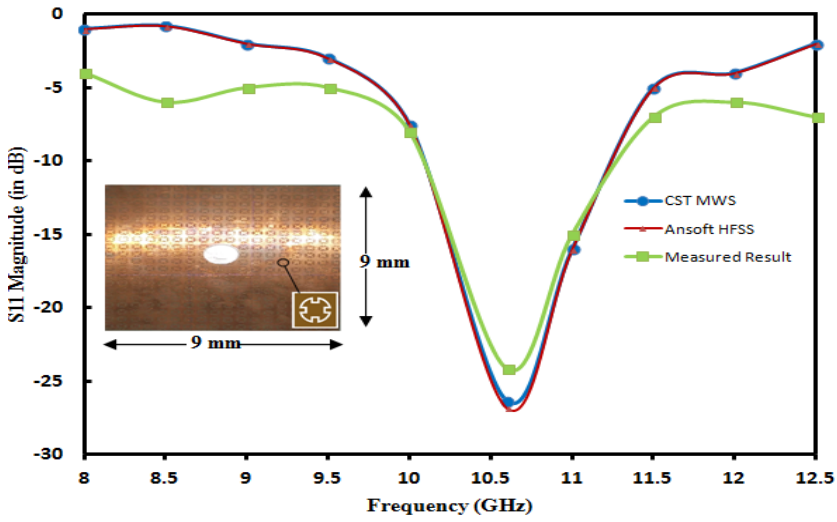

Fig. 4.10 The comparison of measured and simulated frequency response of the proposed bandpass modified circular ring FSS structure CST Microwave Studio and Ansoft HFSS.

Table 4.6 The comparison of angular and polarization stability of the proposed FSS structure with other reported literatures.

AOI	FSS structure	% deviation of f_r
45^o	FSS structure in [92]	3 (TE incidence) and10 (TM incidence)
60^o	FSS structure in [111]	approximately 1 (TE and TM incidence)
45^o	FSS structure in [129]	1.91 (TE incidence) and 1.12 (TM incidence)
45^o	FSS structure in [162]	7 (TE and TM incidence)
45^o	FSS structure in [163]	16.6
45^o	FSS structure in [175]	7.60
60^o	FSS structure in [176]	approximately 5 (TE and TM incidence)
45^o	FSS structure in [177]	5.95
45^o	FSS structure in [178]	5.45
60^o	FSS structure in [181]	0.52 (TE incidence) and 2.1 (TM incidence)
50^o	FSS structure shown in Fig. 4.2(a)	0.84 (TE incidence) and 0.65 (TM incidence)

4.5 CONCLUSION

In this Chapter, we have discussed the miniaturization, angular and polarization stability of the bandpass modified circular ring FSS structure. The bandpass SSLFSS synthesis technique is used to compute the geometrical parameters of the proposed modified circular ring FSS structure, which results ~78 % miniaturization in the proposed bandpass modified circular ring FSS structure as compared to that of the SSLFSS structure at 26 GHz. In addition to this, the significant angular stability of ~1% for the perpendicular polarized wave and ~0.07 % for the parallel polarized wave has been achieved. A prototype of the proposed bandpass modified circular ring FSS structure reveals that the simulation results achieved using CST Microwave Studio and Ansoft HFSS experiences only 0.009% and 0.09% drift in the resonance frequency as compared to the measured results. Moreover, at the normal wave incidence, the return loss obtained in the simulated results such as 26.33 dB and 26.58 dB using CST microwave Studio and Ansoft HFSS, is also comparable with the measured results (24.15 dB). In addition to this, at 0^o AOI, the shift in the resonance frequency due to perpendicular and parallel polarized wave is 0% and 0.3% as achieved through CST Microwave Studio and Ansoft HFSS, respectively, which is significantly small and provides the stable response in terms of the reflection and transmission parameters for dual polarization. As the AOI increases up to 50^o, for the perpendicular polarized wave, the resonance frequency downshifts with 0.85% and

0.84%, respectively and for the parallel polarized wave, the resonance frequency downshifts with 0.76% and 0.65%, through CST Microwave Studio and Ansoft HFSS, respectively at 10.50 GHz. The proposed modified circular ring bandpass FSS structure provides the significantly better angular and polarization stability as compared to that of the active/tunable FSS and different complex geometry FSS structures, which are compared in Table 4.6.

CHAPTER-5

PLANAR MULTIBAND FSS STRUCTURE

5.1 INTRODUCTION

Various researchers/scientists have discussed different geometrical shapes of the FSS structures, which have the potential to provide single-band frequency characteristics [2, 177, 185-187]. However, FSS structures are widely used as sub-reflectors for the satellite communication in which a single main reflector share the different frequency bands and to increase the capabilities of multifunction and multi-frequency antennas, a sub-reflector equipped with FSS structure is required to operate at multi-frequency bands. In order to achieve the multiband frequency response, there are various available approaches, which have been discussed in detail in sub-section 1.4.3. With the consideration of issues discussed in sub-section 1.4.3 taken into account and to achieve the simplified, low profile, light weight and angular as well as polarization stable multiband FSS structure, in this Chapter, we have proposed two single layer multiband FSS structures, which are as follows.

1) Slot type multiband FSS structure consist of a modified circular ring loaded with a concentric conventional circular ring as shown in Fig. 5.1, along with its EC, which offers reflection characteristics in S-band (2-4 GHz)/K_u (12-18 GHz) and transmission characteristics in X-band (8-12 GHz)/K_a-band (24-28 GHz).

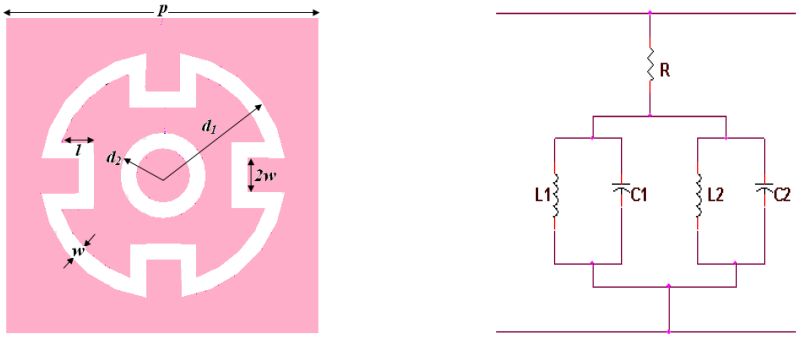

(a) (b)

Fig. 5.1 The proposed inductive loaded modified circular slot type multiband FSS structure (a) unit-cell configuration and (b) its equivalent circuit.

2) Patch type multiband FSS structure, which consist of two concentric modified circular rings as shown in Fig. 5.2, along with its EC and provides transmission

in S-band (2-4 GHz) and reflection in Ku-band (12-15 GHz)/Ka-band (24-26 GHz).

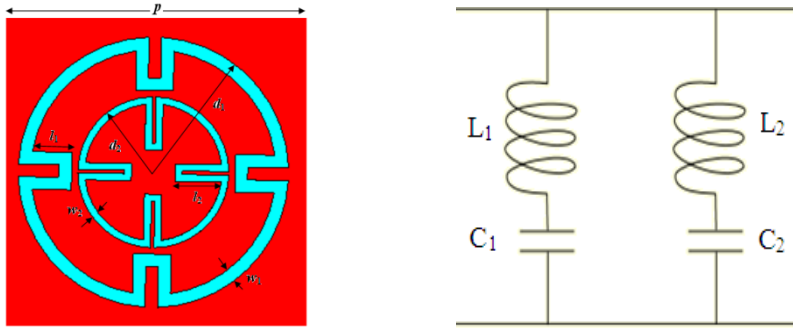

(a) (b)

Fig. 5.2 The proposed tri-band FSS structure (a) unit-cell configuration and (b) its equivalent circuit.

The remainder of the Chapter is organized as follows. Section 5.2 discusses the slot-type multiband FSS structure (shown in Fig. 5.1), which includes the synthesis approach and unit-cell configuration of the proposed multiband FSS along with the material specifications. Section 5.3 discusses the patch-type multiband FSS structure (shown in Fig. 5.2), which includes its parametric optimization. Section 5.4 discusses the effect of slot-length, slot-width, AOIs (up to 50^{o}) and perpendicular/parallel polarization on the frequency response of the slot- type multiband FSS. Section 5.5 discusses the electric field distribution at normal wave incidence and angular/ polarization stability of the patch-type multiband FSS. Finally, Section 5.6 concludes the work.

5.2 THEORY OF OPERATION AND UNIT-CELL CONFIGURATION OF SLOT TYPE MULTIBAND FSS

The proposed slot-type multiband FSS (shown in Fig. 5.1) is achieved through the perforation of copper sheet of thickness t = 0.02 *mm* with electrical conductivity σ = 5.8×10^{7} S/m which is backed with commercially available dielectric substrate Arlon AD 320 of thickness 0.762 *mm*, relative dielectric permittivity ε_r = 3.2 and loss tangent *tan* δ = 0.0038 and shown in Fig. 5.1(a). The geometrical parameters of the proposed slot-type multiband FSS (shown in Fig. 5.1) are as follows: periodicity (p), size of the outer modified ring (d_1), size of the inner circular ring (d_2), slot-width (w) and the length of four-pairs of parallel straight slot (l).

In general, for the multiband applications, the highest frequency of the operating frequency band determines the *p* of the FSS structure [114]. However, in order to avoid the grating lobes to occur in the desired operating frequency band, the *p* must be less than unit wavelength at 0^o AOI and less than half of the free-space wavelength (λ_o) for large angles such as 45^o AOI [117]. According to this, for the proposed slot-type multiband FSS (shown in Fig. 5.1), the *p* computed at K_a-band is significantly small, which is not accommodated the circumference of outer modified circular ring, which is responsible for X-band transmission.

On the other hand, we have computed the value of *p* using the theory discussed in Section 2.2, which modifies the Equation (2.12) for 10^o into Equation (2.13). For $\theta = 10^o$, the value of the *M* is fixed as 0.8520 in Equation (2.13) and we have obtained the value of *p = 9.0 mm* for the proposed multiband FSS (shown in Fig. 5.1). In addition to this, using the mathematical expression shown in second last block of Fig. 4.1, the geometrical parameters of proposed multiband FSS (shown in Fig. 5.1) such as d_1, d_2 and *w* are obtained by the transformation of SSLFSS synthesis technique on the circular ring FSS at each frequency of interest (*X*-band and K_a-band), which is discussed as follows.

5.2.1 1st TRANSMSSION BAND (X-BAND)

According the mathematical expression shown in last block of Fig. 4.1, once the value of *M* is fixed, which is 0.8520 (considering $\theta = 10^o$), for the operating frequency (10.50 GHz), the *w* as fraction of λ and *d* has been obtained. In the X-band, the $d = d_1$ in the mathematical expression shown in last block of Fig. 4.1 and for each value of the w/λ, corresponding value of *w*, d_1 and simulated resonance frequency, which is achieved using Ansoft HFSS, is illustrated in Table 5.1.

Table 5.1 demonstrates that for the fixed value of *p*, with increase in the numerical value of w/λ, the relative percentage deviation from the intended frequency is reduced and further saturates. However, the small amount of the percentage deviation still exist, which is due to the fact that to obtain the mathematical expression shown in second last block of Fig. 4.1 in the synthesis technique, the value of the correction factor as well as inter-element gap has been ignored to simplify the analysis [2]. Table 5.1 discusses that the resonance frequency has been saturated from the 2nd row

onwards, therefore we have chosen the geometrical parameters of the structure from the 2nd row for the outer modified circular slot when l = 0. In order to resonate the circular ring FSS at the same frequency as that of the SSLFSS, we have inserted four pairs of parallel straight slots of the length (l), where *l = 1.08 mm* in the outer circular ring and the chosen geometrical parameters of the 2nd row of the Table 5.1 have been tuned, which provides the geometrical parameters such as: *p = 9 mm*, d_1 *= 6.9 mm*, *w = 0.46 mm* and *l = 1.08 mm* of the unit-cell to obtain the desired frequency response.

Table 5.1 The geometrical parameters of the outer modified circular slot of the structure shown in Fig. 5.1(a) on 10.50 GHz at l = 0 (outer conventional circular slot).

w/λ	p (mm)	w (mm)	d_1	f_r (GHz) (CST MWS)
0.01	9.00	0.286	6.39	10.80
0.02	9.00	0.571	7.60	10.70
0.03	9.00	0.857	8.70	10.70
0.04	9.00	1.140	9.87	10.70
0.05	9.00	1.429	11.1	10.70

5.2.2 2nd TRANSMISSION BAND (K_a-BAND)

The geometrical parameters such as w and d (here, $d = d_2$) at 26.5 GHz have been obtained in the similar way as in X-band. However, the change in the nature of resonance frequency is almost similar in Table 5.1 and Table 5.2. The resonance frequency as shown in Table 5.2, the resonance frequency has been saturated from 4th row onwards therefore we have chosen the geometrical parameters of the structure from the 4th row.

Table 5.2 The geometrical parameters of the inner circular slot of the proposed multiband FSS structure at 26.5 GHz.

w/λ	p (mm)	w (mm)	d_2 (*mm*)	f_r (GHz) (CST MWS)
0.01	9.00	0.113	1.4	27.40
0.02	9.00	0.226	1.72	26.94
0.03	9.00	0.339	1.92	26.93
0.04	9.00	0.452	2.38	26.92
0.05	9.00	0.565	2.68	26.92

We have obtained the geometrical parameters of the proposed multiband FSS structure by combining the parameters obtained at the individual frequency of interest

such as at 10.5 GHz and 26.5 GHz. The resultant geometrical parameters of the proposed multiband FSS (shown in Fig. 5.1(a)) are: *p = 9 mm, d_1 = 6.9 mm, d_2 = 2.4 mm, w = 0.46 mm* and *l = 1.08 mm*. With the consideration of fabrication issues taken into account and to provide a single layer multiband FSS structure with simple unit-cell element, we have used the conventional circular slot, which is responsible for providing the 2nd reflection-null at the K_a-band. With the proposed multiband FSS structure (shown in Fig. 5.1(a)), we have achieved two reflection-nulls such as at 10.5 GHz (X-band) and 26.5 GHz (K_a-band) in the operating frequency band (2-28 GHz), which experiences significant angular and polarization stability. In addition to this, the combination of both the aforementioned structures also affects the resonant frequency response, which has been discussed in the next Section.

5.3 THEORY OF OPERATION AND UNIT-CELL CONFIGURATION OF PATCH TYPE MULTIBAND FSS

5.3.1 PARAMETRIC OPTIMIZATION

In order to achieve the multiband frequency response, we have proposed a dual-resonant element FSS using two concentric modified circular ring as shown in Fig. 5.2(a) along with its EC, which is shown in Fig. 5.2(b). The proposed multiband FSS is a dual concentric modified circular ring of copper with thickness t = 0.02 mm and electrical conductivity $\sigma = 5.8\times10^7$ S/m which is backed with commercially available Arlon AD 320 substrate of thickness h = 0.762 mm with relative dielectric permittivity ε_r = 3.2 and loss tangent $tan\ \delta$ = 0.0038 as shown in Fig. 5.2. The geometrical parameters such as p, size of outer modified circular ring (d_1), strip width of outer modified circular ring (w_1), length of four pair of parallel straight conductors of the outer modified circular ring (l_1), size of inner modified circular ring (d_2), strip width of inner modified circular ring (w_2), length of four pairs of parallel straight conductors of the inner modified circular ring (l_2) of the FSS structure shown in Fig.5.2 are shown in Table 5.3.

Table 5.3 The geometrical parameters of the structure shown in Fig. 5.2.

p (mm)	d_1 (mm)	w_1 (mm)	l_1 (mm)	d_2 (mm)	w_2 (mm)	l_2 (mm)
4.5	4.3	0.2	0.65	2.4	0.11	0.74

However, in order to obtain the intended frequency response of the structure shown in Fig. 5.2, the tuning of the geometrical parameters is performed, which is achieved in following three steps.

1) to tune the size (d_1, d_2) of the unit-cell element, which resonate the FSS structure shown in Fig. 5.2 at the target frequencies such as 15 GHz and 26 GHz,

2) to obtain the appropriate length of pair of parallel straight conductors and

3) to adjust the inter-element gap in the same unit-cell of the FSS structure shown in Fig. 5.2.

We have etched-out four patches of width w_1 from the outer circular ring and of width w_2 from inner circular ring at 0^o, 90^o, 180^o and 270^o, which provides the 1^{st} resonance at the desired frequency (15 GHz), but with small amount of 3-dB bandwidth and 2^{nd} resonance at desired resonance frequency (26 GHz) with significant amount of 3-dB bandwidth, respectively. In order to obtain the significant amount of 3-dB bandwidth at both the resonance frequencies, we have etched-out four patches of width w_1 from the outer circular ring and $w_2/2$ from the inner circular ring at 0^o, 90^o, 180^o and 270^o. Moreover, on reducing the width from $3w_1$ to $2w_1$ and to w_1, keeping the rest of parameters same, the resonance frequency (15 GHz) of the first resonance does not vary, which signifies that the effect of capacitance (C, where $C = C_1$ (at 15 GHz) and $C = C_2$ (at 26 GHz)) on the resonance frequency is negligible and the resonance frequency of the FSS structure shown in Fig. 5.2 mainly depends upon the inductance (L). However, the harmonics of fundamental resonance or onset of the grating lobes which limits the bandwidth of the structure is the main technical issue with the resonating FSS structure. In view of this, we have optimised the proposed tri-band FSS structure without any grating lobes upto the desired frequency range.

5.3.2 NUMERICAL ANALYSIS

The FSS structure shown in Fig. 5.2 consists of two concentric modified circular rings, which are responsible to resonate the structure at 15 GHz and 26 GHz. The outer and inner modified circular ring is responsible for the 15 GHz and 26 GHz resonance, respectively. However, the effect of inter-element gap capacitance is

negligible on the resonance frequency, therefore the resonance frequency of FSS structure shown in Fig. 5.2, mainly depends on the inductance, which is sum of the inductance due to circular ring (L_1) and inductance due to the four-pairs of parallel straight conductors (L_2). The inductance due to circular ring is given by using Equation (3.3). In addition to this, the inductance due to the four pairs of parallel straight conductors is given by using Equation (3.5). In Equation (3.3) and Equation (3.5), the w replaces w_1 (for 15 GHz resonance) and w_2 (for 26 GHz resonance). Moreover, the total inductance (L) is the sum of inductance due to the circular ring and inductance due to the four pairs of parallel straight conductors of appropriate length, which is given by $L = L_1 + L_2$. In addition to this, the inter-element gap capacitance is achieved by using Equation (3.4), where, $C = C_1$ (at 15 GHz) and $C = C_2$ (at 26 GHz) and f_r is the resonance frequency of the FSS structure shown in Fig. 5.2.

Using the geometrical parameters, Table 5.3, we have designed the FSS structure shown in Fig. 5.2 that provides two pole reflection resonances at 15 GHz and 26 GHz and numerically verified. At 15 GHz, the value of L_1 and L_2 is 5.92 nH and 1.24 nH, which is obtained using Equation (3.3) and Equation (3.5), respectively. In addition to this, the value of L and C are 7.16 nH and 1.48 fF, respectively, which provides the 1st resonance of the FSS structure shown in Fig. 5.2 at 15 GHz. Similarly, at 26 GHz, the value of L_1, L_2, L and C is 3.23 nH, 1.76 nH, 4.99 nH and 1.27 fF, respectively, which are obtained using the respective equations and provides the 2nd resonance of the FSS structure shown in Fig. 5.2.

5.4 RESULTS AND DISCUSSION OF SLOT TYPE MULTIBAND FSS STRUCTURE

In this section, the effect of l and w on the frequency response of the proposed multiband FSS structure (shown in Fig. 5.1) is discussed. In addition to this, the angular and polarization stability of the structure shown in Fig. 5.1 is discussed for the plane wave incidence at different polarization angles using Ansoft HFSS by applying master/slave boundary conditions and CST Microwave Studio by applying unit-cell boundary conditions. We have discussed the effect of perpendicular and parallel polarized wave incidence at different polarization angles by assigning the different

values of AOIs in the polarization angle option in Ansoft HFSS and CST Microwave Studio instead of assigning AOIs in the Floquet port option [182, 183].

5.4.1 EFFECT OF SLOT-LENGTH AND SLOT-WIDTH

We have simulated the concentric circular ring FSS for computed geometrical parameters such as: $p = 9\ mm$, $w = 0.46\ mm$, $d_1 = 6.9\ mm$ and $d_2 = 2.4\ mm$ and achieved frequency response, which is shown in 1st row of Table 5.4. The insertion of four pairs of parallel straight slots in the outer circular slot modifies the conventional concentric circular ring to the proposed multiband FSS structure.

On that way, the Table 5.4 demonstrates that with the increase in value of *l*, the 3-dB bandwidth increases and the resonance frequency for both the transmission bands downshifts and approaches the intended frequency without deteriorating its miniaturization. Table 5.5 discusses that with the increase in the value of *w*, the 3-dB bandwidth increases and the resonance frequency up-shifts due to decreasing the inductive effect. Considering the resonance behaviour discussed in Table 5.4 and Table 5.5, the chosen value of *l* and *w* are: *1.08 mm* and *0.46 mm*, respectively.

Table 5.4 The effect of slot-length on the resonance frequency and 3-dB bandwidth.

l (*mm*)	1st Transmission Band (GHz)		2nd Transmission Band (GHz)	
	f_r	3-dB BW	f_r	3-dB BW
0	12.10	1.80	29.6	0.19
0.36	12.00	2.70	29.2	0.28
0.72	11.50	2.90	28.6	0.60
0.99	10.90	3.00	28.2	0.65
1.08	10.50	3.20	27.0	0.90

Table 5.5 The effect of slot-width on the resonance frequency and 3-dB bandwidth.

w (mm)	1st Transmission Band (GHz)		2nd Transmission Band (GHz)	
	f_r	3-dB BW	f_r	3-dB BW
0.13	9.8	1.70	25.2	0.38
0.23	9.85	2.10	25.8	0.40
0.46	10.50	3.20	27.0	0.90
0.56	10.60	3.25	27.4	0.92

5.4.2 POLARIZATION STABILITY

The proposed multiband FSS structure, which provides the reflection in S/K_u-band and transmission in X/K_a-band, is explored to illustrate the effects of perpendicular and parallel polarized wave incidence up to 50^o AOI.

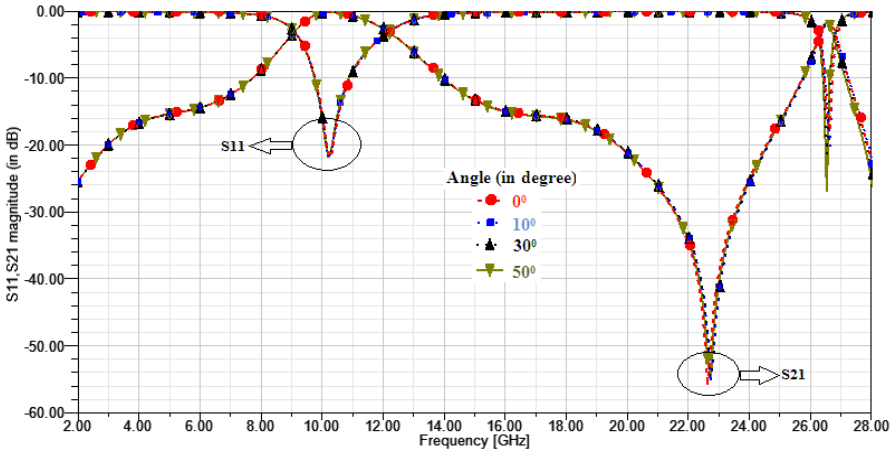

(a)

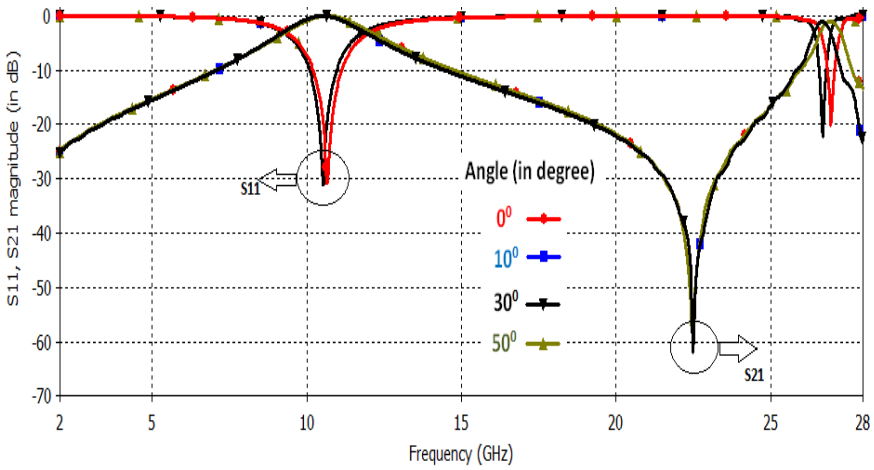

(b)

Fig. 5.3 The frequency response of multiband FSS structure for perpendicular polarized wave incidence up to 50^o using (a) Ansoft HFSS and (b) CST Microwave Studio.

Fig. 5.3(a) demonstrates that the resonance frequency downshifts with 0.93% and 0.74% in the 1st and 2nd transmission band, respectively for perpendicular polarized wave incidence up to 50^o AOI with reference to the normal incidence, which is achieved using the Ansoft HFSS. Further, Fig. 5.3(b) demonstrates that the resonance frequency downshifts with 0.71% and 0.68% in the first and second transmission

band, respectively for perpendicular polarized wave incidence up to 50° AOI with reference to the normal incidence, which is achieved using CST Microwave Studio.

Table 5.6 The effect of perpendicular polarized wave up to 50° on the frequency response of the multiband FSS structure through Ansoft HFSS and CST Microwave Studio.

AOI	Ansoft HFSS				CST Microwave Studio			
	1st Transmission Band (GHz)		2nd Transmission Band (GHz)		1st Transmission Band (GHz)		2nd Transmission Band (GHz)	
	f_r	3-dB BW	f_r	3-dB BW	f_r	3-dB BW	f_r	3-dB BW
0°	10.50	3.30	27.0	0.90	10.570	3.25	26.79	0.98
10°	10.40	3.10	27.0	0.88	10.564	3.25	26.76	0.97
30°	10.40	3.00	26.9	0.88	10.537	3.24	26.69	0.97
50°	10.40	3.00	26.8	0.88	10.495	3.24	26.61	0.96

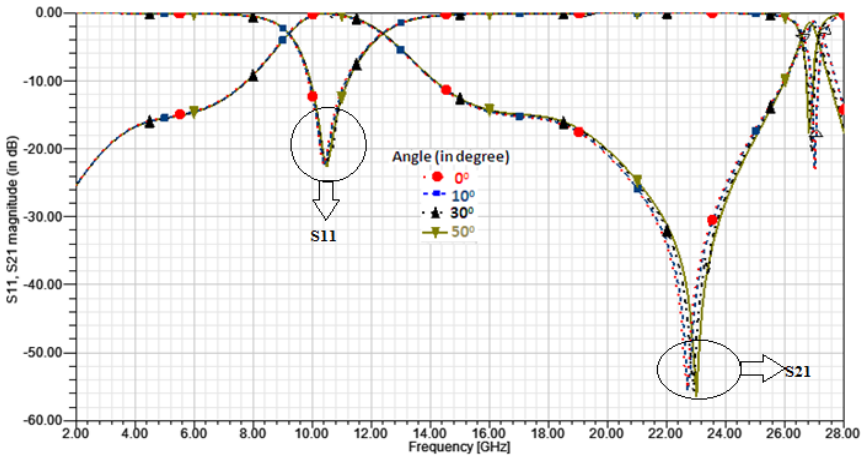

(a)

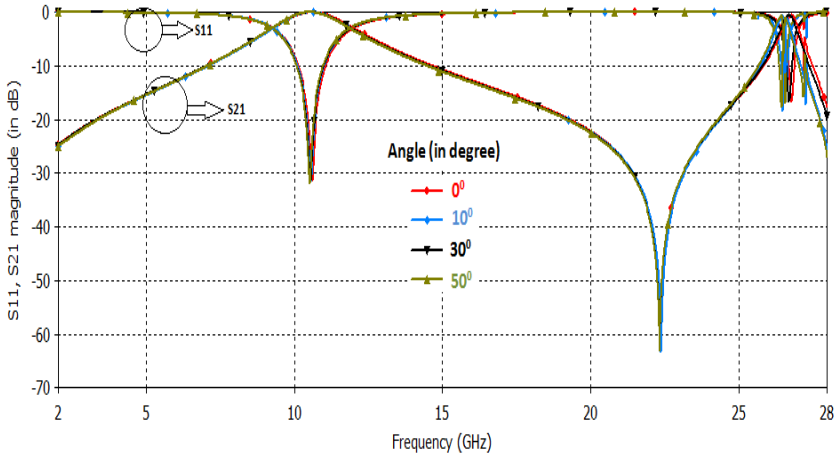

(b)

Fig. 5.4 The frequency response of multiband FSS structure for parallel polarized wave incidence 50° using (a) Ansoft HFSS and (b) CST Microwave Studio.

Table 5.7 The effect of parallel polarized wave incident up to 50^o on frequency response of the multiband FSS structure through Ansoft HFSS and CST Microwave Studio.

AOI	Ansoft HFSS				CST microwave Studio			
	1^{st} Transmission Band (GHz)		2^{nd} Transmission Band (GHz)		1^{st} Transmission Band (GHz)		2^{nd} Transmission Band (GHz)	
	f_r	3-dB BW	f_r	3-dB BW	f_r	3-dB BW	f_r	3-dB BW
0^o	10.50	3.20	27.00	0.90	10.570	3.25	26.793	0.98
10^o	10.40	3.18	27.00	0.88	10.536	3.24	26.774	0.97
30^o	10.40	3.18	26.90	0.88	10.511	3.24	26.693	0.96
50^o	10.40	3.18	26.75	0.87	10.490	3.24	26.596	0.96

In addition to this, Table 5.6 discusses the effect of perpendicular polarized wave incidence up to 50^o AOI on 3-dB bandwidth of the proposed multiband FSS using the Ansoft HFSS and CST Microwave Studio. Further, Fig. 5.4(a) demonstrates that the resonance frequency downshifts with 0.96% and 0.76 % in the 1^{st} and 2^{nd} transmission band, respectively for the parallel polarized wave incidence up to 50^o AOI with reference to the normal incidence, which is achieved through the Ansoft HFSS. Further, Fig. 5.4(b) demonstrates that the resonance frequency downshifts with 0.93% and 0.74% in the 1^{st} and 2^{nd} transmission band, respectively for parallel polarized wave incidence up to 50^o AOI with reference to the normal incidence, which is achieved through CST Microwave Studio. In addition to this, Table 5.7 discusses the effect of the parallel polarized wave incidence up to 50^o AOI on 3-dB bandwidth of the proposed multiband FSS using the Ansoft HFSS and CST Microwave Studio.

In order to validate the downshift achieved in the frequency responses for the wide range of AOIs, we have performed the EC export for 0^o, 10^o, 30^o and 50^o AOI for both perpendicular as well as parallel polarized waves from the Ansoft HFSS in Advanced Design System (ADS) and achieved the values of the associated inductance *L (nH)* and capacitance *C (pF)* for the structure shown in Fig. 5.1. The value of *C (pF)* for perpendicular and parallel polarized wave, which has been incidence at 0^o, 10^o, 30^o and 50^o are approximately same, which is *4.001* pF and the values of *L* (*nH*) at 0^o, 10^o, 30^o and 50^o AOIs are 0.4245, 0.4246, 0.4246 and 0.4246, respectively, for both the perpendicular and parallel polarized wave. However, the slight variations in the resonance frequency as illustrated in Fig. 5.3 and Fig. 5.4 is due to very small variations in the value of inductance *L* (*nH*). In addition to this, the value of the

resistance (R) in all the aforementioned cases is also remain constant and negligible (order of $1\times10^{-6}\,\Omega$).

5.5 RESULTS AND DISCUSSION OF PATCH-TYPE MULTIBAND FSS STRUCTURE

In this section, we have simulated the FSS structure shown in Fig. 5.2 with unit-cell boundary conditions, which is excited by the perpendicular and parallel polarized wave incidence up to 50^{o} AOI to achieve its reflection/transmission characteristics using commercially available simulator CST Microwave Studio. The electric field distribution of the FSS structure shown in Fig. 5.2 plays an important role to understand the physical insight of its filtering/resonance mechanism as discussed in [188]. The FSS structure shown in Fig. 5.2 provides two resonance pole reflection responses at 14.95 GHz and 25.93 GHz, which is well-justified with the electric field distribution as shown in Fig. 5.5. The 1^{st} resonance that occurs at 14.95 GHz is mainly due to the electric field resonance in the outer modified circular ring as illustrated from Fig. 5.5(a). However, the 2^{nd} resonance, which occurs at 25.93 GHz, is mainly due to the electric field resonance in the inner modified circular ring of the structure as shown in Fig. 5.5(b). Moreover, the electric field distribution shown in Fig. 5.5 signifies the resonances (stop-bands) of the modified FSS structure at 14.95 GHz and 25.93 GHz, respectively that arise from the enhanced reflection assisted by two patch resonances.

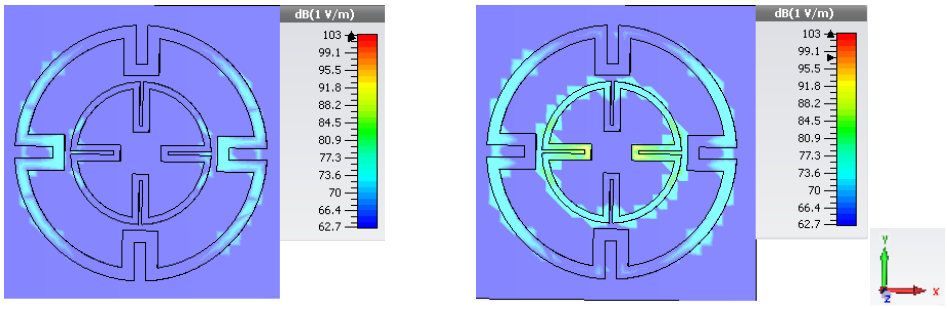

(a) (b)

Fig. 5.5 The simulated electric field distribution of the proposed FSS structure using CST Microwave Studio at two different resonance frequencies (a) 14.95 GHz and (b) 25.93 GHz.

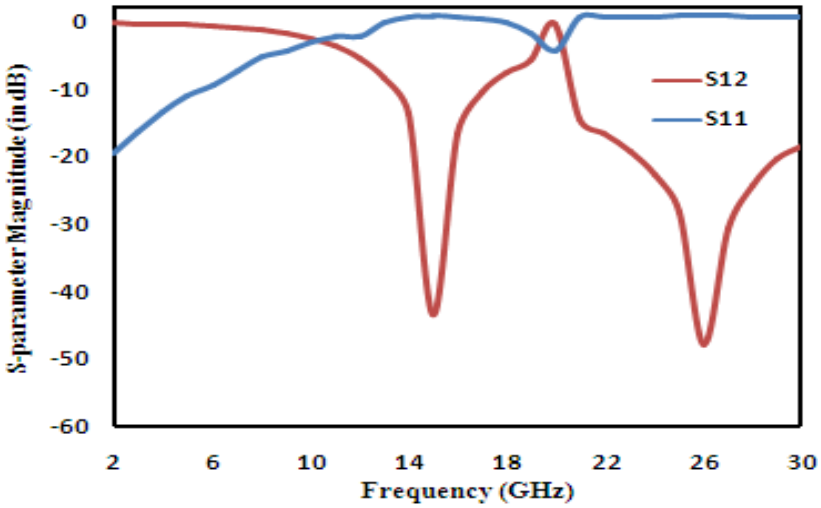

Fig. 5.6 The frequency response of the s-parameters of the FSS structure shown in Fig. 5.2 at normal wave incidence in terms of transmission-line model using ADS.

To validate the frequency response of the s-parameters of the FSS structure shown in Fig. 5.2 at normal wave-incidence, we have imported EC (transmission-line model) as shown in Fig.5.2 (b) of FSS structure (shown in Fig. 5.2(a)) into the Advanced Design System (ADS) [189] and achieved the resonance behavior as shown in Fig. 5.6. The proposed structure provides transmission characteristics in S-band and reflection characteristics in K_a/K_u-band of the electromagnetic spectrum with two resonance pole reflection responses at 14.98 GHz and 25.98 GHz as shown in Fig. 5.6. The frequency response of reflection and transmission parameters of FSS structure shown in Fig. 5.2 for perpendicular and parallel polarized wave incidence up to 50^o AOI are illustrated in Fig. 5.7(a) and Fig. 5.7(b), respectively. The FSS structure shown in Fig. 5.2 illustrates 0.367% and 0.93% downshift at 15 GHz and 26 GHz for perpendicular polarized wave incidence up to 50^o with respect to normal incidence as shown in Fig. 5.7(a), respectively. In addition to this, Fig 5.7(b) demonstrates that for parallel-polarized wave incidence up to 50^o, there is 0.234% and 0.673% downshift at 15 GHz and 26 GHz with respect normal incidence, respectively. The 3-dB bandwidth of proposed structure slightly decreases as the incidence angle increases up to 50^o from the normal incidence, however, for parallel-polarized wave, the 3-dB bandwidth slightly increases as the incidence angle increases up to 50^o from the normal incidence as revealed by Table 5.8.

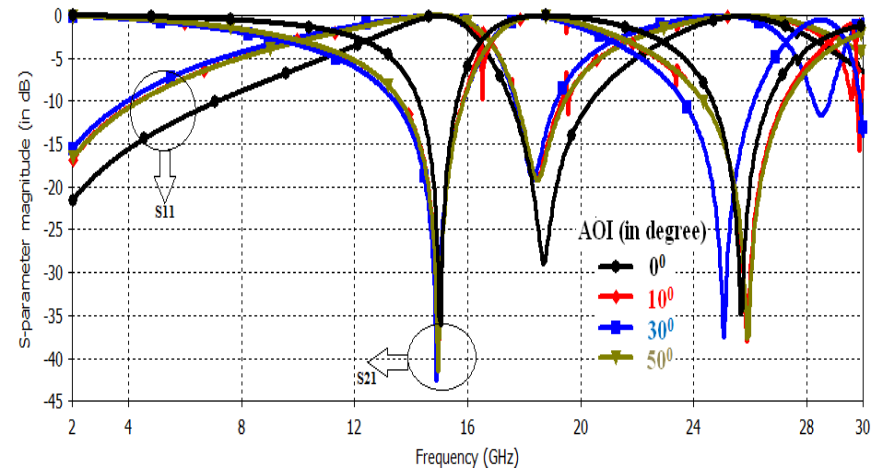

(a)

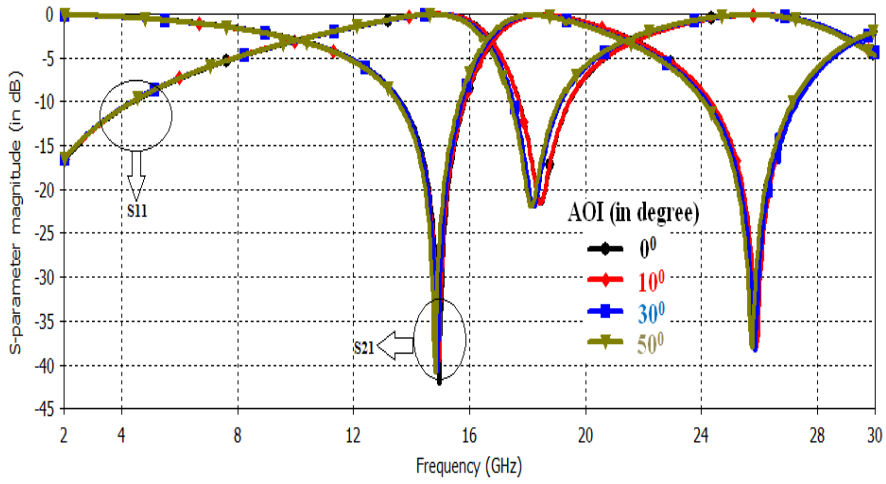

(b)

Fig. 5.7 The frequency response of transmission/reflection parameters of proposed structure using CST Microwave Studio up to 50^{o} AOI for (a) perpendicular and (b) parallel-polarized wave.

Table 5.8 The frequency responses of reflection/transmission frequency parameters and 3-dB of FSS structure shown in Fig. 5.2 at different AOI for perpendicular and parallel polarized wave.

AOI	Perpendicular Polarization				Parallel Polarization			
	1st resonance (GHz)		2nd resonance (GHz)		1st resonance (GHz)		2nd resonance (GHz)	
	f_r	3-dB BW	f_r	3-dB BW	f_r	3-dB BW	f_r	3-dB BW
0^{o}	14.950	6.8131	25.93	7.746	14.95	6.764	25.93	7.354
10^{o}	14.950	6.4656	25.93	7.185	14.95	6.869	25.885	7.394
30^{o}	14.905	6.4086	25.85	6.184	14.905	6.887	25.885	7.613
50^{o}	14.895	6.0350	25.66	5.428	14.915	6.982	25.755	7.858

In addition to this, the FSS structure shown in Fig. 5.2 provides the FBW of about 40% and 21% at 15 GHz and 26 GHz for perpendicular polarized wave incidence up to 50^o as well as about 46% and 36% at 15 GHz and 26 GHz for parallel polarized wave incidence up to 50^o. Moreover, for the comparison of angular and polarization stability of the FSS structure shown in Fig. 5.1(a) and Fig. 5.2(b) with other recently reported literature are listed in Table 5.9.

Table 5.9 The comparison of angular and polarization stability of the proposed multiband FSS structure with the other reported FSS structures.

AOI	FSS structure	% deviation of f_r
60^o	FSS in [111]	1 (TE and TM incidence)
45^o	Concentric circular ring [113]	4.76 (TE incidence) and 1.12 (TM incidence)
20^o, 45^o	One turn helix [119]	6.75 (TE incidence) and 1.65 (TM-incidence)
45^o	Isosceles triangle [120]	6.59 (TE-incidence)
50^o	FSS shown in Fig. 5.1(a)	0.68 (TE-incidence) and 0.74 (TM-incidence)
50^o	FSS shown in Fig. 5.2(a)	0.93 (TE-incidence) and 0.673 (TM-incidence)

5.6 CONCLUSION

In this Chapter, we have discussed two new multiband that is slot-type and patch-type FSS structures which result a single layer, low profile structures and provide significant angular (up to 50^o) /polarization (perpendicular and parallel) stability. The slot type multiband FSS structure has a very thin overall thickness of $0.02\lambda_1$, where λ_1 is the wavelength corresponding to the lower resonance frequency, which prevents the generation of surface waves, especially at the large AOIs and very significant in the shielding applications. In addition to this, the slot type multiband FSS structure experiences 0.68% and 0.74% shift in the resonance frequency for the perpendicular and parallel polarized wave, respectively up to 50^o. Moreover, a single layer, low profile ($0.03\lambda_1$) dual concentric modified circular ring (patch type) multiband FSS structure is discussed, which result maximum frequency downshift of 0.93% (for perpendicular polarized wave) and 0.673% (parallel polarized wave) frequency. In addition to this, the patch type multiband FSS structure provides 40% and 21% FBW in K_u-band and K_a-band, respectively, for perpendicular polarized wave as well as about 46% and 36% for parallel polarized wave incidence up to 50^o with respect to normal incidence, which is very useful for communication applications. Moreover,

the proposed multiband (slot/patch type) FSS structures is compared with various reported literature with reference to the angular/polarization and reveals better angular/polarization stability.

CHAPTER-6

ANALYSIS OF AZIMUTHALLY PERIODIC WEDGE-SHPAED CIRCULAR RING FSS STRUCTURE

6.1 INTRODUCTION

In the Chapter-3 and Chapter-4, we have discussed novel, simple and single layer modified circular ring FSS structure, which offer significantly much better angular/polarization stability, 3-dB bandwidth and miniaturization. In order to enhance the performance of FSS structures, several researchers have investigated the loaded FSS structures as discussed in detail in Section 1.7, which have been classified as active loaded and passive loaded FSS structures [145-155]. However, an actively loaded FSS structure provides tuning characteristics through the implementation of a tuning circuit with significant angular/polarization stability. In addition to provide the significant angular/polarization stability, the passive loaded FSS structures provide the easier fabrication due to the reduced complexity and cost of fabrication as compared to that of the active loaded FSS structure. Therefore, in this Chapter, we have proposed a novel geometrical shape of passive loaded FSS structure, which provide significantly much better frequency response in terms of the angular and polarization stability.

An azimuthally periodic wedge-shaped circular ring FSS structure (as shown in Fig. 6.1) is discussed for the bandstop and bandpass filtering characteristics. This Chapter is organized as follows. Section 6.2 describes the theory of operation and numerical analysis of azimuthally periodic wedge-shaped circular ring bandstop FSS. The numerical optimization of geometrical parameters in order to enhance the performance of the azimuthally periodic wedge-shaped circular ring bandstop structure and the effect of number of vanes on the electrical performance of the azimuthally periodic wedge-shaped circular ring bandstop structure have been discussed. In addition to this, the bandwidth control and angular sensitivity have been presented, which is further compared with the classical circular ring FSS. An azimuthally periodic wedge shaped circular ring FSS structure for the bandpass filtering characteristics using transmission-line approach is also discussed. Further,

Section 6.3 discusses the theory of operation an azimuthally periodic wedge-shaped circular ring bandpass FSS structure. The resonance behaviour of the azimuthally periodic wedge-shaped circular ring bandpass FSS at 3 GHz, 15 GHz and 25 GHz for the perpendicular and parallel polarized wave incidence up to 50^{o} AOI has been discussed. Finally, Section 6.4 concludes the work.

6.2 NUMERICAL ANALYSIS OF PROPOSED BANDSTOP CIRCULAR RING FSS

Using the structural transformation as discussed in Section 3.3 that is from SSLFSS to circular ring FSS structure, we have further modified the circular ring into an azimuthally periodic wedge-shaped metallic vane loaded circular ring FSS structure, as shown in Fig. 6.1. We have obtained the geometrical parameters of the proposed structure at Ku band such as periodicity (p) = 16.39 mm, outer radius of the circular ring (r_3) = 2.6 mm, inner radius of the ring or outer radius of the wedge shaped vane (r_2) = 2.4 mm. However, the inner radius of the wedge shaped vane (r_1) has been chosen equal to the 2.0 mm. An azimuthally periodic wedge-shaped metal vane loaded circular ring made of the Aluminium having electrical conductivity (σ) = 3.5×10^{7} S/m and magnetic permeability (μ) = 1.2566×10^{-6} H/m is placed on the Teflon substrate with relative dielectric permittivity 2.02 and loss tangent (δ) 0.002 has been shown in Fig. 6.1. The thickness of dielectric substrate and wedge shape metallic ring for Ku band has been computed as 1.00 mm and 0.00235 mm, respectively. In [2], it is demonstrated that with the variations in the geometrical structure of the FSS structure, the resonance frequency is also changed significantly. For the structure shown in Fig. 6.1, the inductance has been achieved by the algebraic sum of the inductance of the circular section and the inductance due to the four wedge shape metal vanes. The value of inductance and capacitance of a circular ring is computed by using Equation (3.3) and Equation (3.4), respectively. As, the value of periodicity, width of the conducting strip and the size of the circular ring are same for the structure shown in Fig. 3.4(a) and in Fig. 6.1, which indicates that the inter-element capacitance is same in both structures and the value of C obtained by Equation (3.4) is used to compute the inter element capacitance of the wedge shaped metal vane loaded ring FSS structure. Once the C has been known, the change in the resonance frequency of the structure shown in Fig. 6.1 is controlled by the four wedge

shaped metal vanes and its associated inductance L_2. The inductance due to four metallic vanes has been given by the modified formula, which is obtained by multiplying a constant *n* with a factor $\sin\theta$. The modified expression is given as:

$$L_2(nH) = 2n \times 10^{-4} r_o \left[\ln\left(\frac{r_o}{w+t}\right) + 1.193 + 0.333\left(\frac{w+t}{r_o}\right)\right] \sin\theta \quad (6.1)$$

where, *n* is the number of vanes. In the present analysis, the value of *n* is 4 and *w* is the width of the conducting strip. In Equation (6.1), r_o is the length of the arc of the metal vanes as shown in Fig. 6.1, and *t* is the thickness of the conductor. However, the value of r_o for different cases has been approached to unity, hence to simplify the analysis, we have assumed the value of r_o is equal to the unity. The total inductance (L) is the algebraic sum of L_1 and L_2. The value of L_1 is due to the diameter of the circular ring and it is obtained by using Equation (3.4). In addition to this, there are four wedge shaped metallic vanes which has been used to control the value of L_2. However, the overall inductance of the azimuthally periodic wedge shaped vane loaded structure has been given as:

$$L = L_1 + L_2 \quad (6.2)$$

The resonant frequency (f_r) of azimuthally periodic wedge shaped metallic vane FSS structure is given as: $f_r = \frac{1}{2\pi\sqrt{LC}}$. For any value except the inner radius of the wedge shaped vane (r_1) is equal to zero, the $L > L_1$, otherwise $L = L_1$.

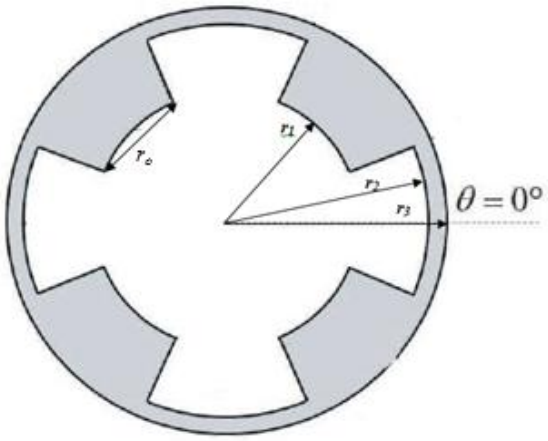

Fig. 6.1 The unit-cell configuration of an azimuthally periodic wedge-shaped metallic vane loaded circular ring FSS structure.

6.2.1 PARAMETRIC OPTIMIZATION OF PROPOSED BANDSTOP FSS STRUCTURE

In order to improve the performance of the proposed FSS structure shown in Fig. 6.1, we have performed the radial optimization for the several values of *M*, where *M* is the ratio of outer radius (r_2) to the inner radius (r_3) of the structure. Considering the minimum deviation in the resonance frequency, which is computed numerically using CST Microwave Studio, Ansoft HFSS and Ansoft Circuit Simulator, for different values of *M* have been discussed in the Table 6.1 and Table 6.2. The radial optimization has been achieved in two different cases:

1) the width (w_2) of the wedge-shape conducting strip, which results from the (r_2-r_1) has been fixed and radially increases the width (w_1) of the circular conducting strip, which results from the (r_3-r_2) and

2) the width (w_1) of the circular conducting strip has been fixed and radially increases the width (w_2).

In both aforementioned cases, the value of the periodicity (p = 16.39 mm) remains same. According to the case-1, to achieve the radial optimization for different values of the *M* through keeping the width (w_2) fixed and radially increasing the width (w_1), we have computed the values of inductance and capacitance numerically and validated the results through the CST Microwave Studio, Ansoft HFSS and Ansoft Circuit Simulator, as shown in Fig. 6.2(a), Fig 6.2(b) and Fig 6.2(c), respectively and Table 6.1. As the width (w_1) of the conducting strip has been changed as 0.4, 0.6, 0.8 and 1.0 mm, the value of the L_1 is also varied, which is calculated as 6.35 nH, 5.35 nH, 4.67 nH and 4.50 nH by Equation (3.3), respectively and provide the significant change in the overall values of the inductance. On the other hand, the width (w_2) of the wedge-shape conducting strip is fixed, because of which the value of L_2 is fixed which has been calculated by Equation (6.1). The overall values of the inductance are 6.423 nH, 5.423 nH, 4.743 nH and 4.503 nH for 0.85, 0.80, 0.75 and 0.70 values of *M*, respectively. In this case, we have considered the change in the value of the capacitance, which is 0.0156 pF, 0.0186 pF, 0.0216 pF and 0.0230 pF for the each value of *M*, respectively. The Fig. 6.2(a), Fig. 6.2(b), Fig. 6.2(c) and Table 6.1,

demonstrate that with the decrease in the value of *M*, the resonant frequency downshifts and approaches the intended frequency, which is 15 GHz and results the optimization of the structure.

Table 6.1 The radial optimization keeping the width (w_2) of the wedge-shaped conducting strip is fixed and radially increasing the width (w_1) of the circular conducting strip.

r_3 (mm)	r_2 (mm)	M= r_2 / r_3	f_r (GHz) (Analytical)	f_r (GHz) (CST MWS)	f_r (GHz) (Ansoft HFSS)	f_r (GHz) Ansoft Circuit Simulator
2.8	2.4	0.85	15.92	16.05	16.32	15.94
3.0	2.4	0.80	15.87	15.82	16.16	15.89
3.2	2.4	0.75	15.70	15.63	15.98	15.74
3.4	2.4	0.70	15.67	15.43	15.83	15.70

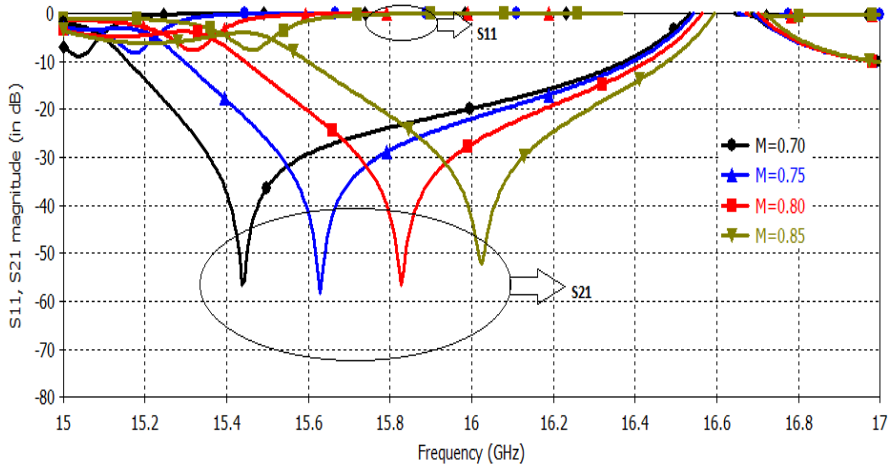

(a)

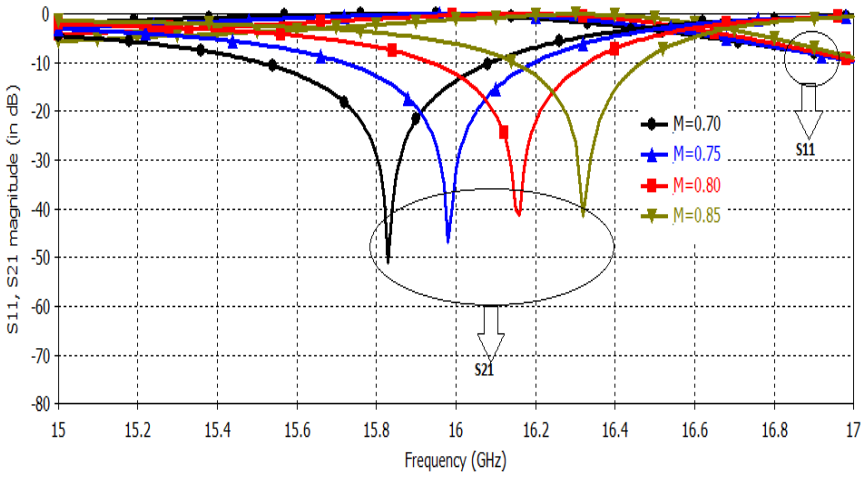

(b)

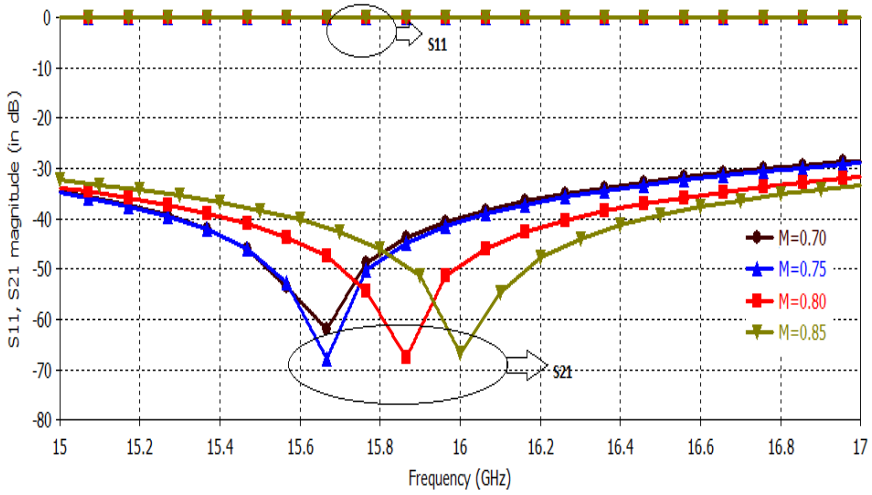

(c)

Fig. 6.2 The radial optimization of proposed structure through simulation, keeping the width (w_2) is fixed and radially increasing the width (w_1), in Ku band using (a) CST Microwave Studio (b) Ansoft HFSS and, (c) Ansoft Circuit Simulator.

Table 6.2 The radial optimization keeping width (w_1) of the circular conducting strip fixed and radially increasing the width (w_2) of the wedge-shaped conducting strip.

r_1 (mm)	r_2 (mm)	$M = r_1/ r_2$	f_r (GHz) (Analytical)	f_r (GHz) (CST MWS)	f_r (GHz) (Ansoft HFSS)	f_r (GHz) Ansoft Circuit Simulator
2.0	2.4	0.83	15.92	16.050	16.32	15.94
1.9	2.4	0.80	15.89	16.030	16.30	15.93
1.8	2.4	0.75	15.87	16.026	16.26	15.90
1.7	2.4	0.70	15.84	16.020	16.25	15.86

According to case-2, the radial optimization has been achieved by keeping the width (w_1) fixed and radially increases the width (w_2). Due to the fixed value of the width (w_1), the value of the L_1 (nH) remain fixed and has been calculated by Equation (3.3), which is 6.35 nH. Moreover, with the change in the width (w_2), the value of L_2 (nH) changes, which results the change in the overall inductance of the proposed structure. We have computed the value of overall inductance from Equation (6.2) which is 6.42 nH, 6.44nH, 6.46 nH and 6.48 nH for 0.83, 0.80, 0.75 and 0.70 values of *M*, respectively. In order to simplify the analysis, we have assumed that the value of capacitance remains same, which is 0.0156 pF because during the analysis negligible change has been achieved in the value of capacitance.

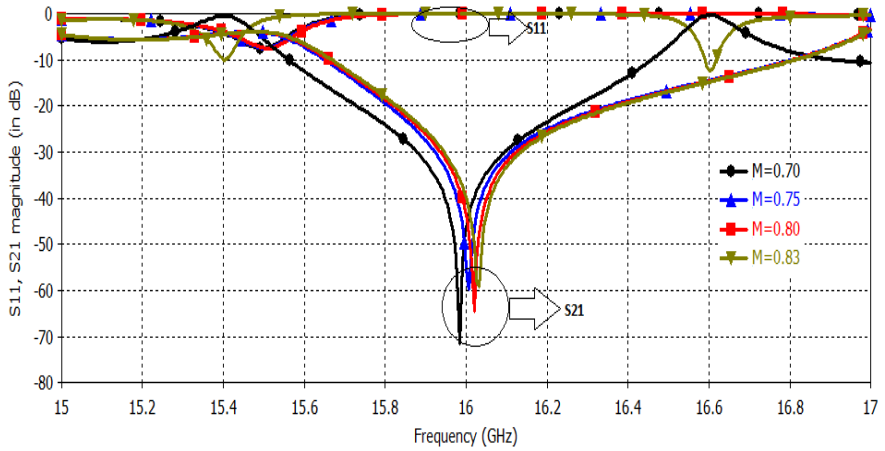

(a)

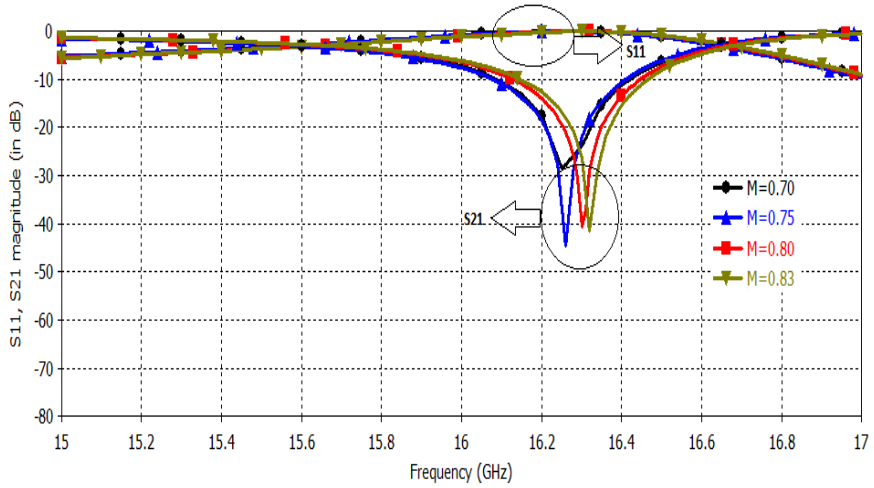

(b)

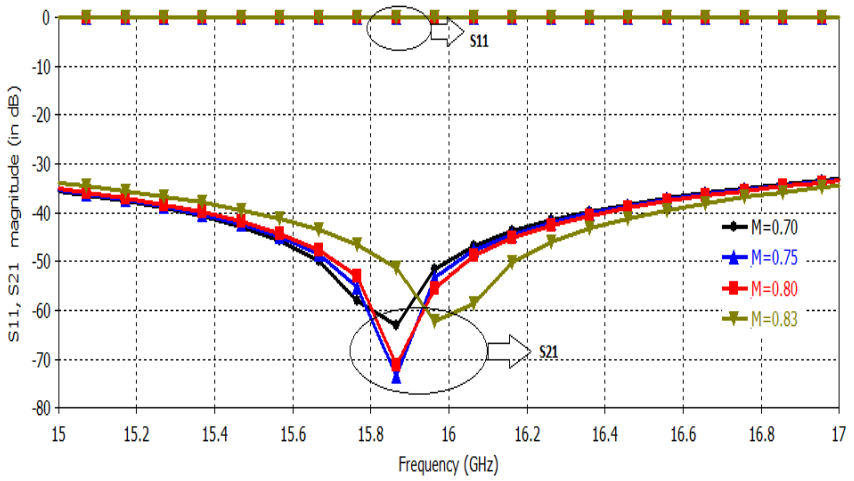

(c)

Fig. 6.3 The radial optimization of the proposed structure through the simulation, keeping width (w_1) fixed and increasing the width (w_2) by using (a) CST Microwave Studio and (b) Ansoft HFSS and, (c) Ansoft Circuit Simulator in Ku band.

To validate the numerical analysis, we have simulated the proposed structure (shown in Fig. 6.1) using CST Microwave Studio, Ansoft HFSS and Ansoft Circuit Simulator, which results in a close agreement between the analytical and simulation results. The analytical technique used by Ansoft Circuit Simulator is based on the mixed potential integral equation (MPIE), which is solved by using the MoM. Moreover, the mixed potential integral equation expresses the electric and magnetic field as a combination of a vector and a scalar potential as discussed in [190]. The comparison of results obtained analytically, using CST Microwave Studio, Ansoft HFSS and Ansoft Circuit Simulator has been shown in Table 6.2. Further, Fig 6.3(a), Fig 6.3(b) and Fig. 6.3(c) obtained using CST Microwave Studio, Ansoft HFSS and Ansoft Circuit Simulator, respectively have demonstrated that with the decrease in the value of *M*, the resonance frequency for transmission/parameters shifts downward, which is due to increase in the inductive effect and approaches the intended frequency of the structure. The results obtained using CST Microwave Studio, Ansoft HFSS and Ansoft Circuit Simulator has achieved the percentage deviation of 0.8%, 2.4% and 0.12%, respectively with respect to the numerical results. The deviation in results of CST Microwave Studio, Ansoft HFSS and numerical approach is due to the different simulation approaches.

6.2.2 EFFECT OF NUMBER OF VANES OF PROPOSED BANDSTOP FSS

In Section 6.2.1, we have achieved the radial optimization of the proposed structure (shown in Fig. 6.1) to ensure the improved performance in terms of the reflection/transmission characteristics. In the present section, we have discussed the angular sensitivity on the proposed optimized structure by increasing the number of vanes in the structure as shown in Fig. 6.1. However, by changing the number of vanes, the periodicity of the FSS unit-cell has been influenced and due to the periodic arrangement of vanes, the field at filter plane is described in terms of the space-harmonics, which are called as Floquet harmonics. Therefore, the total field of FSS has been expanded as the superposition of a finite number of Floquet harmonics [168]. However, the proposed structure has four vanes which are present at an angular periodicity of 45^{o}. We have increased the number of vanes by reducing the angular interval between the vanes as well as angular width of the vanes, which results the downshift in resonance frequency and decreases the 3-dB reflection and transmission

bandwidth as shown in Table 6.3 and Fig. 6.4. This variation is due to the space harmonic expansion of the field occurring because of the increase in the number of vanes in the unit-cell.

Fig. 6.4(a) and Fig. 6.4(b) have demonstrated that with the increase in number of vanes in the proposed structure from 4 to 6, the resonance frequency downshifts with a percentage shift of 0.375 % and 0.123 % through CST Microwave Studio and Ansoft HFSS, respectively. With further increase the number of vanes in the proposed structure from 6 to 8, the resonance frequency up-shifts with the percentage of 0.339 % and 0.245 % through CST Microwave Studio and Ansoft HFSS, respectively. In addition to this, with the increase in the number of vanes in the proposed structure from 4 to 8, the 3-dB reflection/transmission bandwidth has been decreased with a percentage shift of 9.92 % and 9.24 % using CST Microwave Studio as well as 8.63 % and 7.46 % using Ansoft HFSS. In order to validate the simulation results obtained from CST Microwave Studio and Ansoft HFSS, we have performed the analysis by replacing the value of *n* as 4, 6 and 8 in Equation (6.1), which result the overall value of the inductance as 6.420 nH, 6.50 nH and 6.556 nH from Equation (6.2), respectively. Further, the values of the inductance and capacitance achieved through the analytical process have been used to obtain the reflection and transmission coefficient through the Ansoft Circuit Simulator as shown in Fig. 6.4(c) which has demonstrated the maximum percentage shift of 0.162% and 2% in the resonant frequency with respect to that of simulated by CST Microwave Studio and Ansoft HFSS, respectively. Moreover, the nature of shift in the resonant frequency remains same as demonstrated through CST Microwave Simulation and Ansoft HFSS.

Table 6.3 The effect of increase in the number of vanes on the resonance frequency and 3-dB reflection/transmission bandwidth.

AOI	No. of vanes	f_r (GHz)		3-dB Reflection Bandwidth		3-dB Transmission Bandwidth	
		CST MWS	Ansoft HFSS	CST MWS	Ansoft HFSS	CST MWS	Ansoft HFSS
45^o	4	15.99	16.32	1.552	0.996	1.580	1.032
30^o	6	15.93	16.30	1.513	0.926	1.537	0.980
22.5^o	8	15.98	16.34	1.398	0.910	1.434	0.955

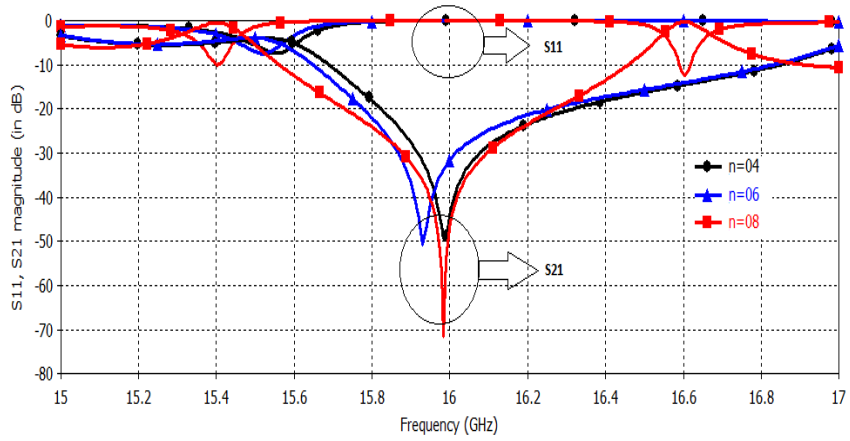

(a)

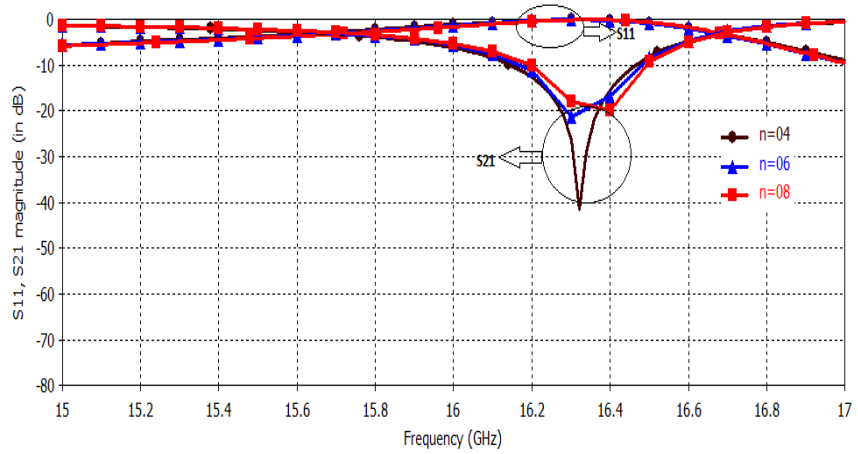

(b)

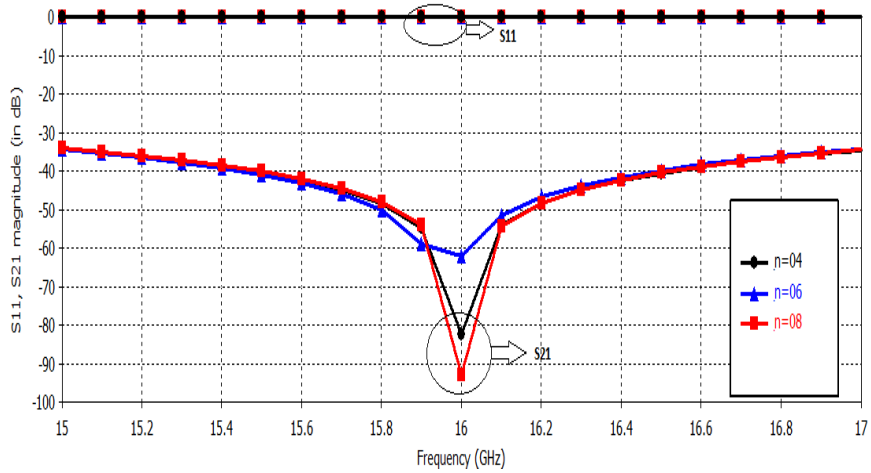

(c)

Fig. 6.4 The effect of increase in the number of vanes on resonance frequency and 3-dB reflection/transmission bandwidth through the (a) CST Microwave Studio, (b) Ansoft HFSS, and (c) Ansoft Circuit Simulator.

6.2.3 EFFECT OF AOI ON PROPOSED BANDSTOP RING FSS

In this section, we have discussed the angular insensitivity of the proposed structure (shown in Fig. 6.1) at different AOIs of the electric field such as at 0^o, 10^o, 30^o and 50^o. The simulation results of proposed optimized structure using CST Microwave Studio and Ansoft HFSS have demonstrated 0.04% and 0.4% up-shift in the resonance frequency, respectively with respect to the normal wave incidence, which is very small as compared to that of the various reported FSS structures, which is given in Table 6.4. As we increase the AOI from 30^o to 50^o, the resonance frequency saturates and results the angular stability. With the increase in the AOI from 0^o to 50^o, the 3-dB reflection and transmission bandwidth has been reduced up to 4.62 % and 3.22 % as obtained using CST Microwave Studio as well as 6.03 % and 5.95 % as obtained using Ansoft HFSS, respectively which is significantly very small as compared to that reported in [154]. When we apply the electric field at oblique angles, the overall value of the inductance has been changed by a factor of $cos\theta$ as compared to the value of inductance obtained from the normal wave incidence electric field. The value of inductance has been computed as 6.42 nH, 6.32 nH, 5.55 nH and 4.12 nH for 0^o, 10^o, 30^o and 50^o, respectively. However, we have computed the value of capacitance from Equation (3.4).

Table 6.4 The comparison of angular and polarization stability of the proposed FSS with other reported literatures.

AOI	Reported Literature	FSS structure	% deviation of f_r
45^o	Lee and Langley [162]	Gridded and Double Square Loop	7
45^o	Reed [163]	Rectangular Dipole	16.6
45^o	Sung et al [175]	Square Loop	10
45^o	Yan et al [176]	Spiral Meander Line	5
45^o	Parker and Hamdy [177]	Circular Ring	5.95
45^o	Hosseinipanah et al [178]	Square Loop	5.45
50^o	Proposed FSS	Azimuthally Periodic Wedge Shaped	0.04 (CST MWS)

Further, through the computed values of inductance and capacitance, we have obtained the reflection and transmission response by Ansoft Circuit Simulator, which have not demonstrated the saturation in resonant frequency, rather experience a small up-shift to 0.125 GHz as shown in Fig. 6.5(c). Moreover, the reflection parameters

obtained through Ansoft Circuit Simulator have demonstrated 100% reflection over the 15-17 GHz as shown in Fig. 6.2(c), Fig. 6.3(c), Fig. 6.4(c) and Fig. 6.5(c), which is due to the fact that the reflection coefficient achieved through the MoM technique (on which Ansoft Circuit Simulator is based) is represented in terms of the induced current (symmetric and anti-symmetric current distributions) on the periodic elements of FSS structure as discussed in [191].

Moreover, the proposed azimuthally periodic wedge-shaped metal vane loaded circular ring FSS structure, which has been achieved through the passive loading of circular ring provides very significant results in terms of the angular stability and bandwidth control as compared to that of the classical circular ring FSS structure as discussed in Table 6.5 and Table 6.6. For the same value of the periodicity (p), outer radius (r_3), inner radius (r_2) of the classical circular ring and width (w_1) of the circular conducting strip, we have discussed the angular stability and bandwidth control for 0^o, 10^o, 30^o and 50^o of AOI.

Table 6.5 The effect of electric field at different AOIs on the resonance frequency and 3-dB transmission/reflection bandwidth of the structure shown in Fig. 6.1.

AOI	f_r (GHz)		3-dB Reflection Bandwidth		3-dB Transmission Bandwidth	
	CST MWS	Ansoft HFSS	CST MWS	Ansoft HFSS	CST MWS	Ansoft HFSS
0^o	16.012	16.32	1.080	1.027	1.084	1.042
10^o	16.018	16.39	1.036	1.000	1.051	0.993
30^o	16.020	16.40	1.032	0.979	1.050	0.988
50^o	16.020	16.40	1.030	0.965	1.049	0.980

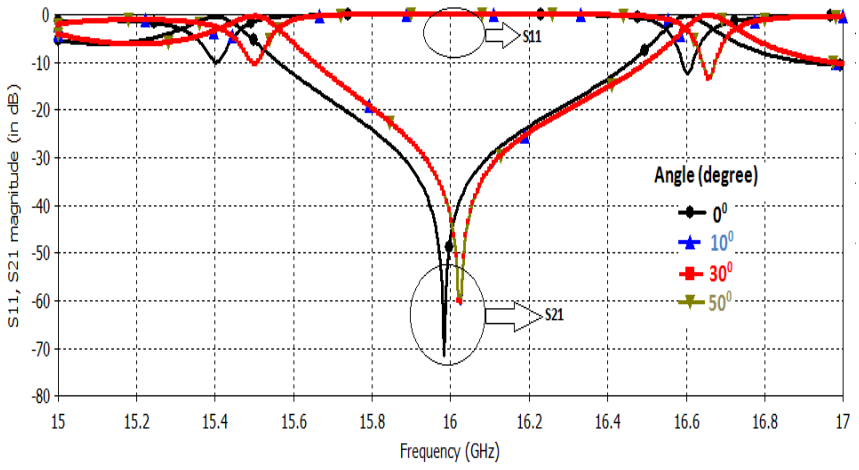

(a)

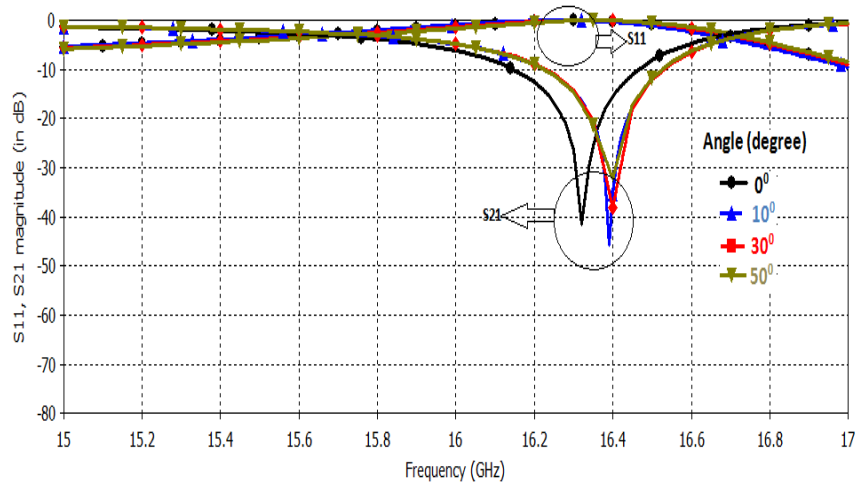

(b)

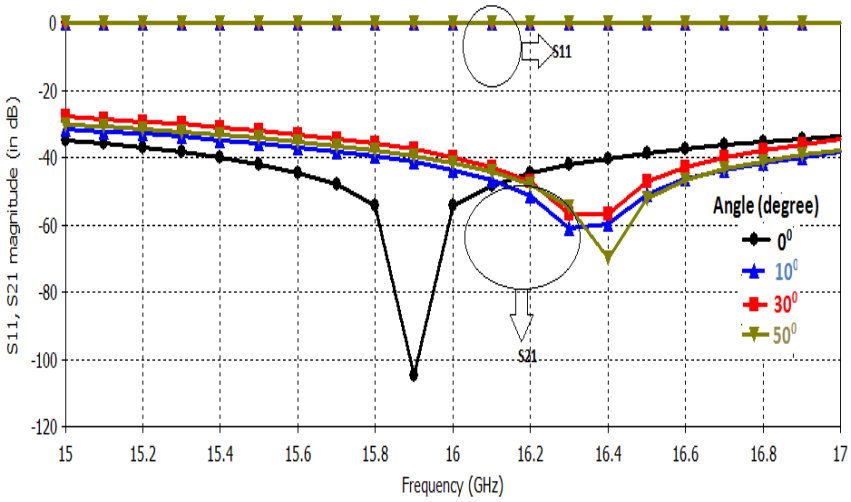

(c)

Fig. 6.5 The effect of electric field at different AOI on the resonance frequency and 3-dB reflection/transmission bandwidth of the proposed structure using (a) CST Microwave Studio, (b) Ansoft HFSS, and (c) Ansoft Circuit Simulator.

Table 6.6 The angular stability and 3-dB reflection as well as transmission bandwidth of the classical circular ring FSS structure.

AOI	f_r (GHz)		3-dB Reflection Bandwidth		3-dB Transmission Bandwidth	
	CST MWS	Ansoft HFSS	CST MWS	Ansoft HFSS	CST MWS	Ansoft HFSS
0^o	16.30	16.88	0.5000	0.2590	0.4563	0.3633
10^o	15.94	16.40	0.4876	0.2158	0.4078	0.3298
30^o	15.73	16.20	0.3987	0.1988	0.3898	0.3022
50^o	15.50	15.98	0.3672	0.1900	0.3565	0.2788

The electrical performance comparison between the proposed conductive loaded circular ring and classical circular ring such as transmission/reflection frequency response and transmission/reflection bandwidth at different AOI are shown in Table 6.4 and Table 6.5, respectively. As for the simulation results of Table 6.5 and Table 6.6, it is illustrated that the downshift of the resonance frequency achieved in case of the classical circular ring FSS structure is 5.16 % and 6.17%, which is significantly higher than 0.04 % and 0.4 % as obtained for the proposed FSS structure up to 50^{o} of AOI with the CST Microwave Studio and Ansoft HFSS, respectively. Also, in the case of classical circular ring FSS structure, the percentage reduction in 3-dB reflection/transmission bandwidth is 26.55 %, 21.87 % with the CST Microwave Studio and 26.64 %, 23.25 % using the Ansoft HFSS which is significantly higher than that of the 4.62 %, 3.22 % as obtained using CST Microwave Studio and 6.03 %, 5.95 % through Ansoft HFSS for the proposed FSS structure.

6.3 ANALYSIS OF AZIMUTHALLY PERIODIC WEDGE SHAPED CIRCULAR RING BANDPASS FSS STRUCTURE

6.3.1 EQUIVALENT CIRCUIT REALIZATION

In this sub-section, the resonance behaviour of an azimuthally periodic wedge-shaped circular ring bandpass FSS structure, which is shown in Fig. 6.1with its geometrical parameters such as periodicity (p), outer radius of the circular aperture (r_3), inner radius of the circular aperture (r_2), inner radius of wedge-shaped aperture (r_1), width of the circular aperture (w_1), which results from the (r_3-r_2) and width of the wedge shaped aperture (w_2), which results from the (r_2-r_1). The resonance behaviour of this bandpass FSS structure is discussed by considering it as the two port network, which has randomly selected input/output port along the circumference of the proposed bandpass structure, and a transmission-line model is used to extract the equivalent lumped circuit elements such as inductance (L) and capacitance (C). The port analysis of the azimuthally periodic wedge-shaped circular ring bandpass FSS provides a parallel RLC circuit, which has resistance (R), capacitance (C) and an equivalent inductance ($L = L_1 \parallel L_2$), where L_1 and L_2 is the inductance due to the conducting portion. For the lossless FSS structure, the value of R vanishes. Moreover, the periphery of circular aperture must be equal or integer multiple of resonance frequency, which provides the equivalent inductance and width of aperture

corresponds to the capacitance of the proposed FSS structure [43, 70]. As discussed in [192], if the width of circular ring is narrow (in the microwave regime), then the circular ring resonator exhibits same dispersion characteristics as that of the transmission-line resonator, therefore the ring resonator has been analyzed using the transmission-line model. Similarly, the electrical equivalent behaviour of the proposed bandpass FSS structure has been analyzed using the two-port network based on the transmission-line model [192]. The bandpass FSS structure has been represented in terms of the parallel RLC circuit using the EC approach as shown in Fig. 6.6.

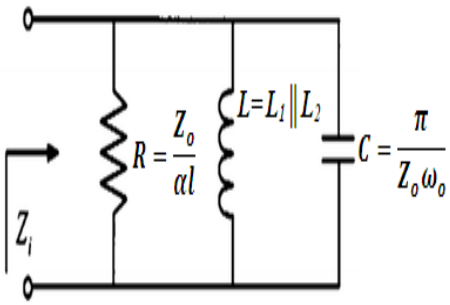

Fig. 6.6 The equivalent circuit diagram of the azimuthally periodic wedge shaped circular ring FSS structure.

However, the input impedance of the azimuthally periodic wedge shaped circular ring bandpass FSS structure in terms of the parallel RLC circuit is given as [193]:

$$Z_i = \frac{R}{1+2j\Delta\omega CR} \tag{6.3}$$

where, Z_i, R and C are the input impedance, resistance in Ω and capacitance of the azimuthally periodic wedge shaped circular ring bandpass FSS structure, respectively. In addition to this, the transmission-line model is used to obtain the input impedance of the proposed bandpass FSS structure. For the transmission-line model, the input impedance in terms of the Y-parameters, which have been achieved through the ABCD matrix, is given as [192]:

$$Z_{ic} = \frac{Z_o \omega_r}{\alpha l \omega_r + 2j\Delta\omega\pi} \tag{6.4}$$

where, Z_{ic}, Z_o, α, l, ω_r and $\Delta\omega$ are the input impedance, characteristic impedance, attenuation constant, length which represents the mean circumference, resonance angular frequency and small deviation in the angular frequency of the transmission-

line model, respectively of the transmission-line model. However, with the comparison of Equation (6.3) and Equation (6.4), we have achieved the resistance and capacitance as follows.

$R = \frac{Z_o}{\alpha l}$ and,

$C = \frac{\pi}{Z_o \omega_r}$ (6.5)

In the azimuthally periodic wedge shaped circular ring bandpass FSS structure, the equivalent inductance (L) is equal to $L_1 \| L_2$. Here, L_1 is computed using Eq. (3.4) as discussed in chapter 3. In addition to this, L_2 is using Eq. (6.1). Moreover, the total inductance $L = L_1 \| L_2$ (6.6)

Therefore, the resonance frequency of the azimuthally periodic wedge shaped bandpass FSS structure is given as: $f_r = \frac{1}{2\pi\sqrt{LC}}$.

6.3.2 PARAMETRIC SYNTHESIS

The mean radius of azimuthally periodic wedge shaped circular ring bandpass FSS structure is given as [2]: $2\pi r = \lambda_o/\sqrt{\varepsilon_{eff}}$, where, r, λ_o and ε_{eff} are the mean radius, operating wavelength and effective dielectric permittivity, respectively. Further, we have computed the value of C for each operating frequency using Equation (6.5) and value of L_1 using Equation (3.3). In addition to this, we have tuned the value of L_2 by varying the associated geometrical parameters in order to achieve the appropriate value of L, which provides the desired/intended resonance frequency. We have computed the values of L and C, which represent the unit-cell of proposed bandpass FSS structure at normal wave incidence for 3 GHz, 15 GHz and 25 GHz. Using the theory discussed in this Section, the geometrical parameters computed at each frequency of interest such as at 3 GHz, 15 GHz and 25 GHz are shown in Table 6.7.

Table 6.7 The geometrical parameters of the proposed bandpass FSS structure at 3 GHz, 15 GHz and 25 GHz.

Operating Frequency (GHz)	r_1 (mm)	r_2 (mm)	r_3 (mm)
3	8.0	12	18
15	2.0	2.4	3.0
25	0.5	1.1	1.9

6.3.3 DESIGN AND SIMULATION

In this sub-section, the azimuthally periodic wedge shaped circular ring bandpass FSS structure is designed at 3 GHz, 15 GHz and 25 GHz using the commercial simulators such as CST Microwave Studio and Ansoft HFSS. To design the unit-cell of azimuthally periodic wedge shaped circular ring bandpass FSS, Arlon AD 320 is used as dielectric substrate (dielectric permittivity, ε_r = 3.2, tanδ = 0.0028 and thickness 0.762 mm) and copper is used as a conductive sheet (electrical conductivity, σ = 5.8 $\times 10^7$ S/m and thickness, t = 0.02 mm). The angular stability, 3-dB reflection/ transmission bandwidth and FBW of the azimuthally periodic wedge shaped circular ring bandpass FSS for perpendicular and parallel polarized wave, which has been incidence up to 50^o AOI at 3 GHz, 15 GHz and 25 GHz, are presented. In addition to this, we have also explored the electric field distribution of the azimuthally periodic wedge shaped circular ring bandpass FSS at each frequency of interest for the normal wave-incidence.

6.3.3.1 ANGULAR/POLARIZATION STABILITY

The values of r_1, r_2 and r_3 at f_r = 3 GHz are as demonstrated in the first row of Table 6.7. In addition to this, the characteristic impedance, Z_o = 377 Ω, mean radius, a = 15 mm, w_1 = 6 mm, w_2 = 4 mm and r_o=6.280 mm. The value of capacitance C is computed using Equation (6.5) that is 0.442 pF. Further, the value of inductance L_1 (using Equation (3.3)) and L_2 (using Equation (6.1)) are computed as 18.68 nH and 9.30 nH, respectively. Moreover, the value of L (nH) is computed using Equation (6.6), which is 18.68 nH ‖ 9.30 nH and results the 6.20 nH. The azimuthally periodic wedge-shaped circular ring bandpass FSS structure resonates at 3.1 GHz for normal wave incidence, which has equivalent circuit parameters such as C and L are 0.442 pF and 6.20 nH, respectively. Table 6.8 discusses the effect of perpendicular and parallel polarized wave incidence up to 50^o AOI on the resonance frequency and FBW of the azimuthally periodic wedge-shaped circular ring bandpass FSS.

For the perpendicular and parallel polarized wave incidence upto 50^o AOI on the azimuthally periodic wedge-shaped circular ring bandpass FSS, the FBW of approximately 59% and 65% have been achieved as illustrated in Table 6.8, respectively. For the perpendicular polarized wave incidence up to 50^o AOI, the

resonance frequency of the azimuthally periodic wedge-shaped circular ring bandpass FSS downshifts up to 0.77% with reference to the normal wave incidence which is computed by using CST Microwave Studio as shown in Fig. 6.7(a). However, this downshift is order of 0.56% when the simulation is performed using Ansoft HFSS as shown in Fig. 6.7(b). Fig. 6.8(a) and Fig. 6.8(b) demonstrate 0.65% and 0.59% downshift in the resonance frequency with reference to the normal wave incidence using CST Microwave Studio and Ansoft HFSS, respectively, for the parallel polarized wave incidence up to 50^{o}.

On the similar way, the Equation (6.5) and Equation (6.6) have been used to compute the value of *C* and *L* at 15 GHz, which are 0.884 fF and 1.29 nH, respectively, and results the resonance frequency of 14.98 GHz at normal wave incidence. Table 6.9 illustrates the effect of the perpendicular and parallel polarized wave incidence up to 50^{o} AOI on the resonance frequency and 3-dB bandwidth of the proposed bandpass FSS structure. Fig. 6.9(a) and Fig. 6.9(b) demonstrate 0.013% and 0.79% downshift in the resonance frequency at 15 GHz with reference to the normal incidence using CST Microwave Studio and Ansoft HFSS, for perpendicular polarized wave up to 50^{o} AOI, respectively. Fig. 6.10(a) demonstrates 0.198% downshift in the resonance frequency with reference to the normal wave incidence for the parallel polarized wave incidence up to 50^{o} using CST Microwave Studio at 15 GHz. However, Fig. 6.10(b) demonstrates not any significant shift in the resonance frequency when the simulation is performed using Ansoft HFSS. In addition to this, Fig. 6.9 and Fig. 6.10 demonstrate that the proposed bandpass FSS structure provide wide-band characteristics in Ku-band. For 25 GHz intended frequency, the value of *C* and *L* is 0.53 fF and 0.768 nH, respectively, which provides the resonance frequency 24.98 GHz for the normal wave incidence. Table 6.10 discusses the effect of perpendicular and parallel polarized wave incidence up to 50^{o} AOI on the resonance frequency and FBW of the proposed bandpass FSS structure. For the perpendicular polarized wave incidence up to 50^{o} AOI, the resonance frequency of the proposed bandpass FSS structure downshift upto 0.055% with reference to the normal incidence when the simulation has been performed by using CST Microwave Studio as shown in Fig. 6.11(a). However, Fig. 6.11(b) shows no any significant shift in the resonance frequency when the simulation is performed using Ansoft HFSS. Fig. 6.12(a)

demonstrates 0.05% downshift in the resonance frequency with reference to the normal wave incidence for the parallel polarized wave incidence up to 50^o using CST Microwave Studio. However, Fig. 6.12(b) shows no any significant shift in the resonance frequency when the simulation is performed using Ansoft HFSS. In addition to this, for the perpendicular and polarized wave incidence up to 50^o AOI on the proposed bandpass FSS, the FBW of approximately 8.2% and 8%, respectively is achieved, as presented in Table 6.10.

Moreover, at each frequency of interest (3 GHz, 15 GHz and 25 GHz), the resonance frequency achieved theoretically, using CST Microwave Studio and Ansoft HFSS experiences a little deviation, which is due to the following reasons.

1) Use of different numerical techniques (EC technique/transmission-line method is used to theoretically compute the resonance frequency (simpler and computationally in-extensive), CST microwave Studio is based on finite integral technique [52] and Ansoft HFSS [53] is based on finite element technique),

2) The CST Microwave Studio and Ansoft HFSS take into account the effect of dielectric permittivity, loss tangent and metal conductivity to compute the resonance response, however, the theoretical computation of the resonance frequency (using equivalent circuit technique/transmission-line method) consider only the effect of dielectric permittivity but not the loss tangent and metal conductivity, and

3) Due to the different mesh types used in CST Microwave Studio and Ansoft HFSS.

Table 6.8 The angular stability and fractional bandwidth of the proposed bandpass FSS structure through CST Microwave Studio and Ansoft HFSS in S-band for perpendicular and parallel polarized wave.

AOI	Perpendicular Polarization				Parallel Polarization			
	CST MWS		Ansoft HFSS		CST MWS		Ansoft HFSS	
	f_r (GHz)	FBW (%)	f_r (GHz)	FBW (%)	f_r (GHz)	FBW (%)	f_r (GHz)	FBW (%)
0^o	3.360	76	3.40	76.47	3.392	70.7	3.40	70.5
10^o	3.356	73.9	3.40	73.5	3.383	69.8	3.40	70.5
30^o	3.342	60.5	3.39	61.9	3.381	66.2	3.38	65.0
50^o	3.334	59.5	3.38	59.1	3.370	65.3	3.38	`65.0

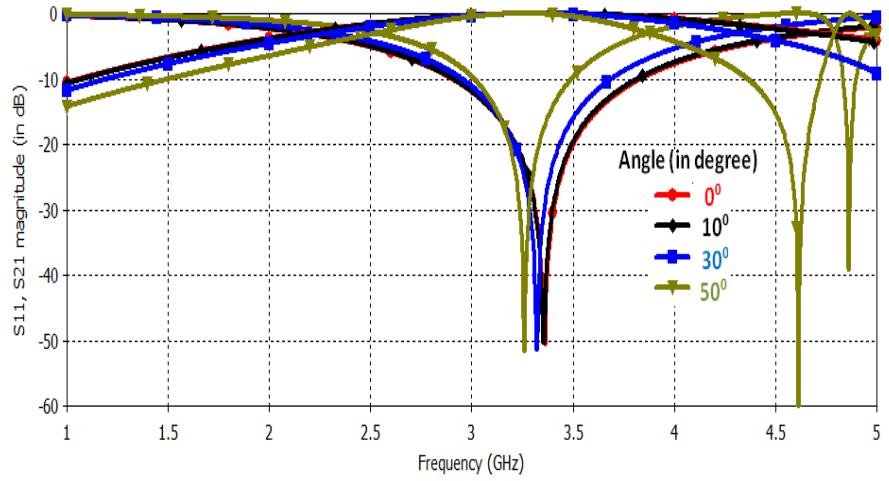

(a)

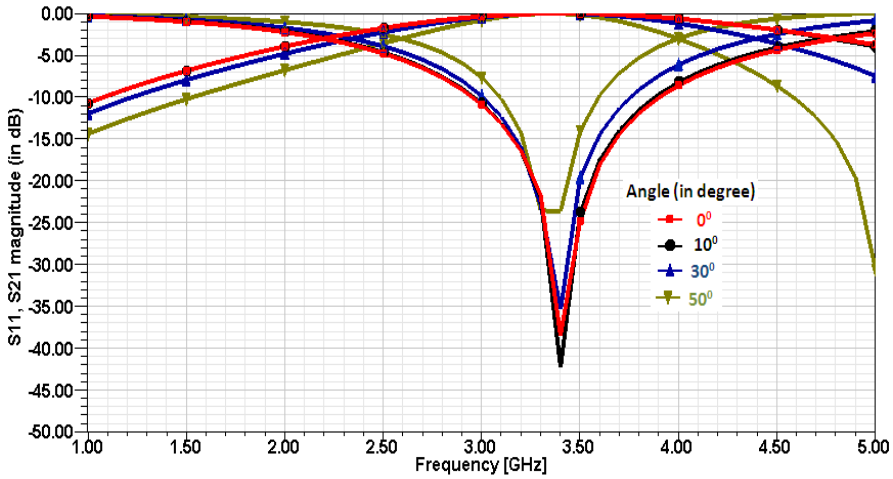

(b)

Fig. 6.7 The frequency response of proposed bandpass FSS structure for perpendicular polarized wave at different AOI in S-band using (a) CST Microwave Studio and (b) Ansoft HFSS.

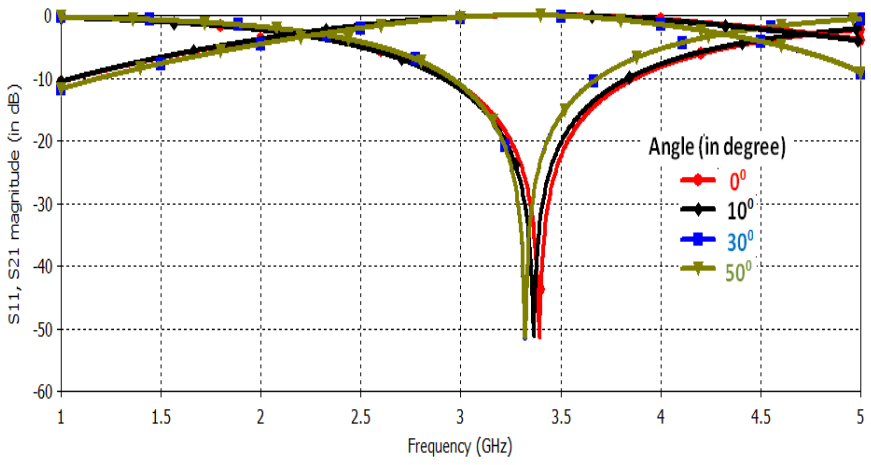

(a)

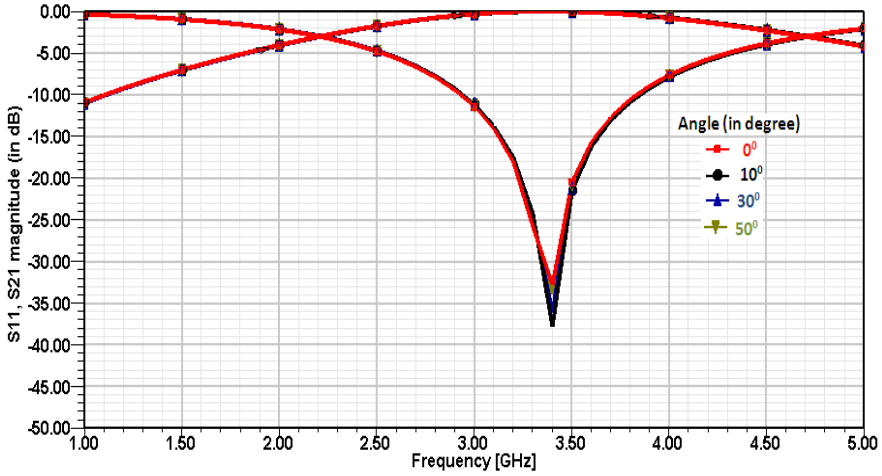

(b)

Fig. 6.8 The frequency response of proposed bandpass FSS structure for parallel polarized wave at different AOIs using in S-band (a) CST Microwave Studio and (b) Ansoft HFSS.

Table 6.9 The angular stability and 3-dB reflection/transmission bandwidth of the proposed bandpass FSS structure through CST Microwave Studio and Ansoft HFSS in Ku-band for perpendicular and parallel polarized wave.

AOI	Perpendicular Polarization		Parallel Polarization	
	CST MWS	Ansoft HFSS	CST MWS	Ansoft HFSS
	f_r (GHz)	f_r GHz)	f_r (GHz)	f_r (GHz)
0^o	15.144	15.15	15.174	15.20
10^o	15.144	15.15	15.168	15.20
30^o	15.142	15.12	15.156	15.20
50^o	15.142	15.03	15.144	15.20

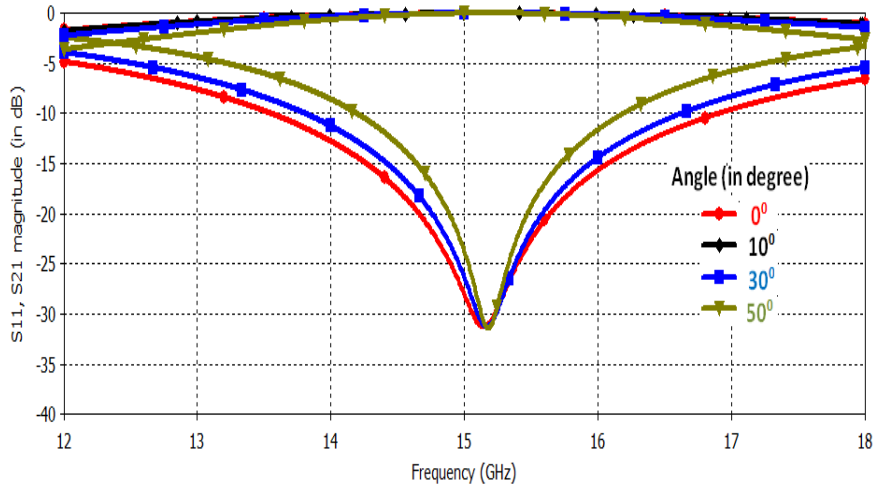

(a)

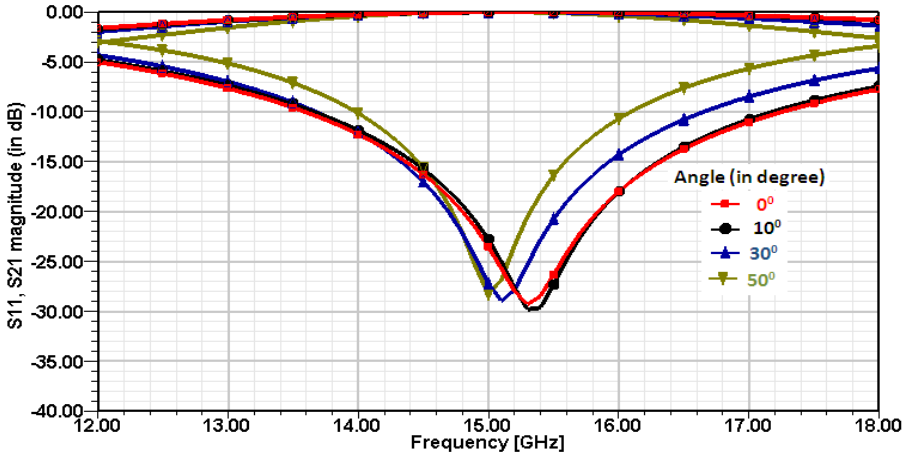

(b)

Fig. 6.9 The frequency response of proposed bandpass FSS structure for perpendicular polarized wave at different AOI in Ku-band using (a) CST Microwave Studio and (b) Ansoft HFSS.

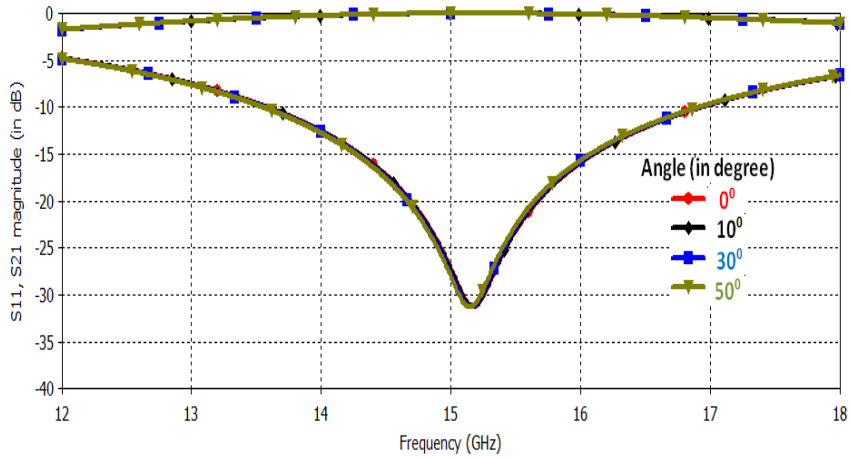

(a)

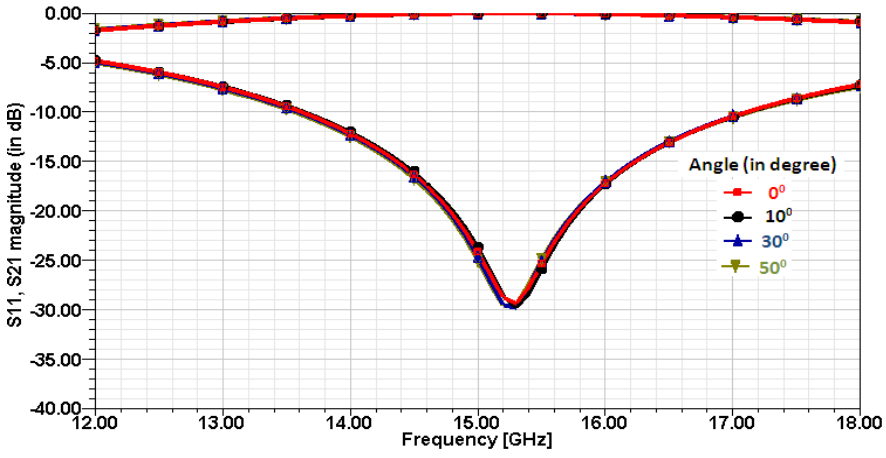

(b)

Fig. 6.10 The frequency response of proposed bandpass FSS structure for parallel polarized wave at different AOI in Ku-band using (a) CST Microwave Studio and (b) Ansoft HFSS.

Table 6.10 The angular stability and 3-dB reflection/transmission bandwidth of the proposed bandpass FSS structure through CST Microwave Studio and Ansoft HFSS in Ka-band for perpendicular and parallel polarized wave.

AOI	Perpendicular Polarization				Parallel Polarization			
	CST MWS		Ansoft HFSS		CST MWS		Ansoft HFSS	
	f_r (GHz)	FBW (%)	f_r (GHz)	FBW (%)	f_r (GHz	FBW (%)	f_r (GHz)	FBW (%)
0^o	25.042	8.4	25.2	8.7	25.0	8.1	25.2	8.3
10^o	25.028	8.3	25.2	8.3	25.0	8.1	25.2	8.3
30^o	25.028	8.2	25.2	8.3	25.0	8.0	25.2	8.3
50^o	25.028	8.2	25.2	8.3	25.0	8.0	25.2	8.3

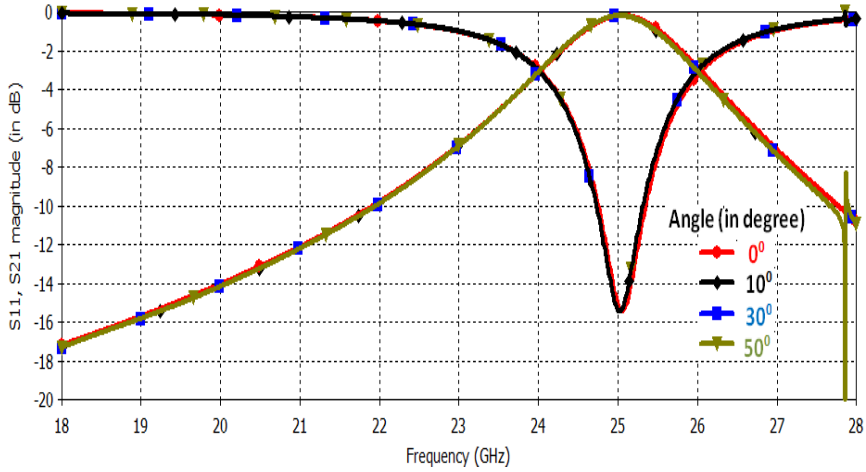

(a)

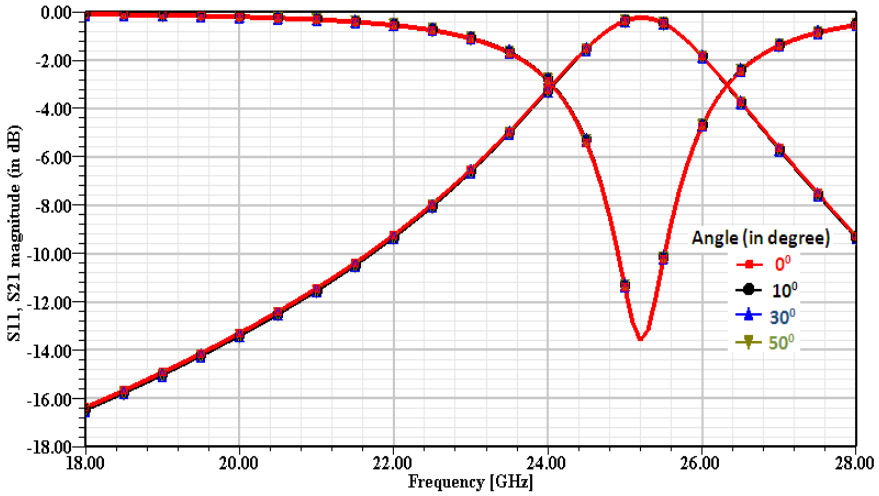

(b)

Fig. 6.11 The frequency response of proposed bandpass FSS structure for perpendicular polarized wave at different AOI in Ka-band using (a) CST Microwave Studio and (b) Ansoft HFSS.

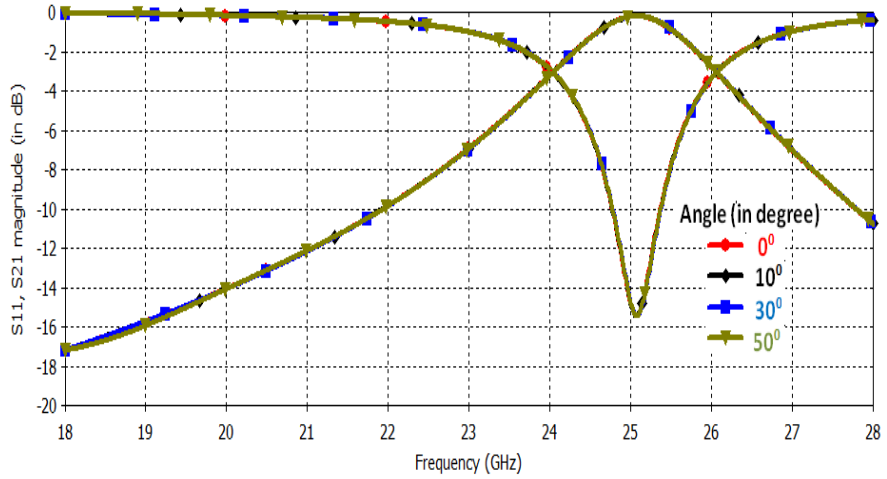

(a)

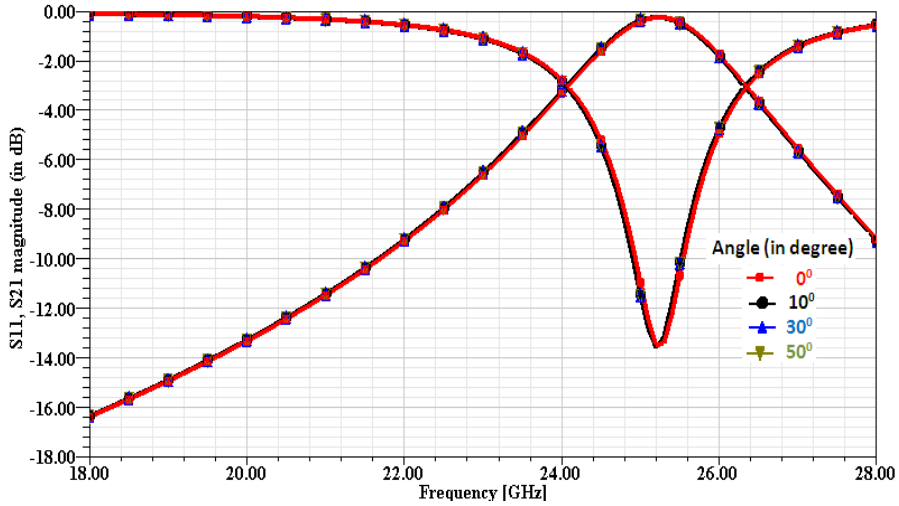

(b)

Fig. 6.12 The frequency response of proposed bandpass FSS structure for parallel polarized wave at different AOI in Ka-band using (a) CST Microwave Studio and (b) Ansoft HFSS.

6.3.3.2 ELECTRIC FIELD DISTRIBUTION

The azimuthally periodic wedge shaped circular ring bandpass FSS structure is designed at each frequency of interest (3 GHz, 15 GHz and 25 GHz) using the geometrical parameters, which are shown in Table 6.7. The structure provides the resonance pole transmission at 3.360 GHz, 15.174 GHz and 25.2 GHz for the normal wave incidence. However, the electric field distribution diagram has the potential to justify the physical mechanism of the bandpass/bandstop filtering characteristics of the FSS structure [156], therefore, we have simulated the electric field distribution at 3.360 GHz, 15.174 GHz and 25.2 GHz for the normal wave incidence. With the electric field distribution, we have observed that the electric field resonance occur in

the aperture (proposed FSS structure) at 3.360 GHz, 15.174 GHz and 25.2 GHz as shown in Fig. 6.13(a), 6.13(b) and 6.13(c), respectively. Moreover, the passband arises due to the enhanced transmission assisted by aperture resonance and outside the circular aperture, the electric field values are significantly weak.

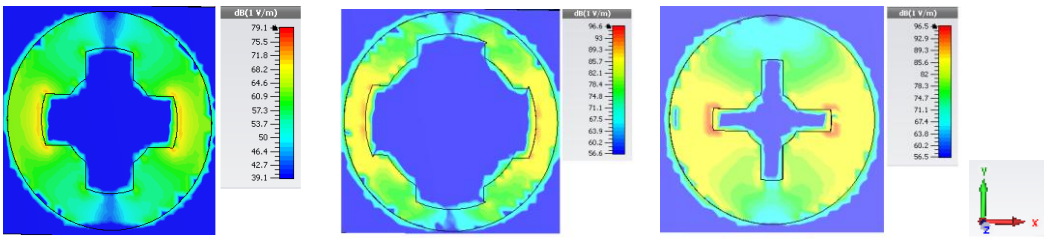

(a) (b) (c)

Fig. 6.13 The electric field distribution of the proposed bandpass FSS structure at (a) 3.360 GHz, (b) 15.174 GHz and (c) 25.2 GHz.

Moreover, the comparison of angular and polarization stability of the azimuthally periodic wedge shaped circular ring bandpass FSS with the other reported FSS structures are listed in Table 6.11, which demonstrates that the azimuthally periodic wedge shaped circular ring bandpass FSS provides significantly better angular and polarization stability upto 50^{o} of AOI.

Table 6.11 Comparison of angular/polarization stability of the azimuthally periodic wedge shaped circular ring bandpass FSS with other reported FSS literatures.

AOI	FSS structure	% deviation of f_r
45^{o}	FSS in [71]	5.00
45^{o}	FSS in [92]	3 (TE incidence) and10 (TM incidence)
60^{o}	FSS in [111]	~1 (TE and TM incidence)
60^{o}	FSS in [154]	~0.1 (TE incidence) and ~1.0 (TE-incidence)
45^{o}	FSS in [162]	7 (TE and TM incidence)
45^{o}	FSS in [163]	16.6
45^{o}	FSS in [175]	7.60
60^{o}	FSS in [176]	~5 (TE and TM incidence)
45^{o}	FSS in [177]	5.95
45^{o}	FSS in [178]	5.45
60^{o}	FSS in [181]	0.52 (TE incidence) and 2.1 (TM incidence)
50^{o}	Bandpass FSS structure	0.65 (TE incidence) and 0.59 (TM incidence) (at 3 GHz) 0.013(TE incidence) and 0 (TM incidence) (at 15 GHz) 0 (TE incidence) and 0 (TM incidence) (at 25 GHz)

6.4 CONCLUSION

In this Chapter, an azimuthally periodic wedge shaped circular ring FSS has been discussed for the bandstop and bandpass filtering characteristics. The radial optimization, effect of number of vanes and angular stability is discussed. The high degree of the angular stability is achieved in azimuthally periodic wedge shaped bandstop circular ring FSS, which is useful in the satellite communication. However, the azimuthally periodic wedge shaped bandstop circular ring FSS provides 0.04% and 0.4% shift in the resonance frequency, which has been achieved through CST Microwave Studio and Ansoft HFSS, respectively up to 50^{o} AOI as compared to that of the normal wave incidence. In addition to this, an azimuthally periodic wedge-shaped circular ring bandpass FSS structure, which provides the angular/polarization stable frequency response with significant FBW in S-band, Ka-band and Ku-band, is also discussed. The transmission-line method is used to obtain the lumped circuit elements of the azimuthally periodic wedge-shaped circular ring bandpass FSS, which offers less computation complexity as compared to that of the other numerical techniques. The azimuthally periodic wedge-shaped circular ring bandpass FSS provides approximately 59% FBW in S-band and wide-band frequency characteristics in Ku-band, which is useful for the satellite communication. However, the azimuthally periodic wedge shaped circular ring FSS structure is practically more feasible because it is single layer and low profile structure, which is very economic from practical perspectives and easy to fabricate compare to the other loaded FSS structures.

CHAPTER-7

CONCLUSION AND FUTURE SCOPE

In order to control the interference in the satellite communication, it is indispensable to use some kind of filter in the antenna system which provides the bandstop and bandpass filtering characteristics. For this purpose, the FSS structures are the potential candidates and likely it is required to study the state-of-the-art of design issues, bandstop/bandpass filtering behaviour and scattering characteristics particularly, the frequency response, bandwidth, and angular/polarization stability of the structures.

In this thesis, we have investigated a synthesis technique to yield the geometrical parameters of the SSLFSS, which is significantly useful for the fast analysis and design of FSS structure. The process of computation of different geometrical parameters is presented, and the parameters achieved by this synthesis technique are supported by the experimental as well as simulation results. At every frequency of interest, the numerical analysis is validated by comparing the resonance frequency with three different commercially available simulators based on different computational techniques. The proposed synthesis technique is used to design bandstop SSLFSS at different frequencies (3 GHz, 22 GHz and 26 GHz) and further extended to design the bandpass SSLFSS structure. Moreover, a way to control the reflection at any chosen frequency is discussed, which may find potential applications in controlling the reflection coefficient at various frequencies of the electromagnetic spectrum. The developed mathematical expression is significantly applicable for both types of free-standing SSLFSS structures such as patch-and slot-type. Furthermore, the dielectric substrate provides the mechanical strength, miniaturization and stable resonant frequency of the FSS structure. Therefore, we have modified the derived mathematical expression of free-standing SSLFSS for that of the dielectric backed, which is further implemented on the circular ring FSS structure. The significant implementation of developed mathematical expression of dielectric backed SSLFSS on the circular ring FSS yields novel modified circular ring FSS structure.

On this way, the proposed synthesis technique is used to design two novel FSS structures (modified circular ring/slot and wedge shaped metal vane/slots) at S-band, Ku-/Ka-band with the controlled FBW for satellite communication systems using the structure transformation technique. The modified circular ring bandpass FSS structure is designed at 3 GHz, 13.5 GHz and 26 GHz with approximately 15% FBW. At each frequency of interest, the resonance responses are discussed in terms of the significant angular (up to 50^{o}) stability, polarization (perpendicular and parallel) stability and bandwidth, which signifies that the simple proposed geometry of FSS structure provides significantly better angular and polarization stability as compared to that of the various reported FSS structures.

Moreover, the resonant frequency of proposed modified circular ring FSS downshifts with 0.85% and 0.84% for the perpendicular polarized wave, and with 0.76% and 0.65% for the parallel polarized wave, which is achieved through CST Microwave Studio and Ansoft HFSS, respectively up to 50^{o} AOI at X-band. At the normal wave incidence, the simulation results achieved through CST Microwave Studio and Ansoft HFSS experiences only 0.009% and 0.09% deviation in the resonant frequency as compared to that of the measured results, which ensures the practicality of the synthesis technique used for the designing of proposed modified circular ring FSS structure. In addition to this, the return loss obtained in the simulated results such as 26.33 dB and 26.58 dB through CST microwave Studio and Ansoft HFSS, is also in the close agreement with measured results (24.15 dB). However, the shift in the resonant frequency due to perpendicular and parallel polarized wave at normal wave incidence is 0% and 0.3% as achieved through CST Microwave Studio and Ansoft HFSS, respectively, which provides the stable response in terms of the scattering characteristics for dual polarization.

Moreover, the proposed modified circular ring FSS structure with four pairs of parallel straight conductors/slot has been extended for the multiband frequency characteristics which provide significant frequency response in the S-, Ku-/Ka-band of the electromagnetic spectrum. In this thesis, using the multi-resonant approach, we have designed two novel geometries of multiband FSS structures, which are of slot-type and patch-type. In addition to this, the proposed multiband FSS structures offer

simple, light-weight, low profile geometry and significant angular/polarization stability.

The proposed slot-type multiband FSS structure has been achieved using passive loading of the inner classical circular ring FSS structure in the outer modified circular ring, which provide reflection in S-band (2-4 GHz)/K_u (12-18 GHz) and transmission in X-band (8-12 GHz)/K_a-band (26.5-40 GHz). Moreover, the proposed patch-type multiband FSS structure is obtained through concentric modified circular ring FSS structure, which provides transmission in S-band and reflection in Ku/Ka-band. The proposed slot-type and patch-type multiband FSS structure offer significant angular and polarization stability as compared to that of the frequency shift in the FSS structure discussed in [111], concentric circular ring FSS structure (4.76%- for TE polarized wave and 1.12%- for TM polarized wave) [113], L-shaped as well as one helix-shaped unit-cell element FSS structure (6.75%- for TE polarized wave and 1.65%- for TM Polarized wave) [119] and triangular conducting element FSS structure (6.59%) [120].

We have also discussed an azimuthally periodic wedge shaped circular ring, which offer single-band bandstop and bandstop filtering characteristics. The azimuthally periodic wedge shaped circular ring bandstop FSS provides 0.04% and 0.4% shift in the resonant frequency through CST Microwave Studio and Ansoft HFSS, respectively for 50^o AOI as compared to that of the normal wave incidence at Ku-band. The frequency response of azimuthally periodic wedge shaped circular ring bandstop FSS is investigated in terms of the number of the vanes in unit-cell. However, the proposed FSS structure is practically more feasible and is easy to fabricate as compare to that of the other loaded FSS structures. In addition to this, the azimuthally periodic wedge shaped circular ring bandpass FSS structure is discussed in S-, Ku- and Ka-band for the significant angular/polarization stability and FBW, which is useful for the satellite communication applications. The azimuthally periodic wedge-shaped circular ring bandpass FSS provides approximately 59% FBW in S-band and wide-band frequency characteristics in Ku-band, which is useful for the satellite communication.

In this thesis, we have considered the negligible thickness of the metallic pattern that is single square loop and circular ring ($t << \lambda$), however it plays very important

role over the circuit parameters and consequently opens the door for 3-dimensional FSS. However, various researchers are working over such structures using the substrate integrated waveguide (SIW) [194], a stepped impedance resonator (SIR) [195] and microstrip line [196-199]. In addition to this, the design as well as fabrication issues of the conical surface FSS structure is also very important issue that will significantly improves the performance of the FSS structure. Moreover, the FSS structures provide significant applications in higher frequency bands (terahertz) such as directivity/gain enhancement in antenna systems, sensing and imaging [200]. Therefore, it is required to exploit the FSS structure in the terahertz regime of the electromagnetic spectrum and various issues such as losses, surface roughness and skin depth need to be investigated in detail while investigating FSS structures in the terahertz regime [59].

REFERENCES

[1] B. A. Munk, "Frequency Selective Surfaces: Theory and Design", Wiley: New York, 2000.

[2] T. K. Wu, "Frequency Selective Surfaces and Grid Arrays", Wiley: New York, 1995.

[3] A. Fallahi, M. Mishrikey, C. Hafner and R. Vahldieck, "Efficient procedures for the optimization of frequency selective surfaces," IEEE Trans. on Antennas and Propagation, vol. 56, no. 5, pp. 1340–1349, 2008.

[4] H. T. Liu, H. F. Cheng, Z. Y. Chu and D. Y. Zhang, "Absorbing properties of frequency selective surface absorbers with cross-shaped resistive patches", Material Design, vol. 28, pp. 2166–2171, 2007.

[5] D. Singh, A. Kumar, S. Meena and V. Agrawal, "Analysis of frequency selective surfaces for radar absorbing materials", Progress Electromagnetics Research B, vol. 38, pp. 297–314, 2012.

[6] D. C. Kohlgraf, "Design and testing of a frequency selective surface based wide-band multiple antenna system", PhD. Thesis, The Ohio State University, USA, 2005.

[7] L. Li, Q. Chen, Q. Yuan, K. Sawaya, T. Maruyama, T. Furuno and S. Uebayashi, "Frequency selective reflect-array using crossed-dipole elements with square loops for wireless communication applications", IEEE Trans. on Antennas and Propagation, vol. 59, no. 1, pp. 89-99, Jan. 2011.

[8] S. Keyrouz, G. Perotto and H. J. Visser, "Frequency selective surface for radio frequency energy harvesting applications", IET Microwaves, Antennas and Propagation, vol. 8, no. 7, pp. 523-531, 2014.

[9] Y. Ranga, L. Matekovits, A. R. Weily and K. P. Esselle, "A low-profile dual-layer ultra-wideband frequency selective surface reflector", Microwave and Optical Technology Letters, vol. 55, no. 6, pp. 1223-1227, 2013.

[10] F. C. G. da Silva Segundo and A. L. P. S. Campos, "Compact frequency selective surface with dual band response for WLAN applications", Microwave and Optical Technology Letters, vol. 57, no. 2, pp. 265-268, 2015.

[11] O. Necibi, D. Hamzaoui, T. P. Vuong and A. Gharsallah, "A novel RFID-HIS-PRS reader antenna for the millimeter wave band 30 GHz", Microwave and Optical Technology Letters, vol. 57, no. 8, pp. 1835-1842, 2015.

[12] G. Sinclair, "Theory of models of electromagnetic systems", Proc. of Institute of Radio Engineers, vol. 36, no. 11, pp. 1364-1370,1948.

[13] E. M. Kennaugh, "Theory of Models of Electromagnetic Systems", US Patent 2,872, 675, 1959.

[14] J. J. S. Fernandez, "Frequency Selective Surface for Terahertz Applications", Ph.D. Thesis, The University of Edinburgh, United Kingdom, 2012.

[15] http://calvin.phys.columbia.edu/group_web/filter_development/download/filter.pdf

[16] B. A. Munk and G. A. Burrell, “Plane wave expansion for arrays of arbitrary oriented piecewise linear elements and its application in determining the impedance of single linear antennas in a lossy half space”, IEEE Trans. on Antennas and Propagation, vol. 27, pp. 331 -343 1979.

[17] C. H. Tsao and R. Mittra, “Spectral-domain analysis of frequency selective surfaces comprises of periodic arrays of cross dipoles and Jerusalem crosses”, IEEE Trans. on Antennas and Propagation, vol. 32, pp.478 -486 1984.

[18] T. A. Cwik and R. Mittra, “Scattering from a periodic array of free standing arbitrarily shaped perfectly conducting or resistive patches”, IEEE Trans. on Antennas and Propagation, vol. 35, pp. 1226 -1234 1987.

[19] A. Fallahi, A. Yahaghi, H. Abiri, M. Shahabadi and C. Hafner, “Large overlapping sub-domain method- of-moments for the analysis of frequency selective surfaces”, IEEE Trans. on Microwave Theory and Techniques, vol. 58, no. 8, pp. 2175-2187, 2010.

[20] http://www.eecs.wsu.edu/~schneidj/ufdtd/ufdtd.pdf

[21] A. Taflove and K. R. Umashankar, “The finite-difference time-domain (FDTD) method for numerical modeling of electromagnetic scattering”, IEEE Trans. on Magnetics, vol. 25, no. 4, pp. 3086-3091, 1989.

[22] F. Kuisheng, Li Na and Xu Jiadong, “Finite element method analysis for the frequency selective characteristics of dielectric periodic structure with arbitrary profiles”, Proc. of 4th IEEE Conf. on Industrial Electronics and Applications, Xian, 25-27 May 2009, pp.1957-1960.

[23] Farhad Khosravi, “Applications of frequency selective surfaces in polarization control of antennas”, MS Thesis, Department of Electrical and Computer Engineering, University of Alberta: Canada, 2014.

[24] C. C. Chen, “Transmission through a conducting screen perforated periodically with apertures”, IEEE Trans. on Microwave Theory and Techniques, vol. 18, no. 9, pp. 627-632, 1970.

[25] T. Gilles, “Advances in the Formulations and Accuracy of the Method-of-Moments Applied to Electromagnetics”, 1st Edition, Presses universitaires de Louvain, Belgium, 2011.

[26] D. S. Weile, E. Michielssen and Kyle Gallivan, “Reduced-order modeling of multi-screen frequency-selective surfaces using Krylov-based rational interpolation”, IEEE Trans. on Antennas and Propagation, vol. 49, no. 5, pp. 801-813, 2001.

[27] V. V. S. Prakash and Raj Mittra, “Characteristic basis function method: a new technique for efficient solution of method of moment s matrix equations”, Microwave and Optical Technology Letters, vol. 36, no. 2, pp. 95-100, 2003.

[28] N. Don, M. Bozzi, A. Kirilenko and L. Perregrini, “Analysis of inductive frequency selective surfaces by the method of moments with entire-domain basis functions”, Microwave and Optical Technology Letters, vol. 49, no. 12, pp. 2929-2932, 2007.

[29] M. Montagna, M. Bozzi and L. Perregrini, "Convergence properties of the method of moments in the modeling of frequency selective surfaces", International Journal of RF and Microwave Computer–Aided Engineering, vol. 20, no. 2, pp. 220-229, March 2010.

[30] D. B. Davidson, "Computational Electromagnetics for RF and Microwave Engineering", Cambridge University Press: Cambridge, 2005.

[31] A. Taflove and S. Hagness, "Computational electrodynamics: The Finite-Difference Time-Domain Method", 2nd Edition, Artech House: Boston, 2000.

[32] http://en.wikipedia.org/wiki/FDTD.

[33] K. Yee, "Numerical solution of initial boundary value problems involving Maxwell's equations in isotropic media", IEEE Trans. on Antennas and Propagation, vol. 14, no. 3, pp. 302-307, 1966.

[34] A. Taflove and K. R. Umashankar, "Review of FDTD numerical modeling of electromagnetic wave scattering and radar cross section", Proc. of IEEE, vol. 77, no. 5, pp. 682-699, 1989.

[35] P. Harms, R. Mittra and W. Ko, "Implementation of the periodic boundary condition in the finite-difference time-domain algorithm for FSS structures", IEEE Trans. on Antennas and Propagation, vol. 42, no. 9, pp. 1317-1324, 1994.

[36] W. Yu, X. Yang, Y. Liu, R. Mittra and A. Muto, "Advanced FDTD Methods: Parallelization, Acceleration and Engineering Applications", Artech House: Norwood, 2011.

[37] W. Yu, R. Mittra, X. Yang, Y. Liu, Q. Rao, and A. Muto, "High performance conformal FDTD techniques", IEEE Microwave Magazine, vol. 11, no. 4, pp. 42-55, 2010.

[38] I. Bardi, R. Remski, D. Perry, and Z. Cendes, "Plane wave scattering from frequency selective surfaces by the finite-element method", IEEE Trans. on Magnetics, vol. 38, no. 2, pp. 641-644, 2002.

[39] J. D'Angelo and I. D. Mayergoyz, "Three dimensional RF scattering by the finite element method", IEEE Trans. on Magnetics, vol. 27, no. 5, pp. 3827-3832, 1991.

[40] T. F. Eibert, Y. E. Erdemli, and J. L. Volakis, "Hybrid finite element-fast spectral domain multilayer boundary integral modeling of doubly periodic structures", IEEE Trans. on Antennas and Propagation, vol. 51, no. 9, pp. 2517-2520, 2003.

[41] M. J. Archer, "Wave reactance of thin planar strip gratings", Int. Journal of Electronics, vol. 58, no. 2, pp. 197-230, 1985.

[42] N. Marcuvitz, "Waveguide Handbook", Peter Peregrinus Ltd.: New York, vol.21, 1986.

[43] R. J. Langley and E. A. Parker, "Equivalent circuit model for arrays of square loops", Electronics Letters, vol. 18, no. 7, pp. 294-296, 1982.

[44] M. A. R. Barrera and W. P. Carpes, "Numerical model of the effective permittivity for square-loop frequency selective surfaces", IEEE Trans. on Magnetics, vol. 51, no. 3, pp. 1-4, March 2015.

[45] J. Yang and Z. Shen, "A thin and broadband absorber using double-square loops", IEEE Antennas and Wireless Propagation Letters, vol. 6, pp. 388-391, 2007.

[46] X. Yao, M. Bai and J. Miao, "Equivalent circuit method for analyzing frequency selective surface with ring patch in oblique angles of incidence", IEEE Antennas and Wireless Propagation Letters, vol. 10, pp. 820-823, 2011.

[47] S. M. A. Hamdy and E. A. Parker, "Influence of lattice geometry on transmission of electromagnetic waves through arrays of crossed dipoles", IEE Proceedings H Microwaves, Optics and Antennas, vol. 129, pp. 7-10, 1982.

[48] E. A. Parker and A. N. A. El-Sheikh, "Convoluted array elements and reduced size unit cells for frequency selective surfaces", IEE Proceedings H Microwaves, Antennas and Propagation, vol. 138, pp. 19-22, 1991.

[49] Y. Shang, Z. Shen and S. Xiao, "Frequency-selective rasorber based on square-loop and cross-dipole arrays", IEEE Trans. on Antennas and Propagation, vol. 62, no. 11, pp. 5581-5589, 2014.

[50] I. Anderson, "On the theory of self-resonant grids", The Bell System Technical Journal, vol. 54, no. 10, pp. 1725-1731, 1975.

[51] https://www.cst.com/

[52] http://anlage.umd.edu/HFSSv10UserGuide.pdf

[53] M. A. Ehsan, Z. Zhou and Yang Yi, "Development of an equivalent circuit model of a finite ground coplanar waveguide interconnect in MIS system for ultra-broadband monolithic ICs", Progress Electromagnetics Research C, vol. 56, pp. 1–13, 2015.

[54] S. N. Zabri, R. Cahill and A. Schuchinsky, "Polarisation independent split ring frequency selective surface", Electronics Letters, vol. 49, no. 4, pp. 245-246, 2013.

[55] M. Beruete, M. Sorolla, I. Campillo, J. S. Dolado, L. Martin-Moreno, J. Bravo-Abad, and F. J. Garcia-Vidal, "Enhanced millimeter wave transmission through quasi-optical sub-wavelength perforated plates", vol. 53, no. 6, pp. 1897-1903, 2005.

[56] K. R. Jha and Ghanshyam Singh, "Terahertz Planar Antennas for Next Generation Communication", Springer: NewYork, 2014.

[57] S. Vegesna, Y. Zhu, Y. Zhao, Z. Fan, A. Bernussi and M. Saed, "Terahertz frequency selective surface with reconfigurable polarization characteristics using vanadium dioxide", Journal of Electromagnetic Waves and Applications, vol. 28, no. 1, pp. 83-90, 2014.

[58] S. Das, K. M. Reza and M. A. Habib, "Frequency selective surface based bandpass filter for THz communication system", Journal of Infrared, Millimeter and Terahertz Waves, vol. 33, pp. 1163-1169, 2012.

[59] Garima Bharti , Kumud Ranjan Jha, and G. Singh, " A synthesis technique for single square loop frequency selective surface at terahertz frequency", Optik-International Journal for Light and Electron Optics, vol. 125, no. 21, pp. 6428-6435, 2014.

[60] S. Islam, J. Stiens, I. Jaeger, G. Poesen and R. Vounckx, "Implementation of dynamic Hadamard diffuser as a frequency selective surface for W-band active millimeter wave imaging", Microwave and Optical Technology Letters, vol. 51, no. 6, pp.1440-1445, 2009.

[61] R. Cahill and E. A. Parker, "Frequency selective surface design for submillimetric demultiplexing", Microwave and Optical Technology Letters, vol. 7, no.13, pp.595-597, 1994.

[62] S. Govindaswamy, J. East, F. Terry, E. Topsakal, J. L. Volakis and G. I. Haddad, "Frequency-selective surface based bandpass filters in the near-infrared region", Microwave and Optical Technology Letters, vol. 41, no. 4, pp. 266-269, 2004.

[63] S. Monni, A. Neto, G. Gerini, F. Nennie, and A. Tijhuis, "Frequency-selective surface to prevent interference between radar and SATCOM antennas", IEEE Antennas Wireless Propagation Letter, vol. 8, pp. 220-223, 2009.

[64] R. Yahiaoui, S. N. Burokur, V. Vigneras, A. de Lustrac and P. Mounaix, "Investigation of spatial filters at microwave frequencies: Application for antenna directivity enhancement", Microwave and Optical Technology Letter, vol. 54, no. 5, pp. 1327-1332, 2012.

[65] R. Ulrich, "Far-infrared properties of metallic mesh and its complementary structure", Infrared Physics, vol. 7, no. 1, pp. 37-50, 1967.

[66] M. S. Durschlag and T. A. Detemple, "Far-IR optical properties of freestanding and dielectrically backed metal meshes", Applied Optics, vol. 20, no. 7, pp.1245-1253, 1981.

[67] G. Kristensson, M. Akerberg and S. Poulsen, "Scattering from a frequency selective surfaces supported by a bi-anisotropic substrate", Progress Electromagnetics Research, vol. 35, pp 83-114, 2002.

[68] Z. Li, P.Y. Papalambros and J.L. Volakis, "Frequency selective surface design by integrating optimisation algorithms with fast full wave numerical methods", IEE Proc. of Microwave, Antennas and Propagation, vol. 149, no. 3, pp. 175-180, June 2002.

[69] A. E. Yilmaz and M. Kuzuoglu, "Design of the square loop frequency selective surfaces with particle swarm optimization via the equivalent circuit model", Radioengineering, vol. 18, no. 2, pp. 95-102, June 2009.

[70] R. Dubrovka, J. Vazquez, C. Parini and D. Moore, "Equivalent circuit method for analysis and synthesis of frequency selective surfaces", IEE Proceedings, vol. 153, no. 3, pp. 213-220, 2006.

[71] G. H. Sung, K. W. Sowerby and A. G. Williamson, "Modeling a low-cost frequency selective wall for wireless-friendly indoor environments", IEEE Antennas Wireless Propagation Letters, vol. 5, pp. 311-314, 2006.

[72] H. G. Foumani and M. K. Amirhosseini, “Compact spatial band-pass filters using frequency selective surfaces”, Progress In Electromagnetics Research C, vol. 21, pp. 59-73, 2011.

[73] E. F. Kent, B. Doken, M. Kartal, “A new equivalent circuit based FSS design method by using genetic algorithm”, Proc. of 2nd International Conf. on Engineering Optimization, Lisbon, Portugal, 6-9 Sep. 2010, pp. 1-4.

[74] J. X. Su, X. W. Xu, M. He and K. Zhang, “Integral equation analysis of frequency selective surfaces using Ewald transformation and lattice symmetry”, Progress In Electromagnetics Research, vol. 121, pp. 249-269, 2011.

[75] E. B. Tchikaya, F. Khalil, F. A. Tahir, and H. Aubert, “Multi-scale approach for the electromagnetic simulation of finite size and thick frequency selective surfaces”, Progress In Electromagnetics Research M, vol. 17, pp. 43-57, 2011.

[76] B. A. Munk, R. G. Kouyoumjian and L. Peters, “Reflection properties of periodic surfaces of loaded dipoles”, IEEE Trans. on Antennas and Propagation, vol. 19, no. 5, pp. 612-617, 1971.

[77] B.A. Munk and R.J. Luebbers, “Reflection properties of two layer dipole arrays”, IEEE Trans. on Antennas Propagation, vol. 22, no. 6, pp. 766-773, 1974.

[78] R. Woo, “A low-loss circularly polarized dichroic plate”, Proc. of International Symposium on Antennas and Propagation Society, USA, 1971, vol. 9, pp 149-152.

[79] R. R. Xu, H. C. Zhao, Z. Y. Zong and W. Wu, “Dual-band capacitive loaded frequency selective surfaces with close band spacing”, IEEE Microwave and Wireless Components Letters, vol. 18, no. 12, pp. 782-784, 2008.

[80] S. N. Azemi, K. Ghorbani and W. S. T. Rowe, “A reconfigurable FSS using a spring resonator element”, IEEE Antennas and Wireless Propagation Letters, vol. 12, pp. 781-784, 2013.

[81] P. S. Taylor, J. C. Bathelor and E. A. Parker, “A passively switched dual-band circular FSS slot array,” Proc. of IEEE-APS Topical Conf. on Antennas and Propagation in Wireless Communications (APWC), Torino, 12-16 Sept. 2011, pp. 648-651.

[82] A. E. Martynyuk, J. I. M. Lopez, and N. A. Martynyuk, “Active frequency-selective surfaces based on loaded ring slot resonators”, Electronics Letters, vol. 41, no. 1, pp. 2-4, 2005.

[83] S. M. Choudhury, M. A. Zaman, M. Gaffar and M. A. Matin, “A novel approach of changing bandwidth of FSS filter using gradual circumferential variation of loaded elements”, Proc. of Progress in Electromagnetics Research, USA, 2010, pp. 1132-1134.

[84] T. K. Chang, R. J. Langley and E. A. Parker, “Active frequency-selective surfaces”, IEE Proc. Microwaves, Antennas and Propagation, vol. 143, no. 1, pp. 62-64, 1996.

[85] L. Zhang, G. Yang, Q. Wu and J. Hua, “A novel active frequency selective surface with wideband tuning range for EMC purpose,” IEEE Trans. on Magnetics, vol. 48, no. 11, pp. 4534-4537, 2012.

[86] C. Mias, “Frequency selective surfaces loaded with surface mount reactive components”, Electronic Letters, vol. 39, no. 9, pp. 724-726, 2003.

[87] C. Guo, H. Sun and L. Xin, “Dual-band frequency selective surface with double-four-legged loaded slots elements”, Proc. of International Conf. on Microwave and Millimeter Wave Technology, Nanjing, 21-24 April 2008, pp. 297-300.

[88] B.A. Munk,” Periodic Surface for Large Scan Angles”, US Patent 3, 789, 404, 1974.

[89] J. Shaker and L. Shafai, “Reduced angular sensitivity frequency selective surface”, Electronics Letters, vol. 29, no. 18, pp. 1655- 1657, 1993.

[90] J. Shaker and L. Shafai, “Removing the angular sensitivity of FSS structures using novel Double-layer structures”, IEEE Microwave and Guided Wave Letter, vol. 5, no. 10, pp. 324-325, 1995.

[91] G. I. Kiani, K. L. Ford, L. G. Olsson, K. P. Esselle and C. J. Panagamuwa, “Switchable frequency selective surface for reconfigurable electromagnetic architecture of buildings”, IEEE Trans. on Antennas and Propagation, vol. 58, no. 2, pp. 581-584, 2010.

[92] B. S. Izquierdo and E. A. Parker, “Dual polarized reconfigurable frequency selective surfaces”, IEEE Trans. on Antennas and Propagation, vol. 62, no. 2, pp. 764-771, Feb. 2014.

[93] J. Romeu and Y. Rahmat-Samii, “Fractal FSS: A novel dual-band frequency selective surface”, IEEE Trans. on Antennas and Propagation, vol. 48, no. 7, pp. 1097-1105, 2000.

[94] G. Q. Luo, W. Hong, H. J. Tang, J. X. Chen and L. L. Sun, “Tri-band frequency selective surface with periodic cell perturbation”, IEEE Microwave and Wireless Components Letters, vol. 17, no. 6, pp. 436-438, June 2007.

[95] D. Wang, W. Che, Y. Chang, K. S. Chin and Y. L. Chow, “A low-profile frequency selective surface with controllable tri-band characteristics”, IEEE Antennas and Wireless Propagation Letters, vol. 12, pp. 468-471, 2013.

[96] M. R. da Silva, C. de L. Nobrega, P. H. da F. Silva and A. G. D’Assunçao, “Dual-polarized band-stop FSS spatial filters using vicsek fractal geometry”, Microwave and Optical Technology Letters, vol. 55, no. 1, pp. 31-34, 2013.

[97] L. M. Araujo, R. H. C. Maniçoba, A. L. P. S. Campos and A. G. d’Assunçao, “A simple dual-band frequency selective surface”, Microwave and Optical Technology Letters, vol. 51, no. 4, pp. 942-944, 2009.

[98] Y. Y. Lv and W. L. Chen, “Dual-polarized multiband frequency selective surface with miniaturized hilbert element”, Microwave and Optical Technology Letters, vol. 55, no. 6, pp.1221-1223, 2013.

[99] S. Uçkun and T. Ege, “Concentric rings as frequency-selective surfaces on isotropic chiral slabs”, Microwave and Optical Technology Letters, vol. 48, no. 1, pp. 79-83, 2006.

[100] A. Ray, M. Kahar, S. Sarkar, S. Biswas, D. Sarkar and P. P. Sarkar, "A novel broad and multiband frequency selective surface", Microwave and Optical Technology Letters, vol. 54, no. 6, pp. 1353-1355, 2012.

[101] Y. S. Im, H. K. Choi and J. H. Park, " Design of double layer frequency selective surfaces with novel multiresonant elements for four-frequency bands", Microwave and Optical Technology Letters, vol. 54, no. 9, pp. 2153-2157, 2012.

[102] E. C. Braz and A. L. P. S. Campos, " Dual/wide band multifractal frequency selective surface for applications in S- and X-band" Microwave and Optical Technology Letters, vol. 56, no. 10, pp. 2217-2222, 2014.

[103] B. S. Izquierdo, E. A. Parker, J. B. Robertson and J. C. Batchelor, "Singly and dual polarized convoluted frequency selective structures", IEEE Trans. on Antennas and Propagation, vol. 58, no. 3, pp. 690-696, March 2010.

[104] A. Ray, M. Kahar, D. Sarkar and P. P. Sarkar, "On fractal FSS suitable for WLAN and WiMAX communication", Microwave and Optical technology Letters, vol. 57, no. 7, pp. 1546-1550, 2015.

[105] A. Qing and C. K. Lee, "An improved model for full wave analysis of multilayered frequency selective surface with gridded square element", Progress Electromagnetic Research, vol. 30, pp. 285-303, 2001.

[106] D. H. Kim and J. I. Choi, "Design of a multiband frequency selective surface", ETRI Journal, vol. 28, pp. 506-508, 2006.

[107] A. D. Chuprin, E. A. Parker and J. C. Batchelor, "Convoluted double square: single layer FSS with close band spacings", Electronics Letters, vol. 36, pp. 1830–1831, Oct. 2000.

[108] A. L. P. S. Campos, T. L. Silva and A. G. Neto, "Multiband frequency selective surfaces with simple modification of a rectangular patch element", Microwave and Optical Technology Letters, vol. 55, no. 12, pp. 2943-2946, 2013.

[109] D. H. Werner and D. Lee, "Design of dual polarized multiband frequency selective surfaces using fractal elements", Electronics Letters, vol. 36, no. 6, pp. 487-488, 2000.

[110] M. Ohira, H. Deguchi, M. Tsuji and H. Shigesawa, "Optimized multiband single-layer frequency selective surface and its experimental verification", Proc. of 32nd European Conf. on Microwave, Italy, 23-26 Sept. 2002, pp.1-4.

[111] C. N. Chiu and W. Wang, "A dual-frequency miniaturized-element FSS with closely located resonances," IEEE Antennas and Wireless Propagation Letters, vol. 12, pp. 163-165, 2013.

[112] R. A. Hill and B. A. Munk, "The effect of perturbating a frequency selective surface and its relation to the design of a dual-band surface", IEEE Trans. on Antennas and Propagation, vol. 44, no. 3, pp. 368-374, 1996.

[113] E. A. Parker, S. M. A. Hamdy and R. J. Langley, "Arrays of concentric rings frequency selective surfaces", Electronics Letter, vol. 17, no. 23, pp. 880-881, August 1981.

[114] J. Huang, T. K. Wu, and S. H. Lee, "Tri-band frequency selective surface with circular ring elements", IEEE Trans. on Antennas Propagation, vol. 42, pp. 166–175, Feb. 1994.

[115] T. K. Wu, "Four-band frequency selective surface with double-square loop patch elements", IEEE Trans. on Antennas and Propagation, vol. 42, pp. 1659–1663, Dec. 1994.

[116] T. K. Wu and S. W. Lee, "Multiband frequency selective surface with multi-ring patch elements", IEEE Trans. on Antennas and Propagation, vol. 42, pp. 1484–1490, Nov. 1994.

[117] Y. T. Lo and S. W. Lee, "Antenna Handbook", Van Nostrand Reinhold Co.: New York, 1988.

[118] Garima Bharti, K. R. Jha, G. Singh and R. Jyoti, "Azimuthally periodic wedge-shaped metallic vane loaded frequency selective surface", International Journal of Microwave and Wireless Technologies, vol. 7, no. 1, pp. 95-106, 2015.

[119] K. Delihacioglu, S. Uckun and T. Ege, "Scattering characteristics of FSS comprised of L-shaped and one-turn helix shaped conductors for TE and TM excitation", Electrical Engineering, vol. 89, pp. 177-181, 2006.

[120] A. Pekmezci and T. Ege, "Scattering characteristics of FSSs with triangular conducting elements", Electrical Engineering, no. 2, vol. 96, pp. 145-155, 2014.

[121] S. Islam, J. Stiens, G. Poesen, I. Jaeger, C. De Tandt, W. Ranson, W. De Raedt and R. Vounckx, "Effect of inter-element spacings variation on the performance of linear grounded frequency selective surface arrays in W-band", Microwave and Optical Technology Letters, vol. 52, no. 1, pp. 155-160, 2010.

[122] F. C. Seman and N. K. Khalid, "Design strategy for optimum planar square loop FSS with different dielectric substrates", Theory and Applications of Applied Electromagnetics Lecture Notes in Electrical Engineering, vol. 344, pp. 87-94, 2015.

[123] F. Costa, A. Monorchio and G. Manara, "Efficient analysis of frequency-selective surfaces by a simple equivalent-circuit model", IEEE Antennas and Propagation Magazine, vol. 54, no. 4, pp. 35-48, Aug. 2012.

[124] B. Mandal, A Chatterjee and S. K. Parui, "Acrylic substrate based low profile wearable button antenna with FSS layer for WLAN and Wi-Fi applications", Microwave and Optical Technology Letters, vol. 57, pp. 1033-1038, 2015.

[125] Hui-Hsia Sung, "Frequency selective wallpaper for mitigating indoor wireless interference", PhD. Thesis, Electrical and Electronic Engineering, University of Auckland, 2006.

[126] T. Larsen, “A survey of the theory of wire grids”, IRE Trans. on Microwave Theory and Techniques, vol. 10, no. 3, pp. 191-201, 1962.

[127] Z. L. Wang, K. Hashimoto, N. Shinohara, and H. Matsumoto, “Frequency-selective surface for microwave power transmission”, IEEE Trans. on Microwave Theory and Techniques, vol. 47, no. 10, pp. 2039-2042, 1999.

[128] R. J. Langley and A. J. Drinkwater, “Improved empirical model for the Jerusalem cross”, IEE Proc. H (Microwaves, Optics and Antennas), vol. 129, no. 1, pp. 1-6, 1982.

[129] G. I. Kiani, K. L. Ford, K. P. Esselle, A. R. Weily, and C. J. Panagamuwa, “Oblique incidence performance of a novel frequency selective surface absorber,” IEEE Trans. on Antennas and Propagation, vol. 55, pp. 2931–2934, 2007.

[130] G. I. Kiani, K. P. Esselle, K. L. Ford, A. R. Weily, and C. Panagamuwa, “Angle and polarization-independent bandstop frequency selective surface for indoor wireless systems”, Microwave and Optical Technology Letters, vol. 50, pp. 2315–2317, 2008.

[131] J. Y. Xue, S. X. Gong, P. F. Zhang, W. Wang and F. F. Zhang, “A new miniaturized fractal frequency selective surface with excellent angular stability”, Progress In Electromagnetics Research Letters, vol. 13, pp. 131–138, 2010.

[132] I. G. Lee and I. P. Hong, “3D frequency selective surface for stable angle of incidence”, Electronics Letters, vol. 50, no. 6, pp. 423-424, 2014.

[133] R. Natarajan, M. Kanagasabai, S. Baisakhiya, R. Sivasamy, S. Palaniswamy and J. K. Pakkathillam, “A compact frequency selective surface with stable response for WLAN applications”, IEEE Antennas and Wireless Propagation Letters, vol. 12, pp. 718-720, 2013.

[134] R. Sivasamy and M. Kanagasabai, “A novel dual-band angular independent FSS with closely spaced frequency response”, IEEE Microwave and Wireless Components Letters, vol. 25, no. 5, pp. 298-300, 2015.

[135] Garima Bharti, Kumud Ranjan Jha, Ghanshyam Singh and Rajeev Jyoti, “Design of dual-polarized and angular stable new bandpass frequency selective surface in X-band”, Telecommunication Systems, (Online), March 2015. DOI: 10.1007/s11235-015-0012-y

[136] Garima Bharti, Kumud Ranjan Jha, Ghanshyam Singh and Rajeev Jyoti, “Design of angular and polarization stable modified circular ring frequency selective surface for satellite communication system”, International Journal of Microwave and Wireless Technologies, 5 March 2015 (online).
DOI: http://dx.doi.org/10.1017/S1759078715000331

[137] M. Sesay, X. Jin and Z. Ouyang, “Frequency selective surface with arbitrary shapes and its application to filter design”, Progress In Electromagnetics Research B, vol. 57, pp. 75–85, 2014.

[138] V. Mizeikis, S. Juodkazis, K. Sun and H. Misawa, “Fabrication of frequency-selective surface structures by femtosecond laser ablation of gold films”, Journal of Laser Micro/Nanoengineering, vol. 5, no. 2, pp. 115-120, 2010.

[139] V. Dmitriev and M. N. Kawakatsu, “Microwave switchable frequency selective surface with high quality factor resonance and low polarization sensitivity”, Journal of Microwaves, Optoelectronics and Electromagnetic Applications , vol. 11, no. 2, pp. 263-268, 2012.

[140] A. D. Panagopoulos, P. D. M. Arapoglou and P. G. Cottis, “Satellite communications at Ku, Ka, and V bands: Propagation impairments and mitigation techniques”, IEEE Communications Surveys & Tutorials, vol. 6, no. 3, pp. 2-14, 2004.

[141] B. R. Elbert, “The Satellite Communication Ground Segment and Earth Station Handbook”, Artech House: Norwood, 2014.

[142] L. J. Ippolito, “Radiowave Propagation in Satellite Communications”, Springer: USA, 2012.

[143] G. V. Stephenson, “Combined Fixed Satellite Service and Mobile Platform Satellite Service Communication System”, US7302226 B2, 2007.

[144] M. Mohajer, M. F. Dana, and S. S. Naeini, “Effects of resonance-based phase shifters on Ka-band phased array antenna performance for satellite communications”, Progress Electromagnetics Research B, vol. 60, pp. 259–274, 2014.

[145] Jia Hong-Yan, Feng Xiao-Guo, and Sheng Cui-Xia, “Tunable frequency selective surface with a shorted ring slot”, Chinese Physics B, vol. 21, no. 5, pp. 054102-1/4, 2012.

[146] M. H. B Ucar, A. Sondas and Y. E. Erdemli, “Switchable split-ring frequency selective surfaces”, Progress Electromagnetics Research B, vol. 6, pp. 65-79, 2008.

[147] E. C. Kinzel, R. L. Brown, J. C. Ginn, B. A. Lail, B. A. Slovick and G. D. Boreman, “Design of an MoM diode-coupled frequency-selective surface”, Microwave and Optical Technology Letters, vol. 55, no. 3, pp. 483-493, 2013.

[148] D. F. Sievenpiper, “Tunable Frequency Selective Surface”, US7173565 B2, 2007.

[149] M. Sazegar, Y. Zheng Y, C. Kohler, H. Maune, M. Nikfalazar, J. R. Binder and R. Jakoby, “Beam steering transmitarray using tunable frequency selective surface with integrated ferroelectric varactors”, IEEE Trans. on Antennas and Propagation, vol. 60, no. 12, pp. 5690–5699, 2012.

[150] Ghaffer I. Kiani , Kenneth L. Ford , Karu P. Esselle, Andrew R. Weily, C. Panagamuwa and J. C. Batchelor, “Single-layer bandpass active frequency selective surface”, Microwave and Optical Technology Letters, vol. 50, no. 8, pp. 2149–2151, August 2008.

[151] B. A. Munk, “Finite Antenna Arrays and FSS”, John Wiley & Sons: USA, 2003.

[152] K. Fuchi, J. Tang, B. Crowgey, A. R. Diaz, E. J. Rothwell and R. O. Ouedraogo, “Origami tunable frequency selective surface”, IEEE Antennas and Wireless Propagation Letters, vol. 11, pp. 473-475, 2012.

[153] Q. Gao, D. Yan, Y. Fu, N. Yuan, “Loaded-frequency selective surface”, Frontiers of Electrical and Electronic Engineering China, vol. 3, no. 1, pp. 96-98, 2008.

[154] T. G. Ming, M. J. Gang and D. J. Ming, "A novel four-legged loaded element thick-screen frequency selective surface with a stable performance", Chinese Physics B, vol. 21, no. 12, pp. 128401/1-8, 2012.

[155] G. I. Kiani, K. P. Esselle, L. G. Olsson, A. Karlsson, and M. Nilsson, "Cross-dipole bandpass frequency selective surface for energy-saving glass used in buildings", IEEE Trans. on Antennas and Propagation, vol. 59, no. 2, pp. 520–525, 2011.

[156] I. S. Syed, Y. Ranga, L. Matekovits, K. P. Esselle and S. G. Hey, "A single-layer frequency-selective surface for ultra-wideband electromagnetic shielding", IEEE Trans. on Electromagnetic Compatibility, vol. 56, no. 6, pp. 1404-1411, 2014.

[157] H. T. Liu, H. F. Cheng, Z. Y. Chu, D. Y. Zhang, "Absorbing properties of frequency selective surface absorbers with cross-shaped resistive patches", Materials & Design, vol. 28, no. 7, pp. 2166–2171, 2007.

[158] H. M. Lee and Y. J. Kim, "Double-layered frequency selective surface superstrate using ring slot and dipole-shaped unit cell structure," Journal of Electromagnetic Engineering and Science, vol. 10, no. 3, pp. 86–91, 2012.

[159] M. Li and N. Behdad, "Frequency selective surfaces for pulsed high-power microwave applications," IEEE Trans. on Antennas and Propagation, vol. 61, pp. 677–687, 2013.

[160] S. Can and A. E. Yilmaz, "Parametric performance analysis of the square loop frequency selective surface", Journal of Electrical Engineering and Computer Science, vol. 80, no. 3, pp. 110-115, 2013.

[161] H. Y. Chen and Y. Tao, " Bandwidth enhancement of a U-slot patch antenna using dual-band frequency-selective surface with double rectangular ring elements", Microwave and Optical Technology Letters, vol. 53, no. 7, pp. 1547-1553, 2011.

[162] C. K. Lee and R. J. Langley, "Equivalent-circuit models for frequency selective surfaces at oblique angles of incidence," IEE Proceedings-H, Microwaves Optics and Antennas, vol. 132, pp. 395-399, 1985.

[163] J. A. Reed, "Frequency Selective Surfaces with Multiple Periodic Elements", Ph.D. Thesis, University of Texas Dallas, USA, 1997.

[164] D. M. Pozar, "Microwave Engineering", 2nd Edition, John Wiley and Sons: NY, USA, 1998.

[165] A. Pirahadi, F. Keshmiri, M. Hakkak, and M. Tayarani, "Analysis and design of dual band high directivity EBG resonator antenna using square loop FSS as superstrate layer", Progress Electromagnetics Research, vol. 70, pp. 1-20, 2007.

[166] Y. J. Lee, J. Yeo, R. Mittra and W. S. Park, "Design of a high-directivity Electromagnetic Band Gap (EBG) resonator antenna using a frequency-selective surface (FSS) superstrate", Microwave and Optical Technology Letters, vol. 43, no. 6, pp. 462-467, 2004.

[167] P. Callaghan, E. A. Parker and R. J. Langley, "Influence of supporting dielectric layers on the transmission properties of frequency selective surfaces", IEE Proc. H Microwave Antennas Propagation, vol. 138, no. 5, pp. 448-454, 1991.

[168] D. S. Lockyer, J. C. Vardaxoglou and R. Simpkin, "Complementary frequency selective surface", IEE Proceedings - Microwaves Antennas and Propagation, vol. 147, no. 6, pp. 501-507, 2000.

[169] J. D. Kraus, "Antennas", 2nd Edition, Tata McGraw Hill: New Delhi, 2001.

[170] P. T. Teo, X. F. Luo, and C. K. Lee, "Transmission of convoluted periodic loop element with selective reflection", Applied Physics Letters, vol. 85, no. 9, pp. 1454-1456, 2004.

[171] M. K. Pain, S. Bhunia, S. Biswas, D. Sarkar and P. P. Sarkar, "A novel investigation on size reduction of a frequency selective surface", Microwave and Optical Technology Letters, vol. 49, no. 11, pp. 2820-2821, 2007.

[172] C. C. Chen, "Scattering by a two-dimensional periodic array of conducting plates", IEEE Transaction on Antennas Propagation, vol. 18, pp. 660-665, 1970.

[173] S. W. Lee, "Scattering by dielectric loaded screen", IEEE Trans. on Antennas and Propagation, vol. 19, pp. 656-665, 1971.

[174] Inder Bahl, "Lumped Elements for RF and Microwave Circuits", 1st Edition, Artech House: Boston, 2003.

[175] G. H. H. Sung, K. W. Sowerby, and A. G. Williamson, "Equivalent circuit modeling of a frequency selective plasterboard wall", Proc. of IEEE International Symposium on Antennas and Propagation, Washington DC, USA, Jul. 3-8, 2005, pp. 400–403.

[176] M. Yan, S. Que, J. Wang, J. Zhang, A. Zhang, S. Xia and W. Wang, "A new miniaturized frequency selective surface with stable resonance", IEEE Antennas and Wireless Propagation Letters, vol. 13, pp. 639-641, 2014.

[177] E. A. Parker and S. M. A. Hamdy, "Rings as elements for frequency selective surfaces", Electronics Letters, vol. 17, no. 17, pp. 612-614, 1981.

[178] M. Hosseinipanah, Q. Wu, C. Zhang, F. A. Minji, and G. Y. Yang, "Design of square-loop frequency selective surfaces utilize c-band radar stations," Proc. of International Conf. on Microwave and Millimeter Wave Technology, China, Apr. 21-24, 2008, pp. 66-68.

[179] M. Raspopoulos and S. Stavrou, "Frequency selective buildings through frequency selective surfaces", IEEE Trans. on Antennas and Propagation, vol. 59, no. 8, pp. 2998-3005, Aug. 2011.

[180] B. S. Izquierdo, E. A. Parker and J. C. Batchelor, "Switchable frequency selective slot arrays", IEEE Trans. on Antennas and Propagation, vol. 59, no. 7, pp. 2728-2731, July 2011.

[181] G. Yang, T. Zhang, W. Li and Q. Wu, "A new stable miniaturized frequency selective surface", IEEE Antennas and Wireless Propagation Letters, vol. 9, pp. 1018-1021, 2010.

[182] Planar EM Technical notes, Getting started with HFSS: Floquet Port help. http://www.scribd.com/doc/27207025/Getting-Started-With-HFSS#scribd

[183] Planar EM Technical notes, CST Microwave Studio: Floquet Port help. http://www.slideshare.net/bundahamka/cst-training-core-module-antenna-2

[184] http://cp.literature.agilent.com/litweb/pdf/5965-7707E.pdf

[185] K. R. Jha, G. Singh and Rajeev Jyoti, "A simple synthesis technique of single square loop frequency selective surface", Progress Electromagnetic Research B, vol. 45, pp. 165-185, 2012.

[186] F. C. G. da Silva Segundo, A. L. P. S. Campos and E. C. Braz, "Wide band frequency selective surface for angular and polarization independent operation", Microwave and Optical Technology Letters, vol. 57, no. 1, pp. 216-219, 2015.

[187] A. G. D'Assunçao Jr., G. Fontgalland, A. G. Neto and H. Baudrand, "Frequency selective surface filters with polarized band pass/band reject performances", Microwave and Optical Technology Letters, vol. 56, no. 2, pp. 438-487, 2014.

[188] Y. Yang, X. H. Wang and H. Zhou, "Dual-band frequency selective surface with miniaturized element in low frequencies", Progress In Electromagnetic Research Letters, vol. 33, pp. 167-175, 2012.

[189]http://www.coe.montana.edu/ee/lameres/courses/eele461_spring12/information/guide_to ads. pdf

[190] Planar EM technical notes, Ansoft Designer help.

[191] A. S. Barlevy and Y. Rahmat-Samii, "On the electrical and numerical properties of high Q resonances in frequency selective surfaces", Progress Electromagnetics Research, vol. 22, pp. 1-27, 1999.

[192] L. H. Hsieh and K. Chang, "Equivalent lumped elements G, L, C, and unloaded Q's of closed- and open-loop ring resonators", IEEE Trans. on Microwave Theory and Techniques, vol. 50, no. 2, pp. 453-460, Feb. 2002.

[193] K. Chang, "Microwave Ring Circuits and Antennas", New York: Wiley, 1996.

[194] G. Q. Luo, W. Hong, Z. C. Hao, B. Liu; W. D. Li, J. X. Chen, H. X. Zhou and K. Wu, "Theory and experiment of novel frequency selective surface based on substrate integrated waveguide technology", IEEE Trans. on Antennas and Propagation, vol. 53, no. 12, pp. 4035-4043, 2005.

[195] B. Li and Z. Shen, "Miniaturized bandstop frequency-selective structure using stepped-impedance resonators", IEEE Antennas and Wireless Propagation Letters, vol. 11, pp. 1112-1115, 2012.

[196] A. K. Rashid and Z. Shen, "A novel band-reject frequency selective surface with pseudo-elliptic response", IEEE Trans. on Antennas and Propagation, vol. 58, no. 4, pp. 1220-1226, April 2010.

[197] A. K. Rashid and Z. Shen, “Scattering by a two-dimensional periodic array of vertically placed microstrip lines”, IEEE Trans. on Antennas and Propagation, vol. 59, no. 7, pp. 2599-2606, July 2011.

[198] A. K. Rashid, Z. Shen, and B. Li, “An elliptical bandpass frequency selective structure based on microstrip lines”, IEEE Trans. on Antennas and Propagation, vol. 60, no. 10, pp. 4661-4669, 2012.

[199] B. Li and Z. Shen, “Three-dimensional dual-polarized frequency selective structure with wide out-of-band rejection”, IEEE Trans. on Antennas and Propagation, vol. 62, no. 1, pp. 130-137, 2014.

[200] Y. Guo, T. Zhang, W. Y. Yin and X. H. Wang, “Improved hybrid FDTD method for studying tunable graphene frequency-selective surfaces (GFSS) for THz-wave applications”, IEEE Trans. on Terahertz Science and Technology, vol. 5, no. 3, pp. 358-367, 2015.